



University of Kentucky
UKnowledge

Theses and Dissertations--Electrical and
Computer Engineering

Electrical and Computer Engineering

2017

REAL-TIME SENSING AND CONTROL OF DEVELOPING WELD PENETRATION THROUGH REFLECTION VIBRATION IN GTAW

Jinsong Chen

University of Kentucky, mr.chenjinsong@gmail.com

Digital Object Identifier: <https://doi.org/10.13023/ETD.2017.046>

[Right click to open a feedback form in a new tab to let us know how this document benefits you.](#)

Recommended Citation

Chen, Jinsong, "REAL-TIME SENSING AND CONTROL OF DEVELOPING WELD PENETRATION THROUGH REFLECTION VIBRATION IN GTAW" (2017). *Theses and Dissertations--Electrical and Computer Engineering*. 98.

https://uknowledge.uky.edu/ece_etds/98

This Doctoral Dissertation is brought to you for free and open access by the Electrical and Computer Engineering at UKnowledge. It has been accepted for inclusion in Theses and Dissertations--Electrical and Computer Engineering by an authorized administrator of UKnowledge. For more information, please contact UKnowledge@lsv.uky.edu.

STUDENT AGREEMENT:

I represent that my thesis or dissertation and abstract are my original work. Proper attribution has been given to all outside sources. I understand that I am solely responsible for obtaining any needed copyright permissions. I have obtained needed written permission statement(s) from the owner(s) of each third-party copyrighted matter to be included in my work, allowing electronic distribution (if such use is not permitted by the fair use doctrine) which will be submitted to UKnowledge as Additional File.

I hereby grant to The University of Kentucky and its agents the irrevocable, non-exclusive, and royalty-free license to archive and make accessible my work in whole or in part in all forms of media, now or hereafter known. I agree that the document mentioned above may be made available immediately for worldwide access unless an embargo applies.

I retain all other ownership rights to the copyright of my work. I also retain the right to use in future works (such as articles or books) all or part of my work. I understand that I am free to register the copyright to my work.

REVIEW, APPROVAL AND ACCEPTANCE

The document mentioned above has been reviewed and accepted by the student's advisor, on behalf of the advisory committee, and by the Director of Graduate Studies (DGS), on behalf of the program; we verify that this is the final, approved version of the student's thesis including all changes required by the advisory committee. The undersigned agree to abide by the statements above.

Jinsong Chen, Student

Dr. Yuming Zhang, Major Professor

Dr. Caicheng Lu, Director of Graduate Studies

REAL-TIME SENSING AND CONTROL OF DEVELOPING
WELD PENETRATION THROUGH REFLECTION
VIBRATION IN GTAW

DISSERTATION

A dissertation submitted in partial fulfillment of the
requirements for the degree of Doctor of Philosophy in the
College of Engineering
at the University of Kentucky

By

Jinsong Chen

Lexington, Kentucky

Director: Dr. YuMing Zhang, Professor of Electrical Engineering

Lexington, Kentucky

2017

Copyright © Jinsong Chen, 2017

ABSTRACT OF DISSERTATION

REAL-TIME SENSING AND CONTROL OF DEVELOPING WELD PENETRATION THROUGH REFLECTION VIBRATION IN GTAW

GTAW (Gas Tungsten Arc Welding) weld pool surface is believed to contain sufficient information to determine the weld penetration, from which skilled welders are able to control the welding process to desired penetration states. However, it is unclear how human welders extract the weld penetration from the observed weld pool surface. In this research, a novel method is studied to determine the weld penetration based on the dynamic change of the weld pool surface.

This study observes/measures/analyzes the development of a weld pool from partial to full penetration and correlates such change to the weld penetration. Similar trends in the weld pool surface are observed when the weld penetration changes from partial to full penetration despite the amperage used and material welded. Correlating the weld pool surface reflecting grayness and the development of the weld penetration from experiments shows: (1) the weld pool reflection intensity will increase while the weld penetration is increasing; (2) the increasing trends of weld pool reflection intensity will decrease when the full penetration is achieved; (3) the weld pool reflection intensity will increase after the full penetration is achieved. Such trend in the weld pool surface reflection intensity when the weld penetration develops is used as feedback signal to detect the weld pool penetration. To control the weld pool penetration, a first-order dynamic model is identified. Model Predictive Control (MPC) is used to control the weld penetration. Experiments verified the feasibility of this proposed method and established system.

KEYWORDS: GTAW, Weld pool, Vibration, Real-Time, MPC

Jinsong Chen
Student's Signature

03 / 03 / 2017
Date

REAL-TIME SENSING AND CONTROL OF DEVELOPING
WELD PENETRATION THROUGH REFLECTION
VIBRATION IN GTAW

By

Jinsong Chen

Yuming Zhang

Director of Dissertation

Caicheng Lu

Director of Graduate Studies

03 / 03 / 2017

Date

ACKNOWLEDGEMENTS

This work is funded by the Oak Ridge National Lab under contract DE-AC05-00OR22725 with DOE.

I would like to give my sincere thanks and appreciations to my advisor Dr. YuMing Zhang for his profound knowledge, patient guidance, continuous encouragement and support during my study at University of Kentucky. I am also thankful to Dr. Larry Holloway, Dr. Fuqian Yang and Dr. Yuan Liao for their helpful instructions and advices for my research and dissertation preparation. I would like to express my appreciation to Dr. Ke Zhang from Shanghai Jiaotong University, China, and Dr. Jiangkang Huang from Lanzhou University of Technology, China who shared experiences and knowledge with me, and cooperated to finish Chapter 5 and Chapter 6. Moreover, I would like to thank my colleagues in the Welding Research Laboratory.

I would like to thank my family for their love, support and faith in me. I want to give my special thanks to my wife Wei Wen for her love, trust and continuously support.

TABLE OF CONTENTS

ACKNOWLEDGEMENTS	iii
TABLE OF CONTENTS	iv
LIST OF TABLES	vii
LIST OF FIGURES	viii
CHAPTER 1 Introduction.....	1
1.1 Background.....	1
1.2 Objectives and Approach.....	3
1.3 Organization.....	5
CHAPTER 2 Literature Review	8
2.1 Weld Pool Oscillation Behaviors.....	9
2.2 Modeling of the Weld Pool.....	11
2.3 Weld Pool Sensing Techniques	13
2.3.1 Vision-based Sensing Technique.....	14
2.3.2 Voltage Variation-Based Sensing.....	16
2.3.3 Infrared-Based Sensing.....	18
2.3.4 Ultrasonic-Based Sensing	19
CHAPTER 3 Weld Pool Penetration Sensing System.....	22
3.1 The Imaging System	23
3.2 The GTAW Welding System.....	25
3.3 The Control System	27
CHAPTER 4 The advantages and the development of the new vision-based method.....	28
4.1 Advantages of the Current Vision-Based Method over Other Methods.....	28
4.1.1 A Two-Dimensional Method.....	28
4.1.2 A None Interruptive Method.....	29
4.1.3 A Noise Immune Method.....	30
4.1.4 A Fast method.....	31
4.2 The Development Process of the New Vision-Based Method.....	32

CHAPTER 5 Analysis of Three-Dimensional Weld Pool Oscillation Behaviors in GTAW	39
.....	39
5.1 Methods and principles	39
5.1.1 Sensing system	39
5.1.2 Characteristics for pool oscillation	40
5.2 Experimental procedure and method	41
5.3 Experimental results and discussion	43
5.3.1 Pool oscillation mode	43
5.3.2 Pool oscillation process for pulsed GTAW	50
5.3.3 Relationship between Amplitude and pulse current difference	59
5.3.4 Discussions	61
5.4 Summary	64
CHAPTER 6 Modeling of the Weld Pool Penetration Stages	66
6.1 The Mathematical model	66
6.1.1 Basic assumptions	68
6.1.2 Governing equations	68
6.1.3 Boundary conditions	69
6.1.4 Simulation parameters	72
6.2 Results and discussion	74
6.2.1 Numerical results	74
6.2.2 Experimental result	80
6.2.3 Discussions	82
6.3 Summary	84
CHAPTER 7 The Grayness Variations of the Laser Dot Images in the Penetration Stages	86
.....	86
7.1 Experiment Setup	87
7.2 Experiment Approaches	88
7.2.1 Observation of grayness variations and quantization of the pixel grayness	88
7.2.2 Quantization of the image grayness variations during welding	94
7.3 Ranges of Applicability	101
7.4 Summary	107

CHAPTER 8 Feed-Back Control Using Grayness Variations of the Laser Dot Image..	109
8.1 The simple feedback control system design	109
8.2 The Model-Predictive-Control feedback system design.....	118
8.2.1 Review of model predictive control.....	118
8.2.2 MPC model development	119
8.2.3 Experiment results using MPC feedback control.....	127
8.3 Summary	131
CHAPTER 9 Conclusions and Future Work	132
9.1 Conclusions.....	132
9.2 Future Work	133
REFERENCES	135
VITA.....	143

LIST OF TABLES

Table 5-1	Welding parameters.....	43
Table 6-1	Material properties of SUS 304 stainless steel	73
Table 6-2	Mathematical oscillation models for weld pools.....	83
Table 6-3	The weld pool oscillation frequency obtained by different researchers.....	83
Table 7-1	Welding parameters.....	87
Table 8-1	Calculated MPC model parameters	124

LIST OF FIGURES

Figure 1-1 Illustration of GTAW processes and weld penetration	2
Figure 1-2 Organization of the dissertation	5
Figure 2-1 Illustration three penetration stages in welding process GTAW	8
Figure 2-2 3D sensing system, captured image and the reconstructed 3-D weld pool	15
Figure 2-3 Schematic of the light rays reflected on the weld pool	15
Figure 2-4 Schematic for weld pool oscillation monitoring using voltage variation-based sensing.....	17
Figure 2-5 Schematic for online weld monitoring using infrared sensing.....	19
Figure 2-6 Schematic for penetration depth measurement using ultrasound.....	20
Figure 3-1 Schematic of the proposed weld pool penetration sensing system	23
Figure 3-2 The StockerYale's Lasiris SNF laser	24
Figure 3-3 Gazelle's GZL-CL-22C5M-C high speed camera	25
Figure 3-4 UR5 robotic arm for handling the arc torch.....	26
Figure 3-5 The GTAW welding system.....	26
Figure 4-1 The relationship between the weld pool oscillation and its penetration stages	35
Figure 4-2 Pixel grayness distribution with welding time	37
Figure 4-3 Pixel grayness variation with welding time	38
Figure 5-1 Sensing system for pool oscillation experiment.....	39
Figure 5-2 Characteristic principles for pool oscillation	41
Figure 5-3 Symmetrical oscillation at the center of pool under partial penetration	45
Figure 5-4 Symmetrical oscillation at the center of the pool under full penetration	47
Figure 5-5 Sloshing oscillation under critical penetration.....	49
Figure 5-6 Pool oscillation process under partial penetration ($I_p=80A$, $I_b=20A$, $f=25Hz$, $T_b=20ms$).....	53
Figure 5-7 Pool oscillation process under greater partial penetration ($I_p=80A$, $I_b=20A$, $f=25Hz$, $T_b=20ms$).....	54
Figure 5-8 Variation of weld pool oscillation surface under full penetration ($I_p=100A$, $I_b=20A$, $f=33.3Hz$, $T_b=10ms$)	57

Figure 5-9 Sloshing pool oscillation under critical penetration ($I_p=80A$, $I_b=20A$, $f=40Hz$, $T_b=20ms$).....	58
Figure 5-10 Variation of maximum and minimum amplitude for sloshing oscillation during 20ms base current time.....	59
Figure 5-11 Oscillation behavior of weld pools oscillation under different peak current ($I_b=20A$, $f=40Hz$, $T_b=5ms$).....	61
Figure 5-12 Pool dynamic behavior under DC-GTAW (welding current $I=60A$)	63
Figure 5-13 Forced pool oscillation under high frequency pulse current ($I_p=80A$, $I_b=20A$, $f=43.5Hz$, $T_b=3ms$).....	64
Figure 6-1 Pulse GTA welding current waveform and arc shape.....	67
Figure 6-2 Physical model of pulsed GTA welding molten pool	67
Figure 6-3 Grid and boundary condition	72
Figure 6-4 Thermal physical properties changed with temperature	73
Figure 6-5 Computed temperature field in the weld pool.....	75
Figure 6-6 Evolution curves of free surface height over time	76
Figure 6-7 The velocity field before full penetration.....	77
Figure 6-8 Bump change of free surface at different time.....	78
Figure 6-9 The velocity field after full penetration	79
Figure 6-10 Oscillation frequency versus time.....	80
Figure 6-11 Acquired reflected images.....	81
Figure 6-12 Oscillation mode.(a. weld pool is concave; b. weld pool is convex).....	81
Figure 6-13 Oscillation period at different time	82
Figure 6-14 Weld morphology at different time.....	82
Figure 6-15 The oscillation frequency comparison obtained by theory, experiment and simulation.....	84
Figure 7-1 Image grayness variations in the different penetration stages and the schematic showing the imaging process while the object is moving.....	89
Figure 7-2 Reflected dot images and their individual pixel's grayness value	93
Figure 7-3 Surface appearances of the finished welds with 1s, 2s and 3s welding time .	94
Figure 7-4 Captured images displaying the evolution of welding.....	96

Figure 7-5 Concavity of the weld pool surface in full penetration leads to convergence of the laser rays	97
Figure 7-6 Grayness variations with welding time with different number of pixels for averaging.....	99
Figure 7-7 Comparison of the grayness variations between different peak welding current.	106
Figure 8-1 Flowchart of the feedback control for stationary welding	111
Figure 8-2 Grayness variations with time using the simple feedback control.....	112
Figure 8-3 Weld beads comparison between controlled and non-controlled welding...	113
Figure 8-4 Flow chart of the feedback control in continuous welding	114
Figure 8-5 Variations of grayness over welding time in continuous welding	116
Figure 8-6 Explanation of the grayness variation behaviors in continuous welding.....	117
Figure 8-7 The bead surface appearance in continuous welding.....	117
Figure 8-8 Schematic of MPC	120
Figure 8-9 Grayness comparison between the simulated (model) data and the real data.	126
Figure 8-10 Grayness and input current variations with time using stationary welding and MPC feedback control.....	128
Figure 8-11 Surface appearance of the finished workpiece using stationary welding and MPC feedback control.	128
Figure 8-12 Grayness and input current variations with time using continuous welding and MPC feedback control.....	130
Figure 8-13 Surface appearance of the finished workpiece using continuous welding and MPC feedback control	131

CHAPTER 1 Introduction

1.1 Background

Gas Tungsten Arc Welding (GTAW), as shown in Figure 1-1, is a welding technique that uses non-consumable tungsten electrode to generate very high temperature arc for welding. Unlike the welding techniques such as Shielded Metal Arc Welding (SMAW) and Gas Metal Arc Welding (GMAW) that use consumable electrode, no weld droplets from the consumables will hit the weld pool and thus there is no pressure from the droplets that could impact the weld pool and that eventually adversely affect the quality of the finished weld. GTAW is commonly used in manual welding since it allows greater welder's control over the welding process than some of the other welding techniques. However, GTAW is more complex and difficult to master than the other competing welding techniques referred to above, it hasn't been of the widest use and is not as popular as GMAW. In order to be skillful in using GTAW, the welder has to coordinate his/her hands to feed a filler metal into the weld area and at the same time manipulate the welding torch. It is also important for him/her to maintain a short arc length while preventing contact between the electrode and the workpiece. Due to the above difficulties for a welder to use GTAW manually, it would greatly alleviate his/her responsibility in GTAW welding if a control system can be developed for GTAW that can automate the welding process, achieving what a skilled welder can do.[1]

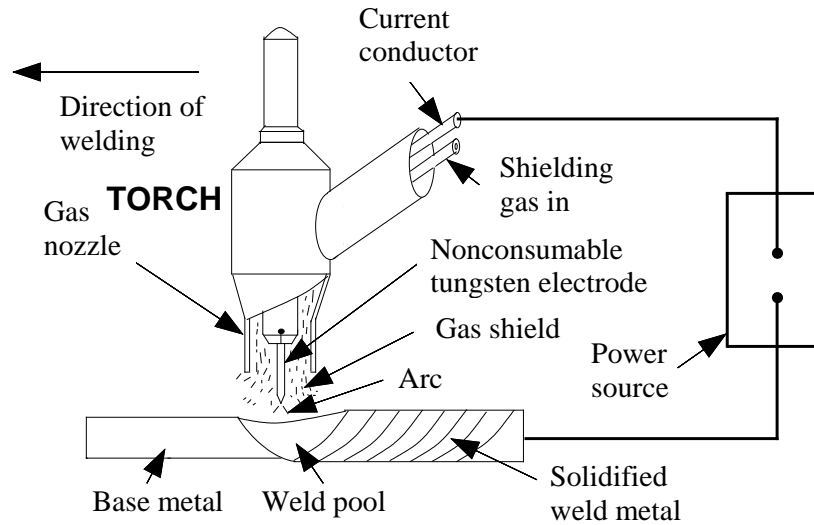


Figure 1-1 Illustration of GTAW processes and weld penetration

There are many factors that can make a finished weld inferior. These include the cleanliness of the workpiece, the quality of the filler metal, the welding current too high or too low, the arc length too long or too short, and insufficient penetration of the weld, etc. Some of these can be easily avoided, such as the cleanliness of the workpiece. However, others, such as full penetration, can be hard to detect during the welding process. This requires significant welding experience on a welder's side. Training a welder to be proficient in detecting full penetration takes countless hours. Besides, one welder's experience cannot be easily transferred to another unless about the same amount of training time has to be spent. On the other hand, if an automated detecting process can be developed, little training on the welders is needed (the training is not for gaining such experience but for using the equipment with the automated system) and the automated system can be installed on as much equipment as needed with little time. Thus, being able to automate the process in finding full penetration is thus of great importance.

1.2 Objectives and Approach

As discussed in Section 1.1, many factors can contribute to a bad weld and some are more easily controlled than others. Full penetration as one is hard to control, and it takes a lot of practice and time for a welder to gain the experience to detect it. Thus, being able to automate the process means great savings on time, effort and resources. Thus, the objective of this study is to find an effective and efficient technique to automatically detect full penetration without a welder's interference. This entails the need to study the weld pool extensively to gain useful information that can be utilized in the detection process.

As we know and has been confirmed by countless research work, the weld pool contains a wealth of information. As will be discussed in Chapter 2, section 2.1, researchers made use of the rich information to achieve different purposes. In this work, the weld pool's properties during partial and full penetrations are studied to identify the useful one to achieve the goal of the study, i.e., automatic control of welding process to reach full penetration.

Following previous studies in the same research group, this work also utilizes pulsed current to ensure appropriate conditions for taking good quality pictures of the weld pool during welding to analyze the evolution of the weld pool for later automatic control of the process. The high current during the first part of the period is for forming the weld pool, while the base (low) current in the second part is for taking pictures. A laser dot matrix is used for imaging.

In order to observe and understand the phenomena during the welding process, a series of experiments were first designed to capture the pool's behaviors under different penetration stages (partial penetration, critical penetration and full penetration) to correlate each stage with its associated pool oscillation mode, and to identify the key characteristics that separate partial penetration from full penetration.

To fully understand the process, a model is built for the dynamic weld pool, taking into consideration factors such as the forces acting on the pool (the arc pressure, the surface tension, electromagnetic force and buoyancy force) and heat flux that involves thermal conductivity, convection, radiation and evaporation. From the result of the model, the different penetration stage can be correlated with the different oscillation magnitude, oscillation frequencies, temperature field and velocity field.

From the model and the experiment observations, it is identified that weld pool has different shapes during partial penetration and full penetration. In addition, pool oscillation characteristics are also different. Based on these, the third part of this work captures the images of the laser dot matrix that is shone on the pool, processes the images to obtain grayness information of the reflected dot matrix, correlated the grayness with the stages of penetration (partial penetration and full penetration).

With good correlation between the grayness and the penetration stages, the fourth part of this work is to convert into control voltages the grayness of the images which carries information about the penetration stage. If the grayness is high, it indicates that the pool is only partially penetrated, and thus control voltage can be increased. The control voltage is further converted to current that passes through the torch. When the

grayness is decreased, it indicates that full penetration is reached, and depending on whether the welding is complete or more locations need to be welded, the current is cut off of the torch or the current is reduced, the workpiece is move to a new location and the process starts again.

1.3 Organization

In this dissertation, a control system is developed that achieves auto-detection of the full penetration of the weld pool, and subsequent control of the welding process in GTAW welding. The main research steps and results are discussed in the following chapters.

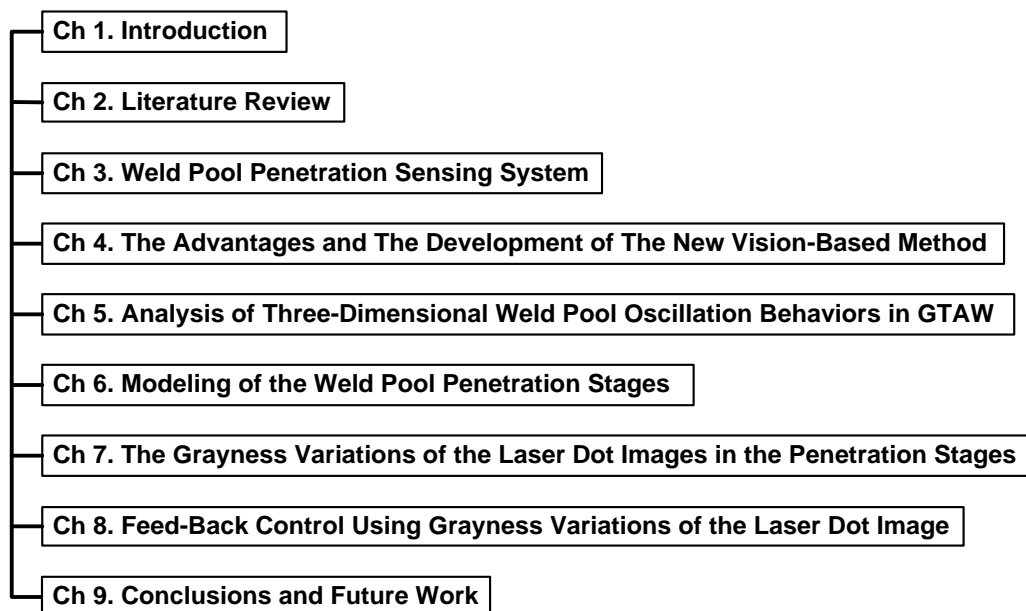


Figure 1-2 Organization of the dissertation

In Chapter 1 “Introduction”, the background knowledge about GTAW welding technique is discussed, including its advantages and disadvantages. This is followed by

outlining the objective and the approach of this research. This chapter concludes with a listing of the contents (chapters) of this dissertation.

In Chapter 2 “Literature Review”, related work is discussed. This encompasses work that studies weld pool surfaces, sensing techniques for detecting weld pool oscillation, as well as models to predict the motion of the pool, etc.

In Chapter 3 “Weld Pool Penetration Sensing System”, an innovative feedback control system is proposed, which encompasses the GTAW system, the image capturing system, and the welding current control system. The GTAW system performs the normal welding; the imaging system shines laser dot matrix lights on the weld pool and subsequently captures the reflected images; the feed-back control system receives the images from the image capturing system, calculates the grayness of the images and adjusts the control voltage based on the grayness values. The control voltage is applied to the GTAW system which is used to adjust the welding current passing through the torch.

In Chapter 4, “The Advantages and the Development of the New Vision-Based Method”, key features/advantages of the new method over the existing methods are highlighted, and the development process (evolution) of the new method is described.

In Chapter 5 “Analysis of Three-Dimensional Weld Pool Oscillation Behaviors in GTAW”, experiments are designed to capture the oscillation behaviors involved in the different stages of pool penetration, and to correlate the oscillation modes with partial, or critical, or full penetrations. It also identifies the amplitude and frequency of oscillation associated with the three penetration stages.

In Chapter 6 “Modeling of the Weld Pool Penetration Stages”, a mathematic model is constructed taking into account the effect of the forces such as arc pressure, the electromagnetic force, the surface tension, the buoyancy force, and the effect of heat transfer including convection, radiation and evaporation.

In Chapter 7 “The Grayness Variations of the Laser Dot Images in the Penetration Stages”, the images captured in the entire welding process are processed to obtain the grayness changes that reflect the stages of the weld pool penetration. First, the 20 brightest pixels in each image are averaged in the range 0-255 in grayness to get one grayness value. Next, for the images captured, the averaged grayness values of 5 contiguous images are averaged again. The resulting average grayness values are plotted against the welding time. The pull penetration can be identified by the grayness change on the plot.

In Chapter 8 “Feed-Back Control Using Grayness Variations of the Laser Dot Image”, a model-predictive control system is constructed, which is used as the feed-back control for adjusting the voltage applied to the GTAW. Experiment results show that the predictive control system utilizing image grayness variation is effective in automating GTAW welding to achieve full penetration.

In Chapter 9, “Conclusions and Future Work”, conclusions are drawn based on this study and future work is outlined and briefly discussed.

CHAPTER 2 Literature Review

The history of welding can be traced back to ancient times. The earliest known example of the welded tool in history was made more than 2000 years ago [2]. However, it is not until the late 19th century when arc welding technique was developed and patented. Over the years, arc welding has been improved by many people. Changes made to perfect the welding technique include selecting materials more suitable for electrode, shielding the arc and the weld area by applying non-reactive gases such as argon, etc.

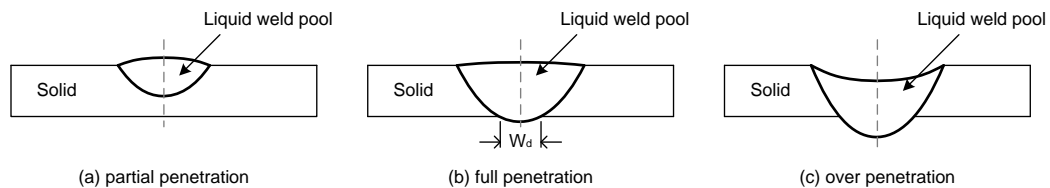


Figure 2-1 Illustration three penetration stages in welding process GTAW

GTAW was developed in the 1940s, but because it used inert gas which was expensive at the time, GTAW was not economical. Nowadays as technology advances, GTAW has seen improvement. The cost of inert gas is no longer a concern, while GTAW has a number of advantages including the high-quality welds it produces, the inexpensive power supplies it uses and the precise control of welding variables, etc. However, as explained in Chapter 1, GTAW is complex and not easy to master compared with other arc welding process, its usage is limited. As shown in Figure 2-1, there are three stages of weld pool penetration. Generally full penetration is desired since the weld produces has high qualities in terms of microstructure, appearance and strength. Partial penetration, though less desired, can be used in certain applications where weld quality is not of

paramount importance. Over penetration, however, should definitely be avoided. Weld produces with over penetration has damaged material properties. To detect the pool penetration stages, it is important to study the behaviors of the weld pool and identify the characteristics that are associated with each stage. Previous studies have shown that the weld pool oscillation can reveal information about pool penetration.

2.1 Weld Pool Oscillation Behaviors

Weld pool is where complex welding phenomena originate playing a fundamental role in determining resultant welds. It has been the subject of many recent studies [3-9]. Among the behaviors of weld pool, the oscillation has received attentions from welding researchers around the world [10-30] , since Kotecki et al. [10] first observed the phenomena of weld pool oscillation in 1972, and has been studied with different interests. Particular interests included its correlation with the weld penetration [20-25, 31-33] and its effect on the grain refinement and defect inhibition using methods like magnetic force stirring, ultrasound vibration [34, 35].

Kotecki et al. [10] studied full penetration weld pool behavior in the case of stationary GTA welding using high-speed motion pictures. They first brought attention to the research community for the oscillations phenomena of weld pool. They found that a relation exists between the natural frequency of the oscillation and diameter of the weld pool. A theoretical model for full penetration was proposed based on a stretched membrane theory. A similar relation was also derived by Zacksenhouse et al. [36] , who developed an analytical model for stationary full penetration pool and verified their mode by experiments.

Richardson et al [31] studied the oscillation frequency for a stationary GTA weld pool by arc voltage signal and arc light intensity signals, and found that the natural oscillation frequency is strongly dependent on the pool geometry and correlates well with the inverse of the square root of pool mass. They found that there exists a distinct boundary for pool oscillation frequency in the intermediate state between the partial and full penetration conditions [32]. They also later found that arc light is the better transducer to detect pool oscillation than arc voltage due to the volume effect of the plasma region [32]. In 1993, Yoo et al.[32] proposed three kinds of oscillation modes for full penetration welding, which are symmetric, sloshing, and mixed modes, respectively. However, these modes were proposed based on simulation without experimental verification.

Xiao et al. [20-22] studied the weld pool oscillation under stationary welding and low speed welding condition, and proposed two pool oscillation modes: oscillation mode for partial penetration and oscillation mode for full penetration under stationary welding conditions. Furthermore, in the low speed traveling welding, there even exists a third oscillation mode: asymmetrical oscillation in addition. They further developed and improved their corresponding theoretical model based on classical hydrodynamics to the liquid metal or a stretched membrane theory on the basis of Kotecki's research [10]. They found that the natural oscillation frequency of a partial penetration pool is considerably higher than the natural oscillation frequency of a full penetration and that an abrupt transition occurs between the partial and full penetration modes of the oscillation. In addition, they found that the oscillation frequency drops after the weld pool changes from partial to full penetration because of the change in the oscillation mode. This result is

fundamental by providing an effective method to distinguish the partial and full penetration.

Preliminary investigations by Nakata et al. showed the effect of current pulsation on the weld solidification structure of aluminum alloy [34]. They also explored the effect of low-frequency pulsed-GMAW welding on the grain refinement of weld metal and the improvement of solidification crack susceptibility in aluminum alloys [35]. They found that weld pool oscillation strongly affects grain refinement, and to some extent, also found that grain refinement has a beneficial effect on the solidification crack susceptibility of the weld metal.

2.2 Modeling of the Weld Pool

Modeling of the weld pool is another direction in studying the pool behaviors, which can reveal information that is not directly visible. Much research work has been carried out to build models that effectively explained observed phenomena and revealed new information.

Kotecki [10] studied the formation mechanism of welding wave during the solidification process of GTAW welding pool, and found that the main reason for the formation of the welding wave was the oscillation in the molten pool. A.S. Tarn [26] presented two models relating weld pool geometry parameters to frequency characteristics of pool motion. But the model did not consider the internal effects of electromagnetic stirring, thermal gradients, etc. Besides the model only predicted the gross motion of the molten region based upon boundary conditions imposed by the geometric constraints. Andersen [29] used pulsed current for inducing and monitoring a

weld pool to predict the state of penetration of the weld pool. Renwick [31, 37] studied the relationship between the weld pool size and the weld pool oscillation frequency, and proposed a method (by arc voltage) to measure the weld pool oscillation frequency. Den Ouden G [20, 22], using GTAW welding pool oscillation behavior, studied the penetration control of the welding process. By comparing the oscillation modes in both partial and full penetration, they proposed a sign of weld penetration. Chen et al.[38, 39], using narrowband filter system, obtained the front and back images of the molten pool in the base current period. By setting up the neural network model between the geometric parameters and the back penetration, the welding penetration control of the dumbbell shaped specimen was achieved. Zhao et al.[40] analyzed the molten pool resonance model in the aluminum alloy GTAW under different penetration states, established the corresponding resonance equation and got the intrinsic frequencies in both partial and full penetration based on experimental conditions. Shi Yu et al.[41] proposed an image processing algorithm with laser characteristics stripes, used Matlab software to write programs to obtain the corresponding oscillation waveform of the molten pool, and used the fast Fourier transform to extract the characteristic frequency oscillation of the molten pool.

Fan et al [42] presented a transient model to describe the heat transfer and fluid flow in a pulsed GTA welding arc. They discussed the steadiness of arc and the regulation between arc pressure and peak current. Traidia et al.[43] developed a finite element model to describe the coupling between the welding arc and the weld pool dynamic in pulsed GTA welding. He analyzed the weld pool's behavior when it was fully penetrated. Wu et al.[44, 45] studied the molten pool behavior in pulsed GTA welding using

numerical simulation method, analyzed the effect of pulse current on the pool flow field, temperature field and pool shape, and investigated the dynamic process of surface deformation in molten pool. An improved method was proposed for the issues existing in the fully penetrated weld pool [46]. It solved the problem of rigidity and reliability in the calculation of the surface deformation of the molten pool in the existing literature [47-50]. When compared to the experimental results, the calculation accuracy was improved. A three-dimensional model of the pulsed laser welding pool based on VOF method was established by Cho et al. [19]. The behavior of the molten pool oscillation under the action of a pulsed laser and the oscillation behavior of the molten pool in the end of the welding process were studied. Karunakaran et al. [51] compared aluminum alloy joints' temperature distribution and weld bead profiles welded by direct-current and pulsed GTA welding. He analyzed the effects of pulsed current welding on tensile properties, hard profiles, microstructural features and residual stress distribution of aluminum alloy joints.

2.3 Weld Pool Sensing Techniques

The previous two sections discussed the weld pool behaviors and the building of the weld pool models to gain knowledge of the weld pool behaviors. However, to acquire weld pool information, the first step is to set up a sensing system to detect the weld pool behaviors.

As discussed before, in order to achieve full penetration, it is important to identify the weld pool behaviors that indicate full penetration. A skilled welder can detect full penetration by observing the surface appearance and change of the weld pool. This requires a lot of training and practicing on the welder and is not easily transferrable as

explained in Chapter 1. To address the issue, a lot of research has been conducted to find an effective method that can automate the detection of full penetration. Being able to detect full penetration requires the ability to sense the difference between partial and full penetration. For a welder, this is done by visually observing the change. But for an automated system, being able to “see” the change can be achieved in many different ways, as will be discussed in the following sections.

Over the years, many different sensing techniques have been developed to detect the weld pool penetration stages. These include vision-based sensing, voltage variation sensing, red infrared light sensing, etc. Of these techniques, vision-based sensing is the most directly observable and may be studied the most.

2.3.1 Vision-based Sensing Technique

In order for a system to detect visually the changes on the pool surface, it first has to “see” the images. To know that there are changes, it has to process the images, do comparisons and make decisions. In order to coordinate the different functional blocks of the system, in addition to a computer, it also needs I/O devices, computer networks and the welding equipment. Vision-based sensing technique is an interdisciplinary study that employs knowledge in computer science, electrical engineering and manufacturing. Generally speaking, vision-based sensing techniques can be categorized into two classes: two-dimensional sensing and three-dimensional sensing. Both sensing techniques make use of camera to take images of the weld pool surface. The difference is that, in three-dimension sensing, 3-D weld pool surface is reconstructed out of the 2-D images. Two-

dimensional technique makes use of the captured images to get the pool's 2-D information, such as length and width).

Figure 2-2 [52] depicts the three-dimensional sensing system developed most recently at University of Kentucky.

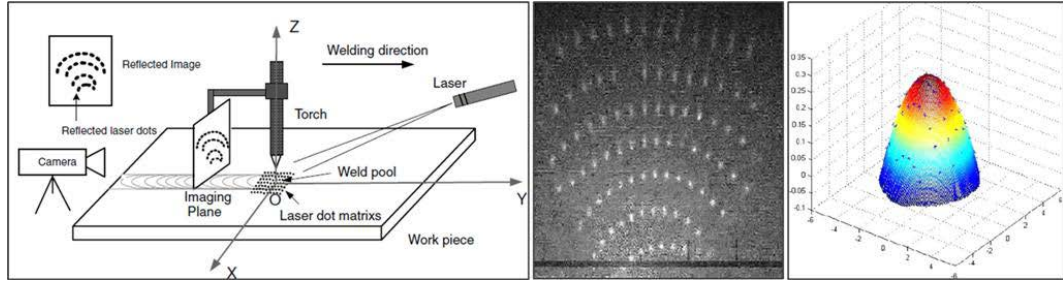


Figure 2-2 3D sensing system, captured image and the reconstructed 3-D weld pool

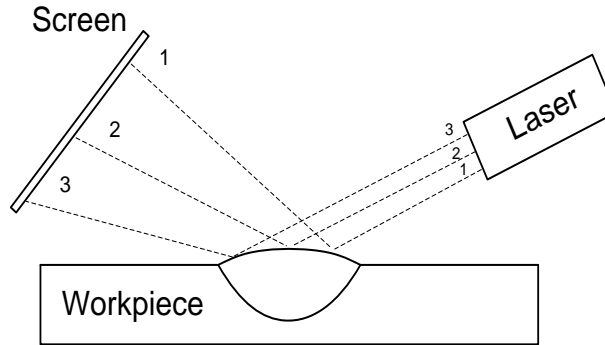


Figure 2-3 Schematic of the light rays reflected on the weld pool

In this system, a laser continuously shines dot matrix light on the weld pool surface. The light is reflected by the weld pool surface and projected on an image plane, which is subsequently captured by a high-speed camera. The captured image is shown in the middle of Figure 2-2. Because the weld pool is as smooth as a mirror, the reflection is

specular and thus the image captured on the image plane reflects the original shape of the light, i.e. dot light. However, since the pool surface has curvature due to natural oscillation, the image has dot arrays that are curved unlike the dot matrix sent out from the laser. As shown in Figure 2-3, the light ray that hit the top of the weld pool is reflected in the middle of the image plane (light ray 2), the ray on the lower right part of the pool is reflected on the top part (light ray 1) while the ray on the lower left part of the pool is reflected on the bottom part (light ray 3) of the image plane. By utilizing the spatial information between the imaged dot light and the weld pool locations, 3-D weld pool can be reconstructed, and this is shown on the right of Figure 2-2. The 3-D weld pool image is subsequently used for controlling the welding process. This is proved to be an effective method. However, there are some disadvantages in this method.

First of all, in order to obtain clear dot-light images, special care has to be taken to reduce the weld pool oscillation as much as possible. In order to achieve this, torch current needs to be kept constant to allow as little disturbance on the weld pool surface as possible. In addition, torch current cannot be too high since too high current will create very bright arc light which interferes with image capturing. Another disadvantage of this method is that the 3-D image reconstruction process is very complex and is sensitive to slight changes in the imaged light dots. Since it is complex and involves many steps, it takes time to rebuild the 3-D image and thus real-time control is not very effective.

2.3.2 Voltage Variation-Based Sensing

Xiao et. al. [22] developed the voltage variation-based sensing technique in their study of weld pool oscillation in mild steel. Figure 2-4[22] is a schematic illustration of

their experiment setup. Unlike the vision-based technique discussed in section 2.1.1, their method made use of weld pool oscillation and then detected arc voltage variations which they correlated with oscillation frequency. In their study, they intentionally created pool oscillation by applying pulsed current on the torch. The current switch caused change in the arc pressure that was applied on the weld pool. This change led to oscillation of the pool. It was found that the pool oscillated at different frequencies in partial penetration and in full penetration. The variation in pool oscillation caused variation in arc voltage. Thus, by measuring the arc voltage variations, they could calculate oscillation frequency and subsequently find out if the pool is partially or fully penetrated.

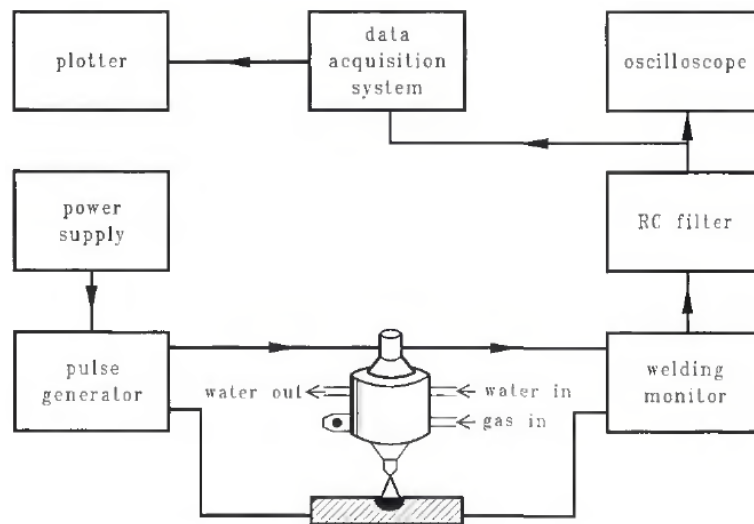


Figure 2-4 Schematic for weld pool oscillation monitoring using voltage variation-based sensing

This method is simple and easy to implement. However, since welding environment is full of noisy sources that could interfere with the arc voltage, detecting arc voltage variations that are solely due to the effect of oscillation is challenging. For example, high electromagnetic forces created during welding as a side effect can also lead to changes in

the arc voltage variation. On the other hand, the changes in arc voltage due to oscillation frequency change are small and can be easily overwhelmed by the effect of noisy sources.

2.3.3 Infrared-Based Sensing

Infrared sensing is based on the thermal properties of the weld pool. Welding is fundamentally a thermal processing method. In an ideal welding condition, the surface temperature distributions of the weld pool show a regular and repeatable pattern. Any disturbance to the ideal condition should result in discernible change in the thermal profile. Thus, using infrared thermal imaging to capture the thermal profile variations seems a natural choice for sensing the weld pool penetration.

Chin et. al.[53] used infrared thermal imaging to study weld pool depth penetration and to estimate bead width. Figure 2-5[53] is the experiment setup. In their study, they used a focal plane array-based thermal imaging system to detect the infrared radiation that characterized the surface temperature distributions of the weld pool. In the imaging system, a lens is used to focus the thermal radiation onto an infrared detector. The detector is very sensitive and can measure a wide range of temperatures (253K to 1773K) with high accuracy (error is within +/-2%). From the capture temperature data, they constructed thermal profiles of the different penetration depths and identified the differences in the profiles of the different penetration depth.

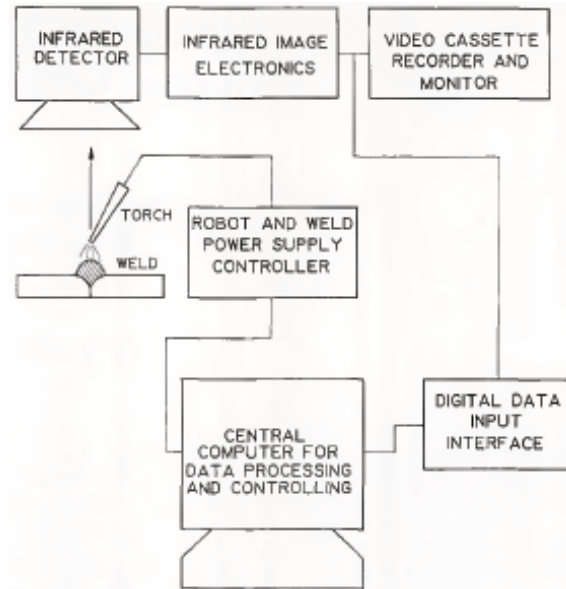


Figure 2-5 Schematic for online weld monitoring using infrared sensing

The advantages of the infrared method are that it is convenient and economical. However, temperature profiles cannot be directly associated with the pool's topographical changes during welding, and thus it is not visually friendly. In addition, the temperature profile is essentially two-dimensional: the concavity or convexity of the pool in oscillation cannot be identified in the temperature profiles.

2.3.4 Ultrasonic-Based Sensing

Ultrasonic sensing is another area of study, especially in the 1980s and 1990s. Early ultrasonic sensing is on-contact and destructive to the workpiece because it used piezoelectric transducers to generate the ultrasound and the transducers had to be placed on either side of the weld pool. Later on, improvement was made to use laser to generate ultrasound. Since the laser was placed a distance away from the workpiece, it is non-contact and non-destructive. Ume et. al. [54] did extensive studies on using ultrasonic

sensing techniques to measure weld pool penetration. Figure 2-6 [54] shows their experimental setup for automated weld pool sensing using ultrasound.

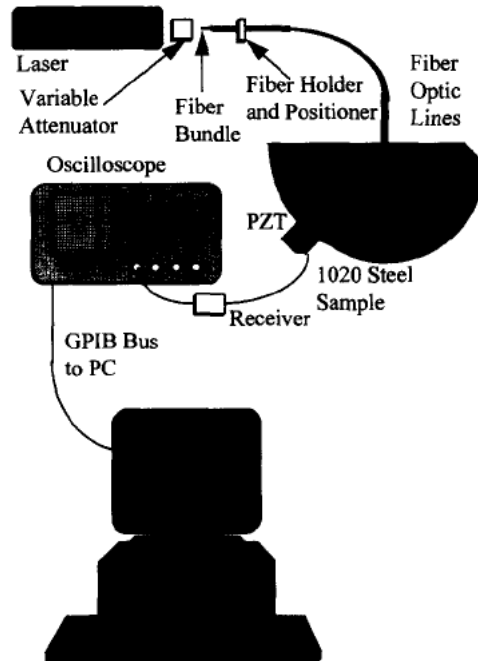


Figure 2-6 Schematic for penetration depth measurement using ultrasound

In their study, they used laser to generate light. The light passed through the fiber optic array where ultrasound was generated. The ultrasound then traveled through the workpiece and was received by a transducer called Electro-Magnetic Acoustic Transducer (EMAT). They collected many transducer signals and averaged them to reduce noise. The averaged signals were sent to a special purpose program which calculated useful information such as the time of flight of the diffracted ultrasound. The pool penetration is approximately proportional to the time of flight. Thus, they could obtain the pool penetration depth information.

The advantages of ultrasonic-based sensing are that it is applicable on all materials and could detect very small irregularities[55]. However, different thermal gradients

within the heat affected zone (HAZ) in the weld pool could reflect ultrasound waves and thus limit the quality and accuracy of sensing.

CHAPTER 3 Weld Pool Penetration Sensing System

In this dissertation research, a pulsed laser-enhanced GMAW process is developed as the second part of the project. In this process, the metal transfer process is monitored in real-time. When the droplet enters the location the laser aims at, a laser pulse is applied. To reduce the need for laser energy to a level achievable using our existing spot laser, the current is pulsed simultaneously with the laser. To make sure the pulses of the laser and current are correctly synchronized, the monitoring of the metal transfer process is done using high speed imaging system and real-time image processing algorithm.

As discussed in the previous chapter, different sensing systems have been developed to capture the weld pool's structures in the penetration stages. This proposed system in this study is an extension of the vision-based sensing discussed in section 2.3.1. However, in the proposed systems, no construction of 3-D weld pool structure is constructed. Instead, it uses the pixel grayness to identify the stages of pool penetration. This proves to be both simple and robust, as will be explained in detail in Chapter 6. Figure 3-1 is the top-level schematic of the entire system. It includes the imaging system, the GTAW welding system and the control system.

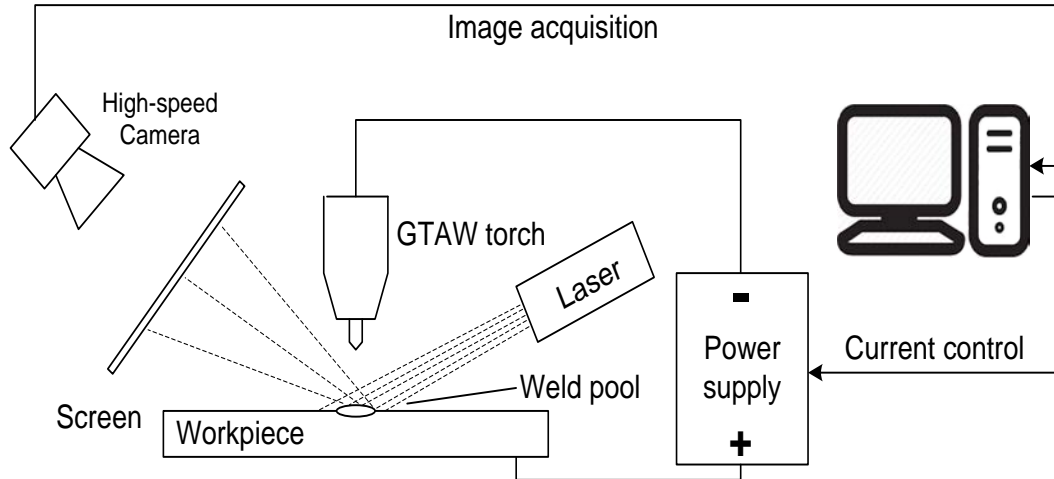


Figure 3-1 Schematic of the proposed weld pool penetration sensing system

3.1 The Imaging System

The imaging system is composed of a laser, a camera and an imaging plane (also called “screen” in Figure 3-1). The laser used is a 20mW StockerYale’s Lasiris SNF laser. Figure 3-2 shows the laser with different optical heads which provides different laser patterns, e.g. dot matrix, lines, etc. The SNF laser is small and has low power. The different optical heads allow different applications requirements; the small size makes it easy to handle; and the low power output (20 mW used in this research) makes it safe to use. Choosing laser instead of normal light source is due to the fact that the laser provides highly concentrated monochromatic light source. Since the arc light spans a wide range of wavelengths and laser light has narrow wavelength, we only need to use a filter to let the light that is in the laser’s wavelength range to pass. By this, the noise from the arc light is filtered out. The concentrated laser light also makes it easy to observe the image. The laser is aligned 30° with respect to the workpiece, and is placed 50 mm away from

the torch. A 19x19 dot matrix structured light pattern is generated for studying the weld pool penetration in this work.



Figure 3-2 The StockerYale's Lasiris SNF laser

Another component of the imaging system is the image screen. It is composed of a piece of white grid paper attached to a glass substrate. The use of grid paper allows easy identification of the relative locations of the imaged laser dots. The image plane is also placed 50mm away from the torch.

The third component of the imaging system is the high-speed camera. In order to capture the slightest change in the pool, the camera has to be able to take pictures in mini-second range. For this, Gazelle's high frame rates, high resolution camera is used. Figure 3-3 shows the front and back of the camera. The camera with the original manufacturer's setup has a speed of 280 frames/second. This is still not fast enough in our application. Thus, in order to make this camera applicable in this study, effort was made to change the setup of the camera. Since in this study the weld pool surface is small, the default image size of the camera can be significantly reduced. This increases the shutter speed. With

this change, the camera can take 1 picture in 1 mini-second. To filter out the arc light, a band pass filter centered at 685 nm and with 20nm bandwidth is installed on the camera.



Figure 3-3 Gazelle's GZL-CL-22C5M-C high speed camera

3.2 The GTAW Welding System

The welding system includes the torch, the robotic arm, the power supply, the workpiece and the inert gas supply. The robotic arm is not shown in Figure 3-1. The gas supply is not visible; however, there is a gas pipe inside the torch along with the power supply cable. During welding, the gas flowing out from the torch covers the entire pool surface, and thus ensures that the surface will not be oxidized. And the gas flowing can cool the tungsten electrode at the same time. The robotic arm is UR5 from Universal Robots. Figure 3-4 shows an image of the robotic arm. It is lightweight, flexible and easy to program.



Figure 3-4 UR5 robotic arm for handling the arc torch

Figure 3.5 includes most of the welding system components. The torch is connected to the robotic arm using a fixture; the power supply is connected to the torch through a cable; and the workpiece is placed flat on the welding workbench, aligned perpendicular to the torch. The power supply is a Miller PM200 DC power supply with a maximum output current of 200A.

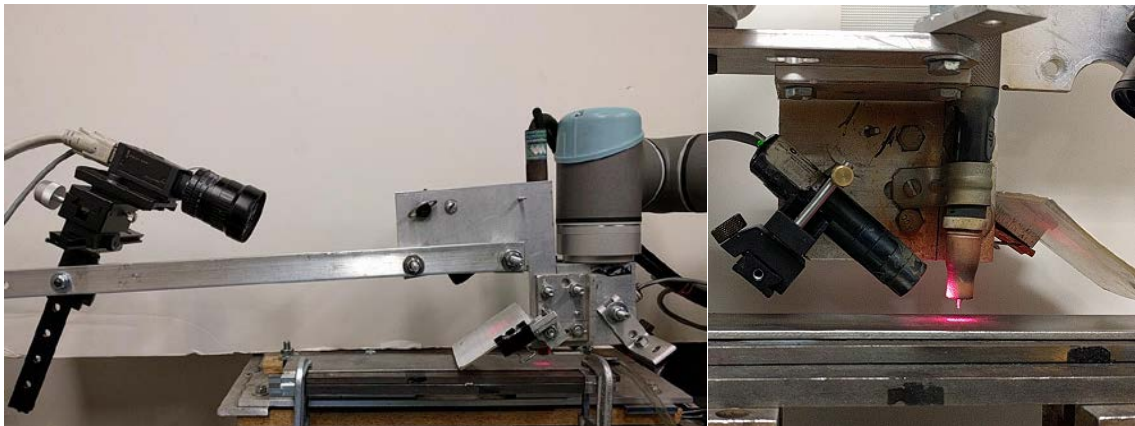


Figure 3-5 The GTAW welding system

3.3 The Control System

The control system includes a computer and NI PCI-6229 data acquisition device which was installed in the computer. The computer collects real-time images from the camera, performs image processing online, and based on the processed grayness results of the images, determines whether welding should continue or is complete, and subsequently send feedback signal to change the torch current through the NI DAQ. In addition, for continuous welding which involves welding on continuous locations of the workpiece, the computer controls the movement of the robotic arm which operates the torch to change locations. The control system is the focus of this research.

CHAPTER 4 The advantages and the development of the new vision-based method

The weld pool penetration has long been identified to have a close relationship with the pool's oscillation characteristics. Generally speaking, when the pool is small and is only partially penetrated, its oscillation frequency is high but the amplitude is small. When the pool is fully penetrated, its oscillation frequency reduces while the amplitude increases. The small amplitude at partial penetration may be explained by the fact that damping is large due to the solid bottom of the weld pool. This solid bottom obstructs the further movement of the pool in that direction and the pool then starts moving in the other direction. The high frequency may be related to the fact that the pool is small and thus light. Since it is light, it can move faster. The low frequency and large amplitude at full penetration can be explained likewise.

4.1 Advantages of the Current Vision-Based Method over Other Methods

The newly developed method is superior to many other methods in a few important aspects, as will be discussed below.

4.1.1 A Two-Dimensional Method

The pool oscillation information has been utilized by many researchers in studying the penetration status. As discussed in Chapter 2, many methods have been developed to detect partial vs. full penetration. However, most of the methods are considered one-dimensional. For example, the voltage detection method measures the arc voltage

changes due to pull oscillation. Voltage itself is only one quantity, and thus one-dimensional. Many other methods, although not necessarily based on pool oscillations, are one-dimensional too, e.g. the infrared-based method, the ultrasonic based method. One-dimensional methods are, generally speaking, simple; however, they cannot reveal enough information about the penetration status. To overcome the inadequacy of the one-dimensional method, many two-dimensional methods have also been proposed. The vision-based method is a two-dimensional method that captures the pool's surface information in the penetration stages. Based on the surface characteristics of the pool, penetration status can be deduced.

The method developed in this research is a two-dimensional method, unlike many others discussed earlier. Thus, the current method can reveal more information about the pool's penetration status. As will be discussed in Chapter 7 and 8, by using this method, we can not only identify the characteristics of the surface images associated with each penetration stage, but can also quantize this information using the pixel grayness values.

4.1.2 A None Interruptive Method

Other methods, such as the voltage detection method, are interruptive. In the voltage detection method, a separate narrow pulsed current is applied on the torch in addition to the based current. The base current is where the welding process occurs, while the narrow current is applied solely for the purpose of indirectly measuring the penetration status. When it is time to measure the penetration status, the pulsed current is applied for a short period of time to induce the pool's oscillation. After that, it measures the arc voltage variations due to the oscillation. From the measured results, the voltage variation

frequency can be calculated. As was found in the voltage detection study, the frequencies due to partial or full penetrations are different. Based on this information, the pool's penetration stages can be identified. Although this method can be effective at characterizing the pool's penetration stages, the separately added measuring current interferes with the normal welding process and it complicates the welding process.

In the new method developed in this study, the measurement procedure is embedded in the welding process by utilizing a pulsed arc current. The peak current is for welding, while the base current is used for measurement, i.e. taking pictures of the weld pool surface. This welding current fulfils the dual purposes of welding and measuring. It is non-interruptive since it does not use a separate current or voltage for detecting the pool penetration.

In addition, the currently developed measurement method is vision-based, which means it uses light. Since light and voltage/current do not interfere, there is no side effect in using the vision-based method. On the other hand, voltage-based method detects arc voltage variations due to the penetration frequency changes, this method could potentially interfere with the normal welding process.

4.1.3 A Noise Immune Method

Many of the methods discussed in Chapter 2 are not robust. They are sensitive to environmental variations. In the voltage-based method, the voltage variation is like a tiny perturbation superimposed on the based arc voltage. On the other hand, the welding environment is noisy; any other disturbances can lead to the arc voltage variations. This makes the method not very accurate.

In the infrared-base method, temperature field gradient is the key parameter used in detecting partial penetration vs. full penetration. However, temperature field gradient is not very sensitive in characterizing the pool's status, especially at the edge of the pool where the solid and liquid parts meet.

By comparison, the newly developed method is very sensitive to the pool's surface changes, which is desired. As can be seen in the images taken during the welding process, even a haphazard glance at them can tell that the images are different, i.e. they reveals the evolution of the welding process. In early stages where the pool is only partially penetrated, the images show clear and bright laser dots (laser light is used for imaging in the study). When the pool is at critical penetration, the imaged laser dots become fuzzy. And the fuzziness increases as the pool continues into full penetration. When full penetration is reached, sometimes a very large and clear dot will form, and sometimes the whole image looks rather dim. To further quantize the penetration stages with the changes of the images, the pixel grayness information can be easily calculated. And it is found that each stage has distinctly different grayness value.

4.1.4 A Fast method

The other methods can be slow. For example, in the voltage-based method [20], it makes no effort to change the speed of welding. In addition, it has to apply a pulsed current regularly just to induce oscillation for measuring the penetration status, which makes the process even slower. The applied pulsed current has a period of 40ms. And this does not taking into account the time spent in measuring. Suppose that only one pulse is enough for generating the oscillation, there is still the step needed to measure the

oscillation. If measurement takes about the same amount of time (40ms), one full measurement can take up to 80ms.

The new method, on the other hand, has the measuring step naturally blended into the welding process. Its measuring step occurs in the base current period which is only 3ms. And the 3ms is the only required time for measuring weld pool image. By comparison, we can see that the new method is more than 20 times faster in terms of measuring pool penetration status. Besides, the pulsed welding current can be easily increased to make the welding process faster.

4.2 The Development Process of the New Vision-Based Method

The new method developed in this study is an extension of the previous vision-based method discussed in Chapter 2. However, in that method, the purpose is to reconstruct the 3-D weld pool structure from the captured images of the laser dot matrix that is reflected by the weld pool. Hence, this method will be called 3-D vision-based method. Unlike many other methods discussed in Chapter 2 and the method in this study, the 3-D vision-based method does not utilize the weld pool oscillation information to recover the weld pool penetration status. On the other hand, in order to take clear pictures, it tries to avoid the weld pool oscillation as much as possible. Thus, it uses constant and relatively low welding current for the welding process when taking pictures. The low current can suppress the natural oscillation of the weld pool, and the constant current is to further avoid the oscillation due to current changes. As we know any disturbances such as pulsed current can cause pool oscillations. The problem in this method is that low current is not very practical in real production welding process. In addition, this method is sensitive to

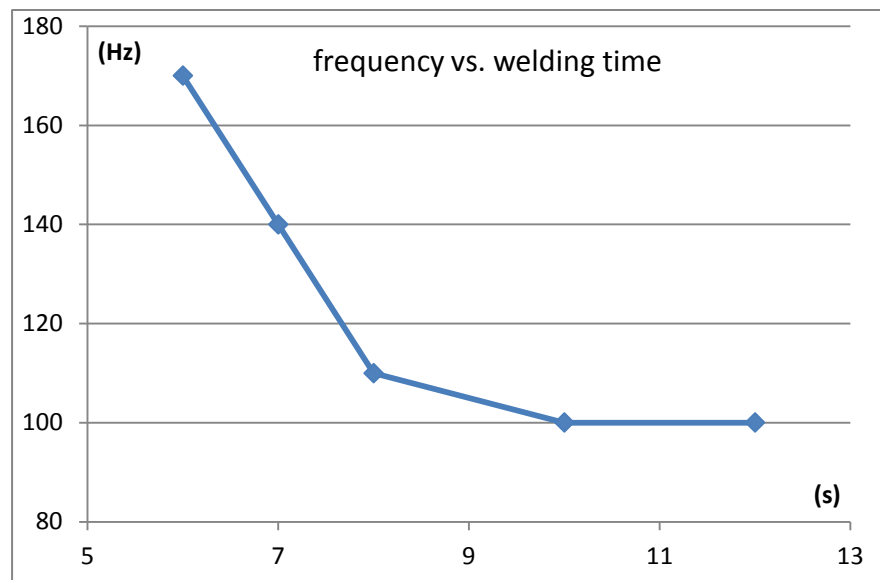
any noises (disturbances) in the welding environment. Noises can lead to oscillation, which makes images unclear.

In order to avoid impractical low current in the 3-D vision-based method, the newly developed method uses higher current. However, high current causes strong arc light which interferes with image taking. Thus, pulsed current is used, as discussed in section 4.1.

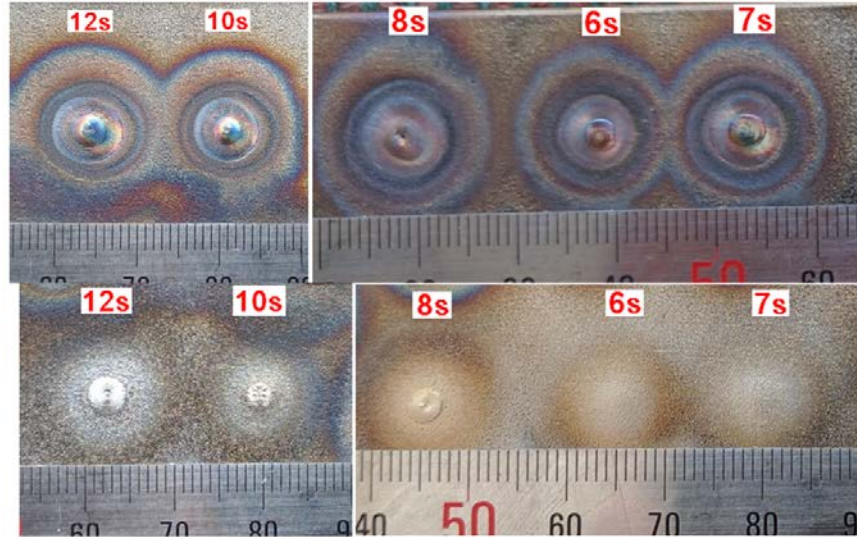
In the new method, although the purpose of using pulsed current is for taking images, it has the added benefit that current changes induce the pool oscillation which is desired.

In the early development stages, the focus was on the pool oscillation frequency. The intention was to find the relationship between the frequency and the pool penetration stage, and use this information to dynamically control the welding process. In order to achieve this, the base current period was set to relatively long, with the maximum of 50ms being used. Figure 4-1 shows the frequency variations with the welding time. The peak current is 150A and the base current is 20A, and the workpiece is a 1/8" 304 stainless steel flat bar. The peak current time and base current time are both 100ms. As can be seen from Figure 4-1(b), the pool is only partially penetrated with welding time of 6s and 7s, but is fully penetrated with welding time reaches 8s, 10s and 12s. Correspondingly, the pool oscillation frequency of 100Hz or 110Hz at full penetration is lower than those at partial penetrations 170Hz and 140Hz. From the frequency vs. time plot, it can be seen that when full penetration is reached, the oscillation frequency changes only slightly.

The frequency vs. the pool penetration relationship, though useful, cannot be used for dynamic welding process control. The main issue was that in order to construct the oscillation frequency, many pictures have to be taken, which takes a long time. In the result shown in Figure 4-1(a), the highest frequency is 170Hz, which is equivalent to a period of 6ms, or 6 pictures at 1 frame/ms shutter speed. In addition, the time taken by sending one picture to computer and that by processing the picture by the computer is about between 15ms and 20ms. The total time to process a whole period is thus about between 90ms and 120ms. This is not only slow, but the pool also has evolved. Thus, this method cannot be used for real-time control. A new method has to be developed.



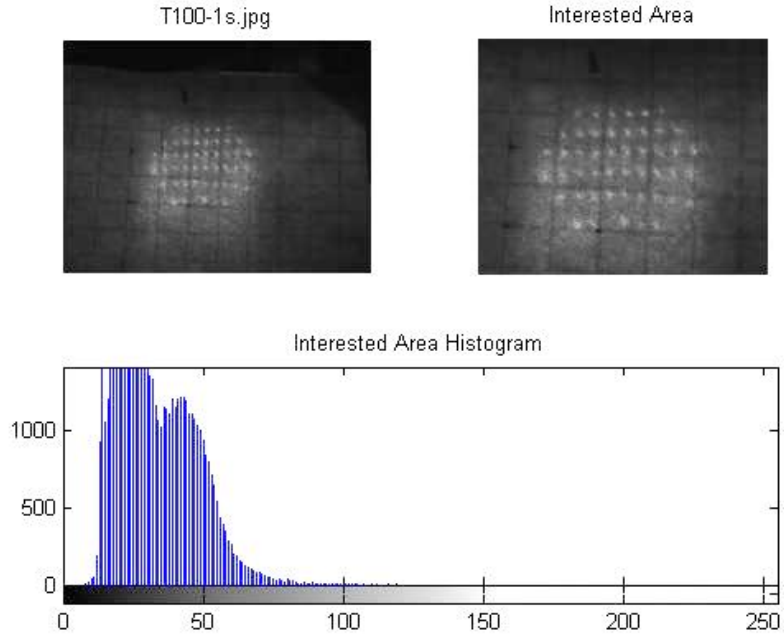
(a) Weld pool oscillation frequency vs. welding time



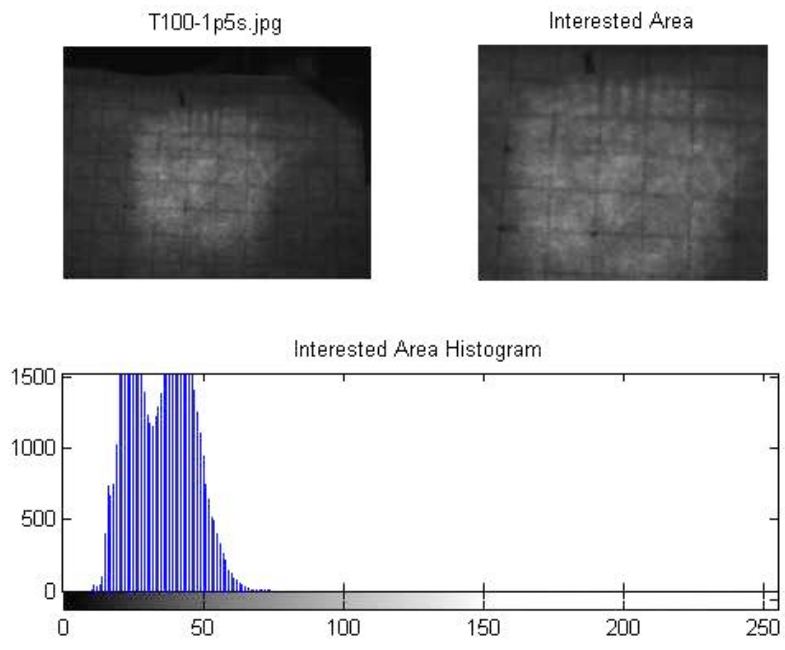
(b) Surface appearances of the weld beads with the welding times

Figure 4-1 The relationship between the weld pool oscillation and its penetration stages

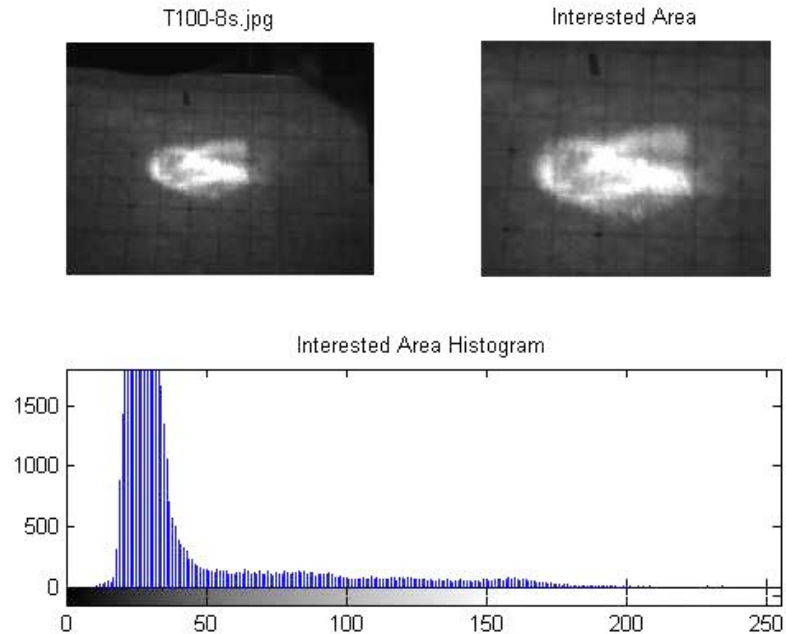
While working on characterizing the pool oscillation frequency, it was discovered that the images taken during the welding process had an evolution pattern. It started with few but bright and clear laser dot images. As time went on, more and more dots were formed until the dots together occupied most of the spaces in a circle. The circle is due to the rounded shape of the weld pool. As welding continued, no more dots images were formed, and those that were already there started to become fuzzy. The fuzziness increased until either one or two very large and clear dots formed or the whole picture looked dim. This is repeatable for every welding process. Figure 4-2 plots the grayness values of the individual pixels. The x-axis represents the grayness in the range of 0 to 255, and the y-axis represents the number of pixels. The peak welding current is 100A and the base current is 20A. The workpiece is a 2mm 304 stainless steel sheet.



(a) Welding time of 1s



(b) Welding time of 1.5s



(c) Welding time of 8s

Figure 4-2 Pixel grayness distribution with welding time

As can be seen in Figure 4-2, in all three welding time, there are more pixels that are in the low grayness value range. This is understandable since there is only limited number of laser dot images, but there is more space that is black. Apart from the common features in the three histograms, in (a) there are more pixels in the larger grayness range than in (b), as can be seen in the grayness between 60 and 120. This difference is also reflected in the difference in the two pictures: the picture in (a) is brighter and clearer than the one in (b). Unlike Figure 4-2 (a) and (b), (c) has many more pixels in the higher grayness range, but fewer pixels in the lower range. We can even see some pixels that have grayness values above 200. This big difference can be clearly seen in the picture too.

The histogram is another indication that the weld pool evolution has a pattern. However, it cannot be used for real-time welding control either, since building the

histograms is not fast. In addition, there is not a decisive division in the histograms that separate the partial penetration stage from the full penetration stage. However, plotting histogram using grayness values points a new and promising direction in finding a real-time control method, i.e. utilizing grayness values.

Figure 4-3 shows the pixel grayness variations with welding time. In this plot, the first 20 pixels with the greatest grayness values are selected and their grayness values are averaged to represent the picture's grayness value. This graph clearly shows a first peak that corresponds to the condition when there are many dot images and they are mostly clear and bright. The subsequent grayness decrease corresponds to the increase in the fuzziness and the reduction in brightness of the imaged dots. The next few peaks are associated with the full penetration stages where extremely large and bright dot is formed. Identification of the first peak and subsequent decrease in grayness can be done in online, which means that grayness information processing can be used in real-time welding process control. More details will be discussed in Chapters 7 and 8.

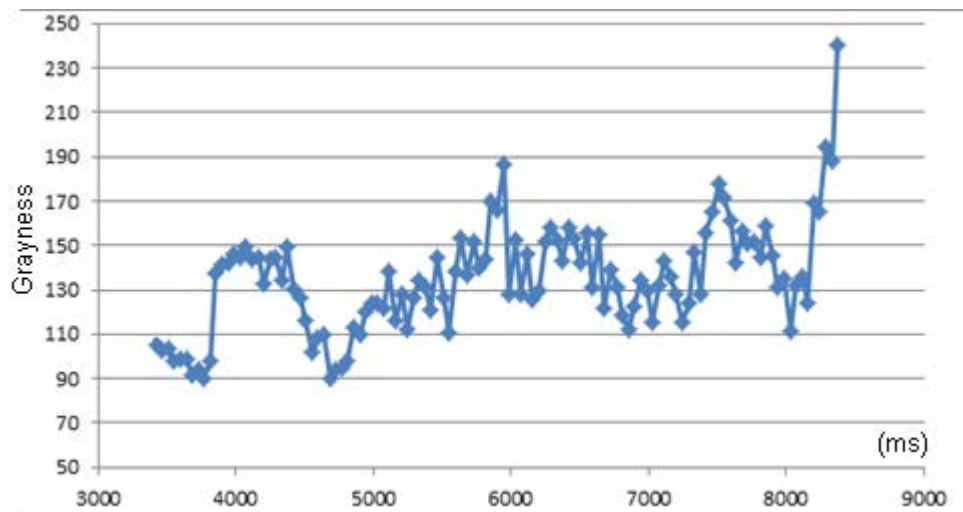


Figure 4-3 Pixel grayness variation with welding time

CHAPTER 5 Analysis of Three-Dimensional Weld Pool

Oscillation Behaviors in GTAW

This chapter focuses on obtaining extensive weld pool oscillation behaviors and detailed analysis of the behaviors in order to fully understand the phenomena. The gained knowledge will help in building up a control system that can achieve the ideal welding condition, i.e. full penetration.

5.1 Methods and principles

5.1.1 Sensing system

The weld pool surface sensing system is shown in Figure 5-1 [56]. This is similar to Figure 3-1 in Chapter 3, but without the feedback control system. This setup is also similar to Figure 2-2 in Chapter 2, section 2.3.1 with the difference that the torch current is pulsed. As discussed before, pulsed current is used both to induce oscillation in the weld pool and to make it easy to capture images.

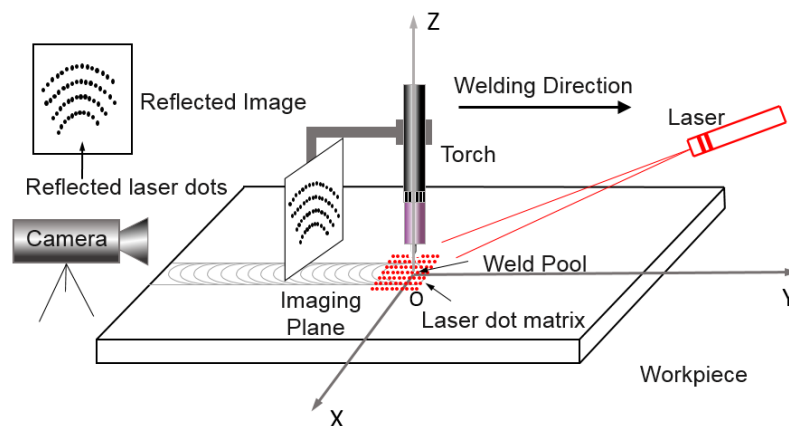


Figure 5-1 Sensing system for pool oscillation experiment

5.1.2 Characteristics for pool oscillation

During the peak current period, the center of the weld pool surface is depressed by the arc jet pressure. During the base current period, the balance among the arc jet pressure, surface tension, and gravity, which are exerted on the weld pool, is broken after the arc plasma pressure is suddenly reduced. As such, the surface tension pulls the pool back toward a new equilibrium position, inducing an oscillation to the pool. On the other hand, the molten specular weld pool surface can reflect, like a mirror, most of the incidental laser light. As a result, the reflected laser dot matrix can respond simultaneously to the motion of the weld pool surface to reflect its oscillation.

When the laser dots matrix project onto the weld pool surface, the laser dots are reflected onto the imaging plane. The reflected dots on the imaging plane have a different mapping relationship corresponding to the different shapes of the weld pool surface [52, 56]: convex, concave and combination. Figure 5-2. Figure 5-2 (1a-4a) are, respectively, the scheme of mapping relationship corresponding to Figure 5-2 (1b-4b), which are the reflected laser dot matrix images of the different weld pool surfaces. The figures show that the adjacent laser dot distance at the center of weld pool changes with the convex or concave state of the weld pool surface. According to the mapping relationship between the projected laser dots and reflected laser dots, the weld pool surface of Figure 5-2(1b) is moderately convex; the weld pool surface of Figure 5-2(2b) is more convex because the distance of reflected laser dots in the center of weld pool is larger than that of Figure 5-2 (1b); the weld pool surface of Figure 5-2 (3b) is moderately concave because the distance of reflected laser dots in the center of weld pool is close; and in Figure 5-2 (4b), the

distance of reflected laser dots in the center of weld pool is closer, showing that the weld pool surface is deeper than that of Figure 5-2 (3b). If the weld pool surface were much deeper downward, the reflected laser dots on the imaging plane would probably converge to a point or even cross up and down. Therefore the amplitude of the change in the pixel distance between two adjacent laser dots in the center of weld pool can represent the amplitude of the weld pool oscillation.

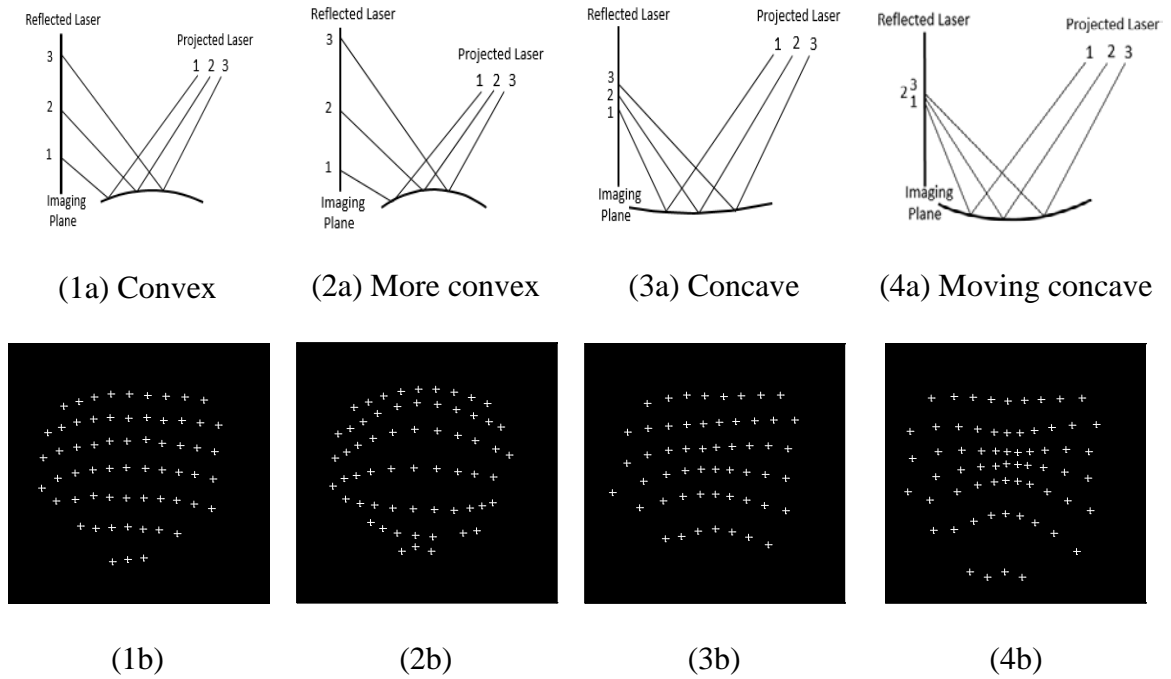


Figure 5-2 Characteristic principles for pool oscillation

5.2 Experimental procedure and method

The experiment aimed to study pool oscillation behavior in different weld penetrations for pulsed GTAW welding under stationary conditions which means zero travel speed. Typical 304 stainless steel bar, 4.7 mm thick, were used as the workpiece, which was placed on a thick copper plate with a backfill of argon. Welding was carried

out using a 2% Thoriated tungsten electrode with a diameter of 2.4mm and a tip angle of 60°, at straight polarity with 99.99% pure Argon as shielding gas at a flow rate of 15 CFH and a distance of 5 mm from the tungsten electrode to the specimen.

The welding-parameters design is given in Table 5-1. The image-capture rate was set to 1000 frames per second. The base time was set to 20 ms to observe the weld pool oscillation process at its natural frequency. The base time was set to 10 ms, mainly for inspecting the pool oscillation behavior of full penetration, whereas the 3 ms base time served in studying the forced pool oscillation behavior when the pulse frequency was greater than the natural frequency of weld pool because of the very short base current time. Experiment No. 1 was designed to judge the pool oscillation under constant welding current conditions. Experiment No.2 and No. 5 were designed for exploring oscillation behavior and partial penetration; Experiment No.3 was designed for exploring forced oscillation. Experiment No.4 and No. 6 were designed for full penetration and oscillation behavior. Experiment No.5 and No. 7 were designed for critical penetration and oscillation behavior. The other experiments were designed for analyzing pool oscillation behavior or amplitude issues.

Table 5-1 Welding parameters

No	Peak current Ip/A	Base current Ib/A	Peak time Tp/ms	Base time Tb/ms	Pulse frequency f/Hz	Captured rate /fps	Target of Study
1	60	60	-	-	-	1000	DC Oscillation
2	60	20	20	20	25.0	1000	Partial / behavior
3	80	20	20	3	43.5	1000	Forced oscillation
4	80	20	20	5	40.0	1000	Full /behavior
5	80	20	20	20	25.0	1000	Mode / behavior
6	100	20	20	10	33.33	1000	Full / behavior
7	100	20	20	20	25.0	1000	Critical / behavior
8	120	20	20	5	25.0	1000	Oscillation behavior
9	140	20	20	5	25.0	1000	Oscillation behavior
10	160	20	20	5	25.0	1000	Oscillation behavior

* Partial –partial penetration, full – full penetration; critical – critical penetration;
mode – partial and critical penetration; behavior – oscillation behavior.

5.3 Experimental results and discussion

5.3.1 Pool oscillation mode

The oscillating weld pool was imaged/captured at 1000 frames per second by the high-speed camera during welding. Both the convexity and concavity of the weld pool surface under the pulse current were observed. The variation in the reflected laser dot matrix presented the dynamic variation in the weld pool surface such that the pool oscillation behavior could be observed clearly. Results of the experiment showed three pool oscillation modes at different depths of penetration.

1. Symmetrical oscillation under partial penetration

Figure 5-3 (1b) and (2b) are the consecutive reflected laser dot-matrix images of the oscillating weld pool at partial penetration, such as those in Experiment No.2, and 5 in Table 5-1. The pixel distance of adjacent laser dots in the weld pool center in Figure 5-3 (1b) is relatively large, while it in Figure 5-3 (2b) is much smaller. This concurs with the characteristic principles discussed in Section 5.1.2. The center of the weld pool shrank toward the inside [Figure 5-3 (1b)], and correspondingly, the shape of weld pool oscillation surface was concave, whereas the center of the weld pool expanded toward the outside [Figure 5-3 (2b)], correspondingly, and the shape of weld pool oscillation surface was convex.

Figure 5-3 (1b) and (2b) show that the weld pool oscillation in the partial penetration is symmetrical about the center of weld pool. As was presented in reference [20, 22], the oscillation model can be described with the first harmonic mode of Bessel function.

The arc pressure is known to be caused by a magnetic pressure differential along the length of the arc, which accelerates the arc plasma and entrains the gas toward the workpiece to form a dynamic jet pressure [10, 31]; it increases with the square of current and decreases from electrode to workpiece as the arc radius increases. Thus, the arc jet pressure derived from the peak current is much greater than that derived from the base current.

When the welding current is switched to the base current from the peak current, the arc jet pressure suddenly releases from the top of the pool and induces pool oscillation at a natural frequency. The surface tension pulls the pool back toward its equilibrium position. The pixel distance at the central region of the weld pool enlarges [Figure 5-3

(2b)], and the weld pool continues to expand upward after it reaches its point of equilibrium, due to the inertia. When the weld pool expands upward to its highest position, the surface tension and gravity drag the pool back toward its point of equilibrium, and the pixel distance at the central region of the weld pool shrinks [Figure 5-3 (1b)]. The weld pool continues to depress downward after it reaches its point of equilibrium position, again due to the inertia. More detailed evolution process can be seen in Section 5.3.2.1.

Due to the support of the solid metal in the bottom of the pool, the liquid metal around the pool edge is pushed upward when the liquid metal at the central pool is depressed downward. The scheme of the pool oscillation mode for partial penetration is illustrated in Figure 5-3 (1a) and (2a). The oscillation mode is consistent with the mode 1 proposed by Xiao, et al. in literature [20]. Figure 5-3 (3a) and (3b) are the top and bottom for the weld associated with partial penetration.

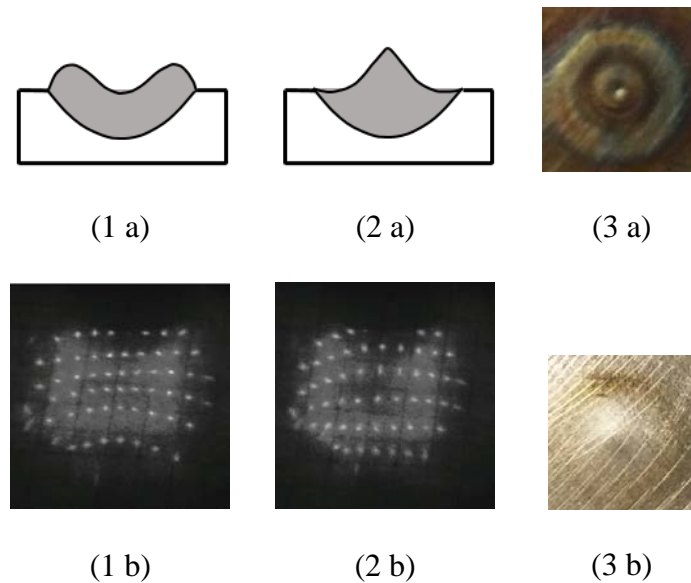


Figure 5-3 Symmetrical oscillation at the center of pool under partial penetration

2. Symmetrical oscillation under full penetration

Images of the oscillating weld pool in Figure 5-4 (1b) and (2b) show full penetration occurring as it did in Experiment No.4 and 6, Table 5-1. Figure 5-4 (3a) and (3b) are the top and bottom of the weld, respectively, corresponding to full penetration oscillation. To a first approximation, the oscillation under full penetration can be described in terms of a stretched membrane or classical hydrodynamics to the liquid metal in the weld pool [10, 20, 22].

In Figure 5-4 (1b), a bright region appears in the central region of the molten pool. The brightness is much higher there than that in other regions of molten pool. Under the condition of full penetration, the bottom metal of the work-piece has also been melted, as shown in Figure 5-4 (3b). The bottom of the weld pool loses the support of the solid metal, and instead, it is maintained by the surface tension of liquid metal from the bottom pool. Therefore, the liquid weld metal in the full penetration pool has an extra degree of freedom (normal to the surface of the pool) [22], and the surface tension along the top and bottom surface of the pool as the main driven force have a significant influence on the oscillation behavior. When the arc jet pressure acts on the top of weld pool surface, the weld pool surface depresses to such a low position that the reflected laser dot–matrix shrinks into a large bright point in the center of weld pool. At this time, the shape of weld pool surface is concave. The scheme of the pool oscillation mode is shown in Figure 5-4 (1a).

Figure 5-4 (2b) shows a brighter circle in the edge of the pool. When the arc jet pressure on the top of the weld pool surface is suddenly released, the surface tension on the top and the bottom of the weld pool pulls together the pool back toward its

equilibrium position. The center of the weld pool first expands upward, and then the edge of weld pool follows with the motion of the center of weld pool. However, because of the lack of support of solid metal in the bottom of the pool, the weld pool surface is pushed down to a relatively low position by the high arc pressure which derived from the pulse current. Therefore, the edge of the weld pool does not easily drag back to the convex when the center of the pool reaches the highest point, and in the most of time, the reflected image of the weld pool surface, like Figure 5-4 (2b), is a bright circle around the edge of the pool. According to Section 5.1.2, that shows that the shape of the central region of the weld pool is convex and that of weld pool edge is concave, as shown in Figure 5-4 (2b). The scheme of the oscillation mode is illustrated in Figure 5-4 (2a).

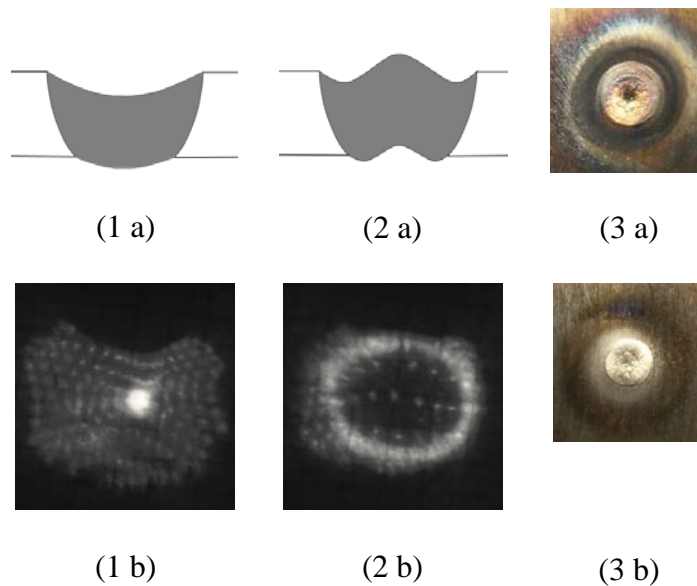


Figure 5-4 Symmetrical oscillation at the center of the pool under full penetration

It is apparent from the reflected laser dot characteristic that the pool oscillation under full penetration is also radial symmetrical with respect to the axis of the arc. However, both the top and bottom of the weld pool are liquid film, and the pool

oscillation morphology is significantly different, and the corresponding image of the oscillating weld pool surface [Figure 5-4 (1a)] is also considerably different from the image under partial penetration [Figure 5-3 (1a)]. Figure 5-4 (1b) and (2b) show that the pool oscillation amplitude is much greater than that under partial penetration. The results coincide with mode 2 proposed by Xiao, et al [20-22], and the experimental phenomena also verify the hypothesis proposed by Richardson, et al [32], i.e., there exists a kind of symmetrical oscillation mode under full penetration as described above.

3. Sloshing oscillation under critical penetration

Figure 5-5 (1b) and (2b) show the pool oscillation under the critical penetration, such as in Experiment No.5 and 7, Table 5-1. In Figure 5-5 (1b) and (2b), the symbol “ \ominus ” and “ \oplus ” represent the valley and the peak of weld pool oscillation, respectively.

The minimum of the pixel distance in Figure 5-5 (1b) is located on the right side of the pool oscillation image, whereas the minimum pixel distance in Figure 5-5 (2b) is located on the left side of the pool oscillation image, neither at the center of the weld pool. Unlike the pool oscillation under full or partial penetration, the extreme position (oscillation center hereafter) of the oscillating pool under critical penetration is not always at the center of the weld pool but instead shifts like a wave of water in a pool. It is possible that the oscillation center would shift to another position in the next moment. The oscillation behavior is somewhat like a wave of water in a puddle, so the pool oscillation mode is defined as sloshing oscillation or swing oscillation. The scheme of the oscillation mode is given in Figure 5-5 (1a) and (2a).

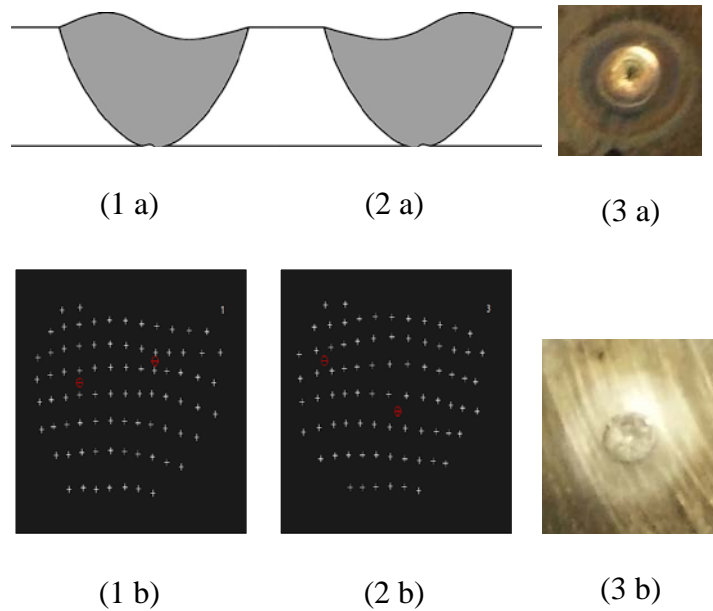


Figure 5-5 Sloshing oscillation under critical penetration

Why did the oscillation center shift? When the weld pool grows, the bottom metal of the work-piece also gradually melts into liquid state. Because the microstructure, crystal structure, and defects/imperfection are not uniform and continuous, it is possible that the earliest spot which is melted is not exactly at the center of the weld pool. The melting process of the bottom pool is thus not perfectly uniform and symmetrical (in stationary welding). Therefore, the asymmetrical position results in that the forces of the weld pool are off-balance and not uniform, and the force of the unbalance causes asymmetrical movement, like a sloshing wave of water, in the oscillating pool.

In the situation of critical penetration, only a very small part of the bottom metal is melted. A large part of the weld pool is still backed by the solid metal. Under the arc pressure, only a small part of the liquid metal is pushed downward, with the increasing of the pool size, less liquid metal is backed by solid material and more liquid metal is

pushed in downward direction. Only after the bottom size of the pool reaches a certain threshold, the oscillation would become the mode of full penetration.

Our series of experimental results have also shown that this oscillation behavior did occur under the critical penetration, i.e., after the full penetration is achieved until the area of the bottom liquid surface reached approximately 0.3 and 0.5 time of that of the top surface as suggested by literature [32]. Thus, the critical oscillation is not at a specific position as its oscillation center but in a transition stage. This is consistent with the results which are obtained in terms of oscillation frequency characteristics[22]. Figure 5-5 (3a) and (3b) are the top and bottom of corresponding weld with critical penetration in which the bottom pool surface area is less than 0.3 and 0.5 time of that of the top pool surface.

5.3.2 Pool oscillation process for pulsed GTAW

To investigate the evolution process of pool oscillation during pulsed GTAW welding, a series of consecutive reflected weld pool images based on laser dot-matrix were captured at 1000 frames per second. The peak time and base time of the pulsing current were both 20 ms. The other welding parameters are given in Table 5-1. Within a pulse period, 20 frames of images under peak current and 20 frames of images under base current were captured and processed. The feature points were extracted, the missing points were added by interpolation, and the point in the laser dot matrix in the image corresponding to the oscillation center was replaced by the symbol “+”, as shown in Figure 5-6.

As previously mentioned, the pixel distance between two adjacent laser dots around the oscillation center of a weld pool is defined as the amplitude of pool oscillation. When the current switches from the peak to base current, the arc plasma pressure suddenly

releases. The surface tension pulls the pool back toward the equilibrium position and the natural oscillation occurs due to the surface tension and gravity. A different penetration state has a different pool oscillation behavior which can be observed and analyzed from the consecutive oscillation behavior within a 40-ms pulse period.

1. Pool oscillation under partial penetration

Again, 40 frames of consecutive weld pool oscillation images were captured and processed including 20 frames for the peak and 20 frames for the base time such as Experiment No.5, Table 1. Some typical oscillation images taken after processing are shown in Figure 5-6 (b). Figure 5-6 shows that the oscillation dynamic evolution process is very clearly observable. The reflected laser pattern is distorted because of the pool oscillation, and its variations respond to the regular and periodic contraction and expansion during the entire period.

As previously mentioned, the pixel distance between two adjacent laser dots at the oscillation center of the weld pool is defined as the amplitude of the pool oscillation. The amplitude in each image was calculated. The relationship between the amplitude and welding time is shown in Figure 5-6 (a). The following phenomena can be discerned from Figure 5-6 (a):

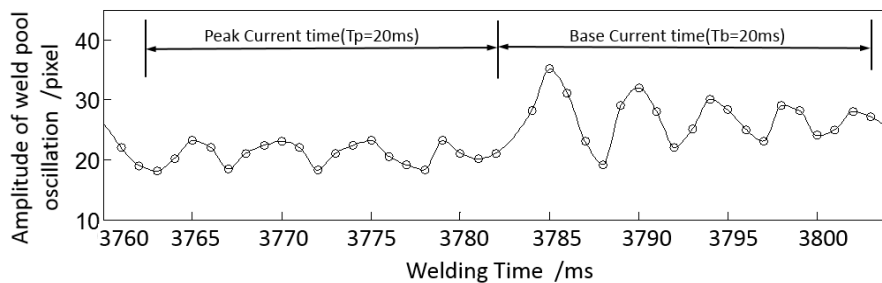
During the base current time when the arc plasma pressure on the top of the weld pool surface is released, the weld pool oscillates at a natural frequency, and the amplitude gradually decreases with weld pool solidification because of the reduced heat input under the base current.

The variation in the amplitude of weld pool surface is from 19 to 36 pixel during the base time period, while the variation in the amplitude of weld pool surface is from 17 to

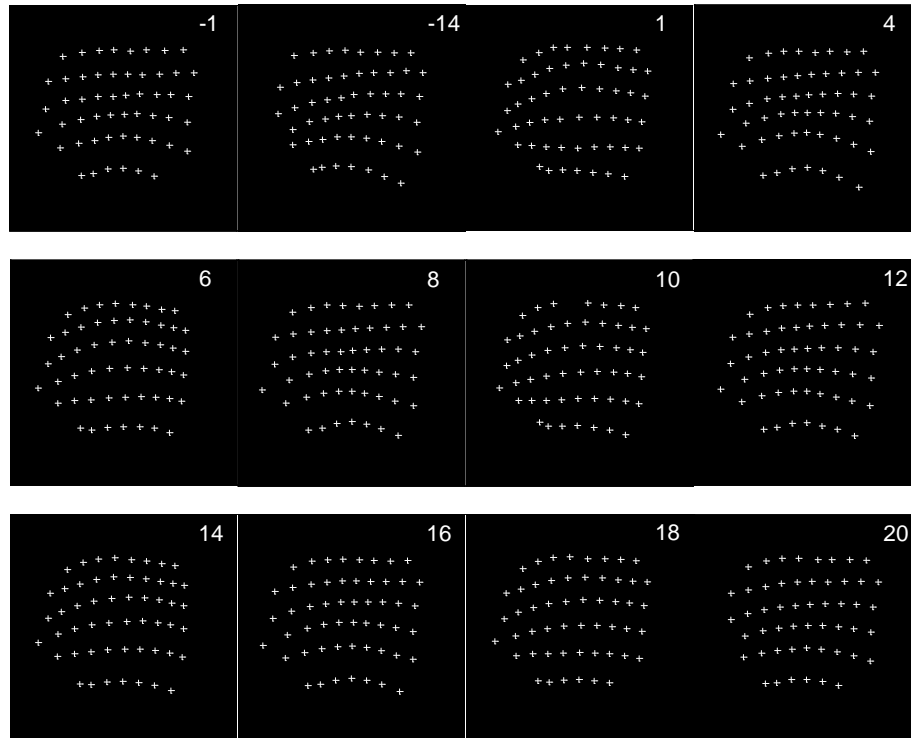
23 pixel during the peak time period. Because of the support of the solid metal in the bottom (Figure 5-6), it is very difficult for the surface of the pool to be pulled to a lower position only by the surface tension than that by the pulse arc jet pressure, therefore, in general, the lowest value of amplitude is not lower than the values during the peak current period.

During the peak current time, the weld pool surface is not also completely still, possibly because of the effect of the ‘natural’ oscillation in the base current period, the surface tension on the weld pool surface which prevents the pool oscillation from stopping immediately, instead, oscillation continues at a lower amplitude [Figure 5-6 (a)].

In addition, the natural frequency of the pool can be calculated easily from the pool oscillation process shown in Figure 5-6 (b). The pool oscillation has 4.5 cycles within 20 ms when the welding time is from 3783 to 3803ms, thus, the oscillation frequency at the moment is approximately 225Hz. The oscillation phenomena for the other experiments are similar to those in Experiment No.5.



(a) Amplitude variation of pool oscillation (welding base time from 3760ms to 3804ms)

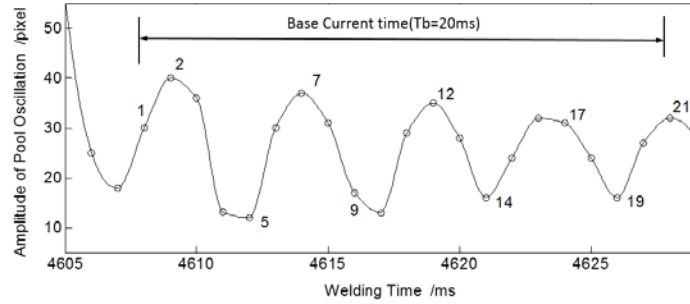


(b) Some typical pool oscillation images (welding base time from 3760 to 3804ms)

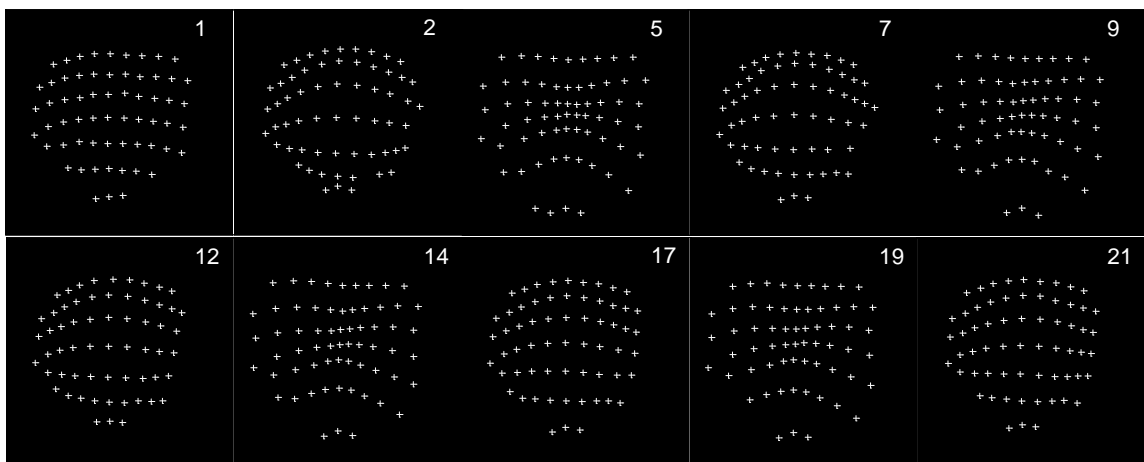
Figure 5-6 Pool oscillation process under partial penetration ($I_p=80A$, $I_b=20A$, $f=25Hz$, $T_b=20ms$)

Figure 5-7 shows the pool oscillation process when the welding time is from 4608 to 4628 ms with same welding parameters as for the experiment shown in Figure 5-6. Because the welding time is longer than that of Figure 5-6, the depth of penetration is correspondingly deeper, the oscillation process is sharper, and the oscillation amplitude from 10 to 40 pixel is much greater than that of the oscillation of welding time from 3782 to 3802ms.

According to Figure 5-7, it can be calculated that the natural oscillation frequency is approximately 200Hz, which is less than 225Hz of Figure 5-6. The results are consistent with the other studies indicating that the natural frequency decreases with the increases the geometry or mass of weld pool [10, 31].



(a) Amplitude variation of pool oscillation (welding base time from 4608ms to 4628ms)



(b) Some typical pool oscillation images (welding base time from 4608 to 4628ms)

Figure 5-7 Pool oscillation process under greater partial penetration ($I_p=80A$, $I_b=20A$, $f=25Hz$, $T_b=20ms$)

As can be seen in Figure 5-6 and 5-7, compared with the arc voltage variation, arc light intensity [32], or shadowgraph image techniques [33], with the help of three dimensional laser dot matrix sensing method and high speed camera, the variation of oscillation morphology can be observed more easily, and dynamic evolution process of weld pool surface oscillation can be clearly observed and analyzed.

2. Pool oscillation under full penetration

Figure 5-8 shows the variation of the oscillating weld pool surface and several corresponding pool oscillation images that are typical for full penetration, such as those in Experiment No.6, Table 5-1, with the welding time t_0 being equal to 6080 ms. The reflected images from the pool oscillation surface were taken at 1, 4, 7, and 10 ms after the arc plasma pressure is suddenly removed. The pool oscillation process is just as the scheme of oscillation under the time axis of Figure 5-8.

As indicated in Section 5.3.1.2, the pool oscillation mode and phenomena of full penetration is similar to that of the partial penetration. However, when the weld is at full penetration, the metal in the bottom of weld pool is also molten such that the bottom of the weld pool loses the support of the solid metal. Instead, it is maintained by the surface tension of the liquid metal in the bottom pool. The weight of the weld pool itself has a significant effect on pool oscillation. The amplitude of pool oscillation is much greater than that under partial penetration, and the motion of weld pool oscillation is sharper (Figure 5-8).

Apparently, the pool surface is lower than the top of the workpiece due to the effect of surface tension and the lack of support from bottom solid metal. When the welding current switches from peak to base current such that the arc jet pressure on the top of the pool is suddenly removed, the surface tensions of the top and the bottom of the weld pool pull together the pool back toward its equilibrium position and the oscillation occurs at a natural frequency. The oscillation process is as shown in Figure 5-8. As can be seen, the weld pool gradually expands to up from the bottom to top. The pool morphology is as shown in the scheme of Figure 5-8 in the corresponding images t_0+1 ms to t_0+10 ms.

Then the oscillation process repeats as described previously, but the amplitude of the pool oscillation decreases with the solidification of liquid pool. During the next 40ms period, the pool oscillation process is similar.

Because of the lack of the support of bottom solid metal and the weight of weld pool itself, the weld pool shrinks downward to a lower position, and the reflected laser dot-matrix at the center of pool gradually converge to a litter area as shown in the image of $t_0+1\text{ms}$ in Figure 5-8. The image of $t_0+4\text{ms}$ in Figure 5-8 shows that the weld pool continues to shrink, and the brightness is the largest in the entire weld pool area. When the pool surface expands upward, the distance between adjacent laser dots at the center of the pool gradually becomes larger. However, the shape of the weld pool edge might still be concave, and the reflected laser dot-matrix converges. As a result, the brightness of the area is larger, looking like a bright ring, as shown in the image of $t_0+7\text{ms}$, Figure 5-8. The bright ring in the image of $t_0+10\text{ms}$ becomes bigger, and shows that the edge part of pool expanded upward. If the pool were to continue to expand upward, and the concaveness of the pool edge would gradually become flat, even convex, and then the bright ring would gradually disappear.

When the arc jet pressure, once again, exerted on the top of the weld pool surface, the weld pool surface curved downward to the very low level because of the forced action of the arc pressure, as shown in the last scheme of Figure 5-8.

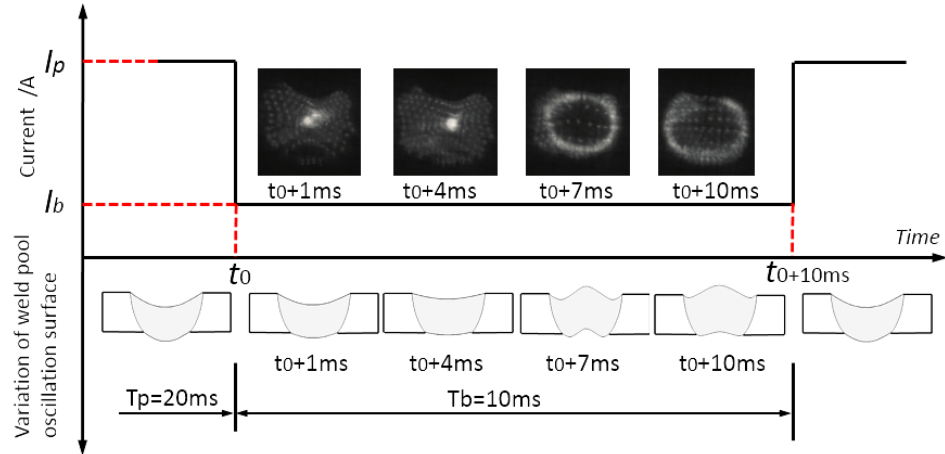


Figure 5-8 Variation of weld pool oscillation surface under full penetration ($I_p=100A$, $I_b=20A$, $f=33.3Hz$, $T_b=10ms$)

3. Pool oscillation under critical penetration

As mentioned previously, when the penetration is between the partial and full, the pool oscillation dynamic process is in the critical penetration stage as can be seen from Figure 5-9, which includes 20 frames from 20 ms base current time, such as those in Experiment No.5, Table 5-1. The lowest positions of the oscillating pool surface in the following 1-20 images are labeled with the sign “ Θ ”. The dynamic variation of pool oscillation by the shift of the sign “ Θ ” in the following 1-20 images is clearly evident. The maximum amplitude and lowest oscillation position distribution are shown in Figure 5-9.

Figure 5-9 indicates that the pool surface is not symmetrically and vertically oscillated as is the case in partial penetration and full penetration, and the pool oscillation center is no longer fixed at the center of the weld pool, but constantly moves like the waves on a water surface. The pool behavior looks like the swing or sloshing wave of water in a pool.

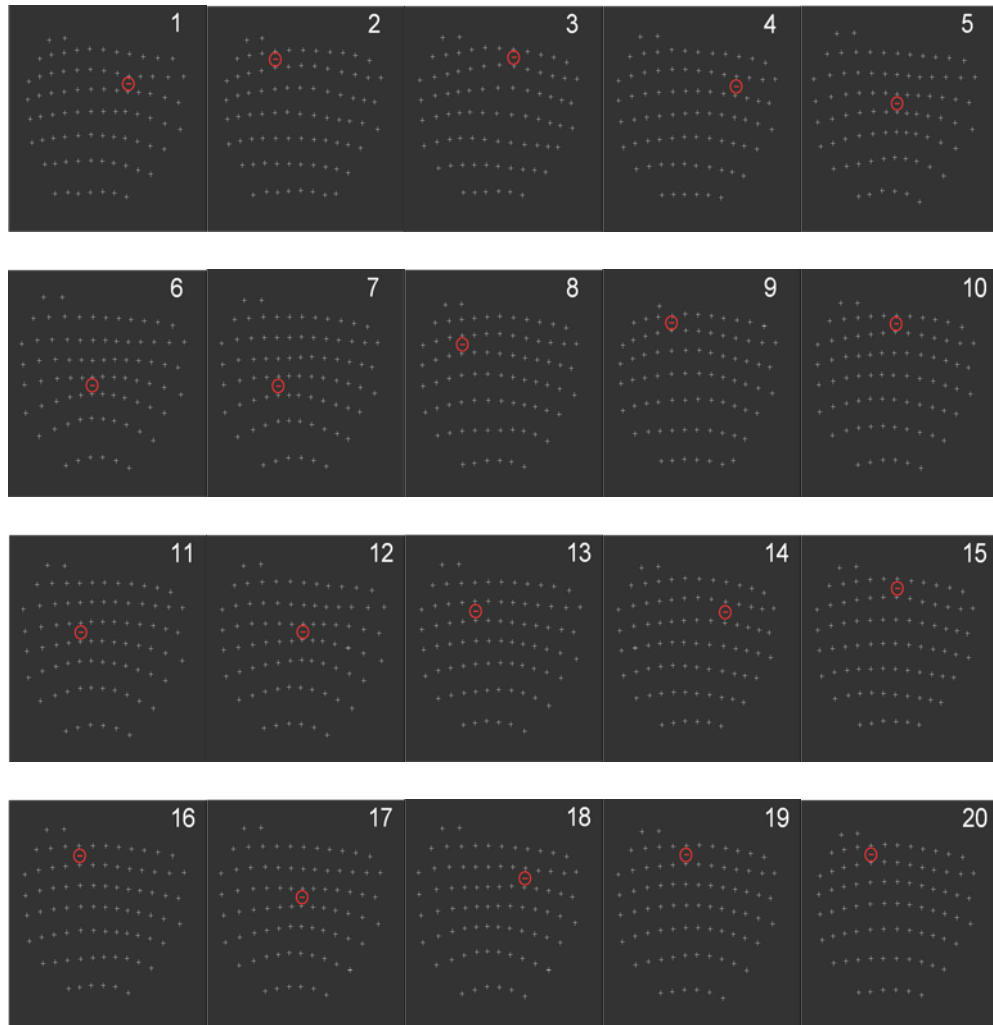


Figure 5-9 Sloshing pool oscillation under critical penetration ($I_p=80A$, $I_b=20A$, $f=40Hz$, $T_b=20ms$)

Figure 5-9 shows that the variation of maximum and minimum amplitude for sloshing oscillation during a 20 ms base current time. Again, the peak current has a amplitude of 80 A peak and duration of 20 ms. The base current has a amplitude of 20 A and duration of 20 ms. In Figure 5-9, When the welding time reaches 7084 ms, the critical penetration process occurs, and the natural oscillation process is forcedly stopped after the base time of 20 ms, because the arc jet pressure, once again, is exerted on the top of the weld pool surface, which is derived from the pulse current.

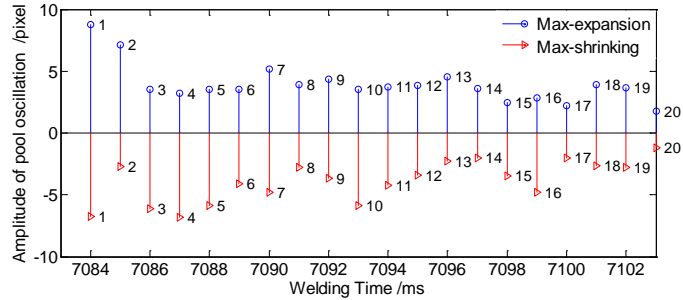


Figure 5-10 Variation of maximum and minimum amplitude for sloshing oscillation during 20ms base current time

Compared with partial penetration (Figure 5-6, 7) and full penetration (Figure 5-8), the oscillation amplitude of critical penetration (Figure 5-9) is minimum, and the oscillation frequency is not a fixed value but varies.

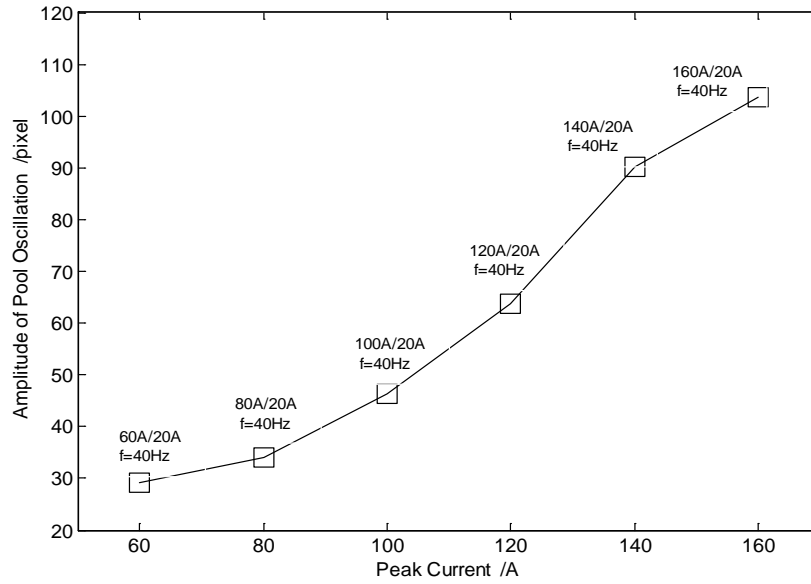
In the critical penetration, the oscillation center dynamically changes. The weld pool surface morphology is abruptly different from those in partial penetration and full penetration. The pool oscillation mode is also essentially different from those in partial penetration and full penetration. It is apparent that the morphology variation of weld pool surface that is clearly observable from the reflected images is not obtainable from one dimensional arc voltage or arc light signal that were used in pool oscillation studies in literature.

5.3.3 Relationship between Amplitude and pulse current difference

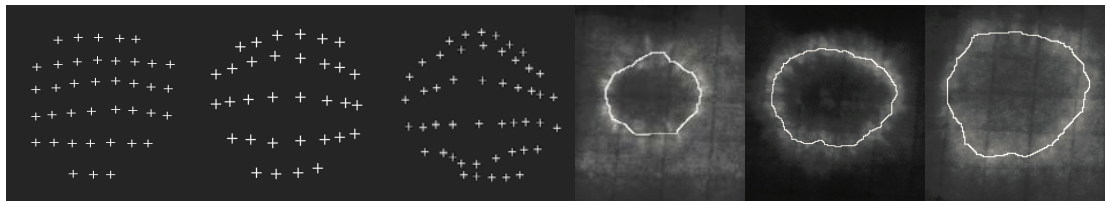
To observe the pool oscillation amplitude in different peak currents, all other welding parameters were kept the same: 20 A base current, 5 ms duration for the base current, and 20 ms duration for the peak current. Different peak currents were applied in different experiments (Table 5-1).

To ensure the conditions the same, only after the weld pool had grown up to the same size, the weld pool oscillation was observed. Figure 5-11 (b) shows typical pool oscillation images after processing when the peak current were 60, 80, 100, 120, 140, and 160 A, respectively. Figure 5-11 (a) shows the amplitude of pool oscillation at the different peak currents. The arc pressure increases with the square of current and decreases from electrode to workpiece as the arc radius increases. The pressure accelerates the arc plasma and entrained gas toward the workpiece to form a dynamic jet pressure, and the jet acts on the pool surface to create a pressure. As shown in Figure 5-11 (a), the amplitude of pool center oscillation gradually increases from 30 pixel to approximately 100 pixel when the corresponding welding peak current gradually increases from 60 to 160 A.

The conclusion can be drawn that, under the condition of the same base current, the greater the peak current the greater the pool oscillation amplitude. The appropriate amplitude of pool oscillation helps to improve the weld quality, gain refinement, and defect inhibition [31, 32], however, improper amplitude might influence on the stability of welding process. Thus, the relationship between amplitude and arc pressure needs to understand.



(a) Amplitude variation of pool oscillation in the different peak current



$I_p=60\text{ A}$ $I_p=80\text{ A}$ $I_p=100\text{ A}$ $I_p=120\text{ A}$ $I_p=140\text{ A}$ $I_p=160\text{ A}$

(b) Typical Pools Oscillation images for different peak current

Figure 5-11 Oscillation behavior of weld pools oscillation under different peak current
($I_b=20\text{ A}$, $f=40\text{ Hz}$, $T_b=5\text{ ms}$)

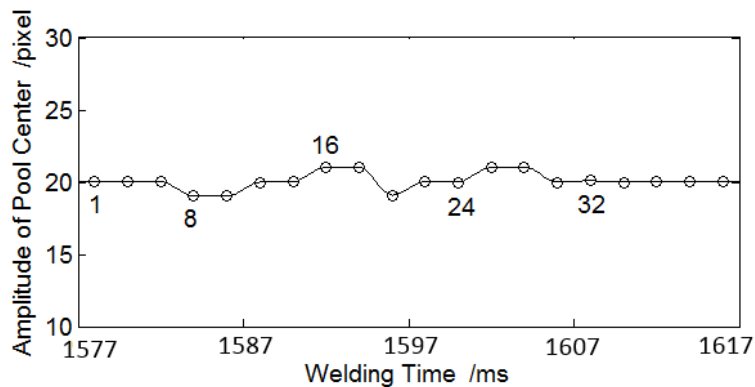
5.3.4 Discussions

As such, the oscillation modes and oscillation dynamic behaviors have been studied in detail. However, the studies were done under pulsed current with moderate frequency. To gain broader and more complete view, we wish to briefly study the oscillations under

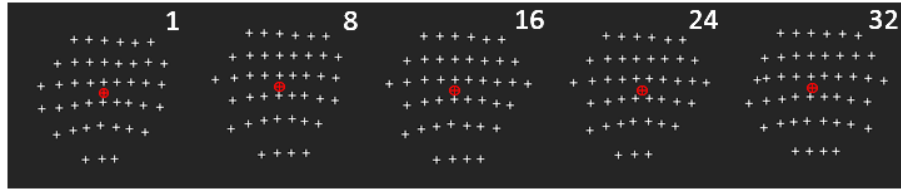
extreme frequencies by using DC current as the extreme for low frequency and pulsing current with high frequency.

1. Pool dynamic behavior under direct current GTAW

To study the behavior under ultra-low frequencies, direct current is used. As shown in Figure 5-12, the amplitude of pool center during direct current (DC) GTAW welding was also measured based on the same method described previously. Figure 5-12 (b) shows typical images for DC-GTAW after imaging processing. The symbol “ \oplus ” still represents the weld pool oscillation center. Figure 5-12 (a) shows amplitude variations from consecutive 1-40 ms welding time from 1577 to 1617 ms. Figure 5-12 (a) shows that the amplitude of the pool oscillation center almost remains constant since the welding current stays nearly constant during DC-GTAW despite some slight changes possibly caused by minor disturbances. According to Section 5.3.2.1 and 5.3.2.2, the pool behaviors during DC-GTAW differ entirely from those in pulsed GTAW during the peak period.



(a) Amplitude variation during DC-GTAW



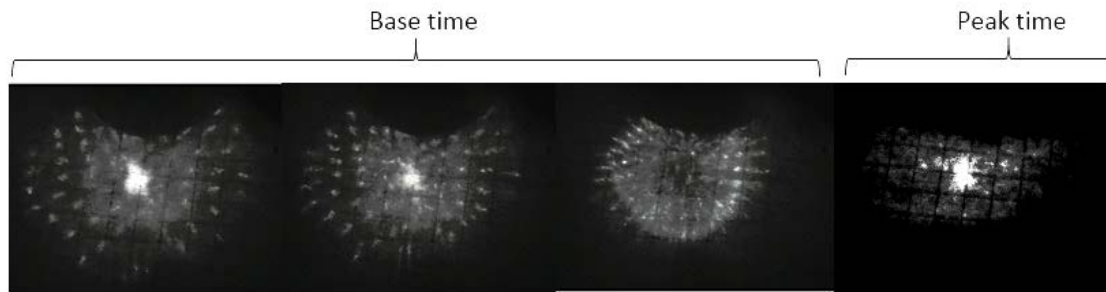
(b) Some typical images for DC-GTAW

Figure 5-12 Pool dynamic behavior under DC-GTAW (welding current $I=60A$)

2. Forced pool oscillation under high frequency pulsing current

As mentioned previously, when the arc jet pressure on the top of the weld pool is released, the pool oscillate is excited at the natural frequency corresponding to the geometry of the weld pool. However, when the base time is shorter than the period of the pool oscillation at the national frequency, the oscillation process would be forcedly terminated. Figure 5-13 shows that, after the current is switched at 4608 ms from 80 A peak current to 20 A base current which lasts 20 ms, the natural oscillation frequency of the weld pool is 200 Hz. The oscillation period is 5 ms. Clearly, if the base time is less than 5 ms, such as that in Experiment No.3, Table 5-1, the oscillation process will be terminated before a complete natural oscillation cycle is finished. The natural oscillation will not occur. The pool oscillation frequency is expected to be equal to that of the pulse frequency of pulsed GTAW. In this case the oscillation will be much stronger such that the images become blurrier. To analyze such oscillation, the images have been enhanced to increase the contrast as in Figure 5-13 in which the base current is 3 ms where the fourth image was acquired three milliseconds after the peak current had been applied. Despite the relatively bluer images, it is still clear that the reflection in the fourth image

shows a concave pool surface (as indicated by the bright spot in the center) rather than a convex pool surface as it should be if the natural oscillation continues.



(a) $W_{\text{Time}} = 3498+1\text{ms}$ (b) $W_{\text{Time}} = 3498+2\text{ms}$ (c) $W_{\text{Time}} = 3498+3\text{ms}$ (d) $W_{\text{Time}} = 3498+6\text{ms}$

Figure 5-13 Forced pool oscillation under high frequency pulse current ($I_p=80\text{A}$, $I_b=20\text{A}$, $f=43.5\text{Hz}$, $T_b=3\text{ms}$)

5.4 Summary

The pool oscillation behavior have been characterized by and analyzed from the reflection laser dot-matrix pattern from the oscillating weld pool surface. From reflection laser dot-matric pattern based analyses, the following conclusions can be drawn for the pools oscillation in pulsed GTAW:

- (1) Pool oscillation dynamic behaviors can be clearly observed and easily measured according to the reflected images derived from the laser dot –matrix sensing method.
- (2) The dynamic evolution process of the oscillating weld pool and the variation in the weld pool surface morphology can be clearly presented using the innovative three dimensional weld pool surface sensing method.

- (3) There exist three oscillation modes: symmetrical oscillation for partial penetration, sloshing oscillation for critical penetration, and symmetrical oscillation for full penetration which differs significantly from that of partial penetration.
- (4) The amplitude of the pool oscillation gradually increases as the peak current increases. This is because the arc plasma pressure on the top of pool surface increases with the peak current increases.
- (5) The natural frequency oscillation can be excited after the current is reduced to the base level but its continuation to finish a complete cycle requires the base current period is sufficiently long in comparison with the period of the natural frequency. A relatively short base current period will result in a forced oscillation at the frequency of the pulsed current.
- (6) Oscillations with smaller amplitude still exist in the weld pool during the peak current period. However, during welding with a constant current, the oscillation in the weld pool is insignificant.

CHAPTER 6 Modeling of the Weld Pool Penetration

Stages

In this chapter, a model is built for the weld pool for the different penetration stages. It takes into account the forces existing in the weld pool and the heat flux and heat loss factors. It makes a number of assumptions to simplify the model while still capture the important factors. Simulation results based on the model revealed the differences between partial and full penetrations in terms of velocity field and temperature field.

6.1 The Mathematical model

During pulsed GTA welding, the peak value and the base value of the pulsed current are alternated with a certain frequency, as shown in Figure 6-1. Meanwhile, the arc shape is also alternated. The workpiece temperature rises and the molten pool increases during the peak current; the workpiece temperature decreases and the molten pool cools when the base current is applied. Pulsed GTA welding pool's physical model is shown in Figure 6-2, in which (a) is the heat transfer model of pulsed GTA welding molten pool. In this model, the heat flux produced by the arc melts the base metal and forms the molten pool. Through the heat conduction, the heat flux spreads everywhere of the base metal. The primary heat loss of the molten pool is convection, radiation and evaporation. Figure 6-2 (b) shows the mechanical model of the pulsed GTA welding pool, in which the arc pressure and surface tension are surface forces; electromagnetic force and buoyancy force are volume forces.

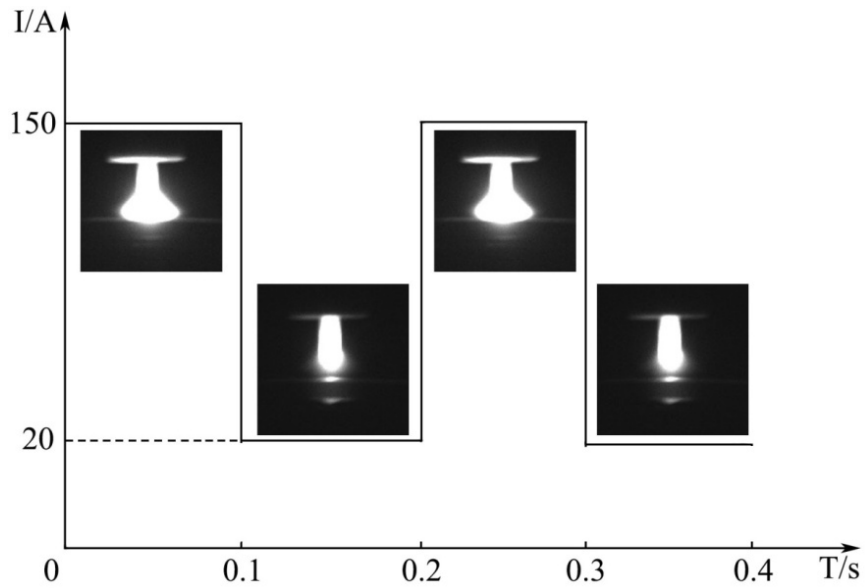
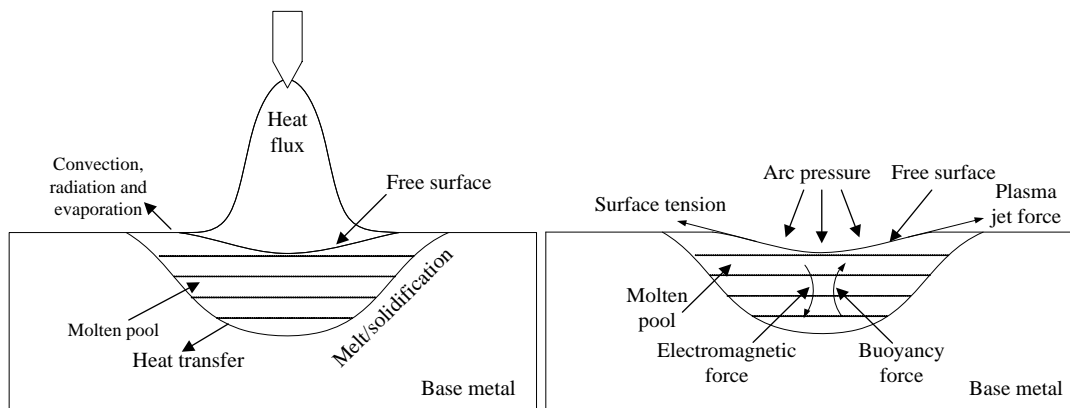


Figure 6-1 Pulse GTA welding current waveform and arc shape



(a) Heat transfer model of pulsed GTA

(b) Mechanical model of pulsed GTA

welding pool

welding pool

Figure 6-2 Physical model of pulsed GTA welding molten pool

6.1.1 Basic assumptions

According to the actual situation of the transient pulsed GTA welding process, the following assumptions are made to simplify the calculation:

Liquid metal in the molten pool is viscous incompressible Newtonian fluid, and its means of flow is laminar.

Except for the surface tension, thermal conductivity, viscosity and specific heat, the other thermal physical parameters are independent of temperature.

Only in the momentum equation does the gravity term take into account the change of density, following the Boussinesq hypothesis.

6.1.2 Governing equations

The governing equation is shown below (6-1):

$$\frac{\partial(\rho\phi)}{\partial t} + \frac{\partial(\rho u\phi)}{\partial x} + \frac{\partial(\rho v\phi)}{\partial y} + \frac{\partial(\rho w\phi)}{\partial z} = \frac{\partial}{\partial x}(\Gamma \frac{\partial\phi}{\partial x}) + \frac{\partial}{\partial y}(\Gamma \frac{\partial\phi}{\partial y}) + \frac{\partial}{\partial z}(\Gamma \frac{\partial\phi}{\partial z}) + S \quad (6-1)$$

Where ρ is density of fluid; u 、 v 、 w are the fluid velocity components in the x 、 y 、 z direction. ϕ is a general variable, which can represent speed, temperature and other variables; Γ is the generalized diffusion coefficient; S is the generalized source term, including the quality of source term, the momentum source term and heat source term.

The Volume of Fluid (VOF) method is used to track the free surface, and the volume fraction $F(x, y, z, t)$ is introduced to represent the proportion of fluid in the unit volume:

$$\frac{dF}{dt} = \frac{\partial F}{\partial t} + (\vec{V} \cdot \nabla) F = 0 \quad (6-2)$$

F is the volume fraction of the fluid in the unit, and the average value is calculated in the grid cell.

6.1.3 Boundary conditions

(1) The welding heat input is a very important boundary condition in the dynamic simulation of the free surface in the weld pool. Because this paper only studies the stationary pulsed GTA welding, the Gauss surface heat source is used. The heat flux expression is:

$$q(r) = \frac{\eta UI}{2\pi\sigma_H^2} \exp\left(\frac{-r^2}{2\sigma_H^2}\right) \quad (6-3)$$

Where U and I are arc voltage and current, σ_H is the Gauss heat distribution parameter, which is used to adjust the heat input distribution of the free surface in the weld pool, η is the welding heat efficiency.

(2) The total pressure P of the free surface of the molten pool satisfies the following formula [57]:

$$P = P_{arc} + \gamma_T \kappa \quad (6-4)$$

Where P_{arc} is the arc pressure, which is calculated as follows:

$$P_{arc}(r) = \frac{\mu_0 I^2}{8\pi^2 \sigma_p^2} \exp\left(-\frac{r^2}{2\sigma_p^2}\right) \quad (6-5)$$

Where μ_0 is the vacuum permeability; I is the current; r is the Gaussian distribution radius; σ_p is the radius distribution parameters for the arc pressure; γ_T is the surface tension coefficient; κ is the curvature of the surface, which is expressed as the following formula:

$$\kappa = - \left[\nabla \cdot \left(\frac{\vec{n}}{|\vec{n}|} \right) \right] = \frac{1}{|\vec{n}|} \left[\left(\frac{\vec{n}}{|\vec{n}|} \cdot \nabla \right) |\vec{n}| - (\nabla \cdot \vec{n}) \right] \quad (6-6)$$

Where \vec{n} is a free surface normal vector, expressed as the gradient of the volume fraction $F(x, y, z, t)$:

$$\vec{n} = \nabla F \quad (6-7)$$

Due to the change of surface tension with temperature, the surface tensions in the center and at the edge of the weld pool are different, which makes the molten pool flow. Surface tension is defined as the surface traction force, and the expression is as follows:

$$F_{\gamma-i} = - \frac{\partial \gamma}{\partial T} \frac{\partial T}{\partial x_i} \quad (6-8)$$

Where $\frac{\partial \gamma}{\partial T}$ is the temperature coefficient of the surface tension.

(3) In this model, the volume forces including the electromagnetic force and the buoyancy force caused by temperature change are taken into account. The electromagnetic force and the buoyancy force are given by the following formulas:

$$F_x = - \frac{\mu_m I^2}{4\pi^2 \sigma_j^2 r} \exp\left(-\frac{r^2}{2\sigma_j^2}\right) \left[1 - \exp\left(-\frac{r^2}{2\sigma_j^2}\right)\right] \left(1 - \frac{z}{H}\right)^2 \frac{x}{r} \quad (6-9)$$

$$F_y = - \frac{\mu_m I^2}{4\pi^2 \sigma_j^2 r} \exp\left(-\frac{r^2}{2\sigma_j^2}\right) \left[1 - \exp\left(-\frac{r^2}{2\sigma_j^2}\right)\right] \left(1 - \frac{z}{H}\right)^2 \frac{y}{r} \quad (6-10)$$

$$F_z = \frac{\mu_m I^2}{4\pi^2 H r^2} \left[1 - \exp\left(-\frac{r^2}{2\sigma_j^2}\right) \right]^2 \left(1 - \frac{z}{H} \right) - \rho g \beta (T - T_0) \quad (6-11)$$

Where H is the workpiece thickness, σ_j is the current distribution parameter, ρ is the density of the liquid metal, β is the thermal expansion coefficient of the liquid metal.

(4) The initial temperature of the workpiece is the same as that of the ambient temperature. The initial velocity of the molten metal is zero, that is, $u=0$, $v=0$, $w=0$. Assuming that the heat loss includes convection loss and radiation heat dissipation, the thermal boundary condition of the workpiece is [58]:

The upper surface boundary condition is expressed as:

$$-\lambda \frac{\partial T}{\partial z} = q(r) - \alpha(T - T_0) - \sigma \varepsilon (T^4 - T_0^4) \quad (6-12)$$

The thermal boundary conditions of the lower surface are the convection and radiation heat transfer conditions between the workpiece and the environment:

$$-\lambda \frac{\partial T}{\partial z} = -\alpha(T - T_0) - \sigma \varepsilon (T^4 - T_0^4) \quad (6-13)$$

Where α is the convective heat transfer coefficient, λ is the heat transfer coefficient of the fluid, σ is the Stefan-Boltzmann constant, ε is the surface radiation coefficient.

The boundary conditions applied to the computational domain as illustrated in Figure 6-3 is assumed continuous in order to model the semi-infinite state. The black cuboid represents the substrate. The boundary conditions used in the upper and bottom

surface include convection and radiation. The simulation was modeled in three-dimensional Cartesian system for description of the transport phenomena. The computation domain has dimensions of 200mm in length(x-direction), 200mm in width (y-direction) and 6mm in height (z-direction) for transient flow. The ambient temperature assumed for material and environment is 300K. Subroutines developed with FLOW SCIENCE FLOW-3D are used to compute the mathematical model.

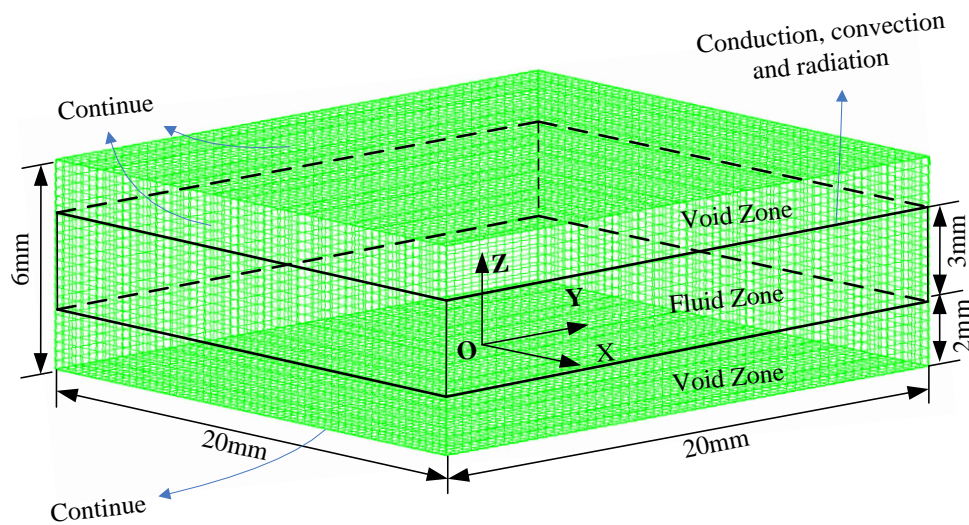


Figure 6-3 Grid and boundary condition

6.1.4 Simulation parameters

The material used in the simulation is 304 stainless steel, and the changes in thermal conductivity, viscosity, specific heat and density of the material with temperature are shown in Figure 6-4 [59]. The parameters used in the simulation are shown in Table 6-1 [60].

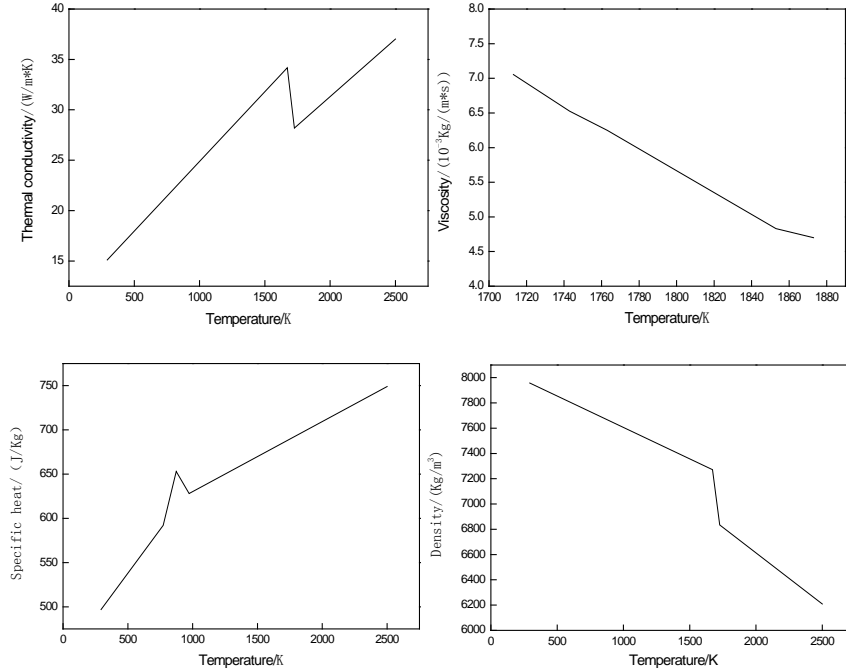


Figure 6-4 Thermal physical properties changed with temperature

Table 6-1 Material properties of SUS 304 stainless steel

Symbol	Property	Value
σ	Stenfan-Boltzmann constant/[W/(m ² *K ⁴)]	5.67*10 ⁻⁸
ε	Emissivity	0.4
ΔH	Latent heat of vaporisation/[J/Kg]	7.343*10 ⁶
μ_m	Permeability of vacuum [T*m/A]	4 π *10 ⁻⁷
γ^0	Surface tension of pure iron at reference temperature [N/m]	1.943
R	Gas constant[J/(K*mol)]	8.314
Γ_s	Surface excess in saturation[mol/m ²]	1.3*10 ⁻⁵
k_{ent}	Entropy factor	-1.38*10 ⁻²
ΔH^0	Enthalpy of segregation/[J/g*mol]	1.463*10 ³
β	The coefficient of thermal expansion/[K ⁻¹]	10 ⁻⁴

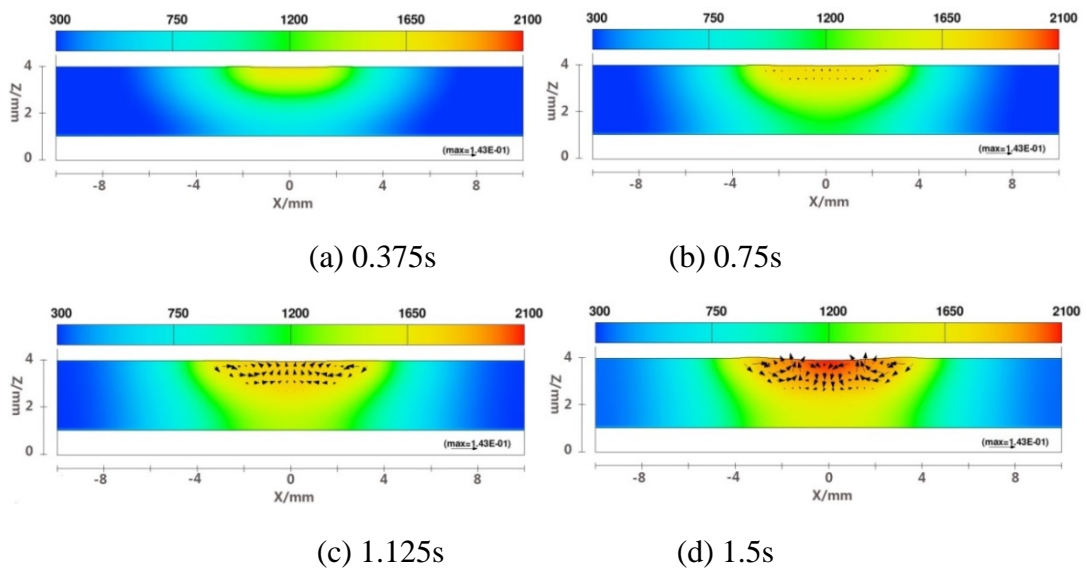
6.2 Results and discussion

6.2.1 Numerical results

The welding parameters are as follows: the peak current is 150A, the base current is 20A, the pulsed frequency is 5Hz, the duty cycle is 50%; the base material is 1/8" thick 304 stainless steel; the shielding gas is pure Argon with 15 CFH flow; the workpiece backside shielding gas is pure Argon with 30 CFH flow.

1. The effect of pulsed current on the oscillation of GTA welding molten pool

Figure 6-5 shows the simulated dynamic evolution of the temperature field on the xz cross section of the weld pool area. It can be clearly seen from the figure that as the welding time increases, the temperature in the workpiece gradually increases and the range of the temperature field becomes larger and both the penetration depth and melting width increase. The free surface is deformed with welding time.



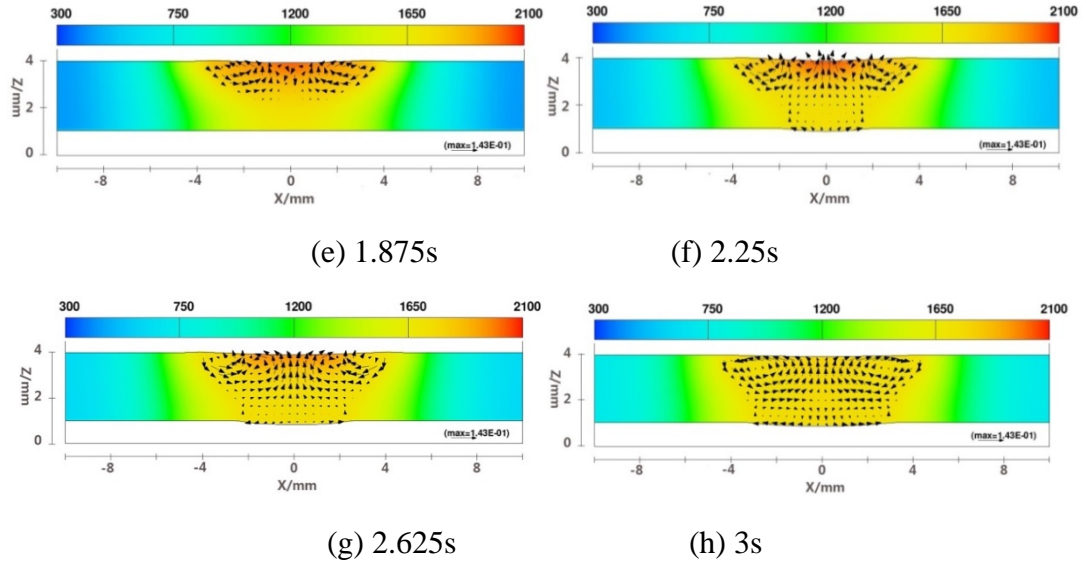


Figure 6-5 Computed temperature field in the weld pool

Figure 6-6 depicts the evolution curve of the free surface height in the center of the weld pool during the welding process. The oscillation frequency of the weld pool with time is recorded. As can be seen from the figure, free surface fluctuates under the action of the pulse cycle. When the current changes from the peak to the base or from the base to the peak, the free surface experiences a damped oscillation. The free surface begins to fluctuate at 0.06s and the oscillation amplitude of the molten pool increases gradually, which indicates that the molten pool starts to format at 0.06s. During the peak current, the free surface declines quickly and starts damped oscillation under the action of the surface tension, arc pressure, electromagnetic force and the buoyancy force. Under the action of the base current, the free surface begins to rise, and does a higher frequency damping vibration after the current changes from peak to base. Also, due to the decrease of the heat input in the molten pool, temperature field distribution in the molten pool is changed, which causes changes in the surface tension and buoyancy. The forces in the molten pool

are changed, which aggravates the flow of liquid metal. With the increase in the welding time, the oscillation amplitude gradually decreases, as shown in the inset in Figure 6-6.

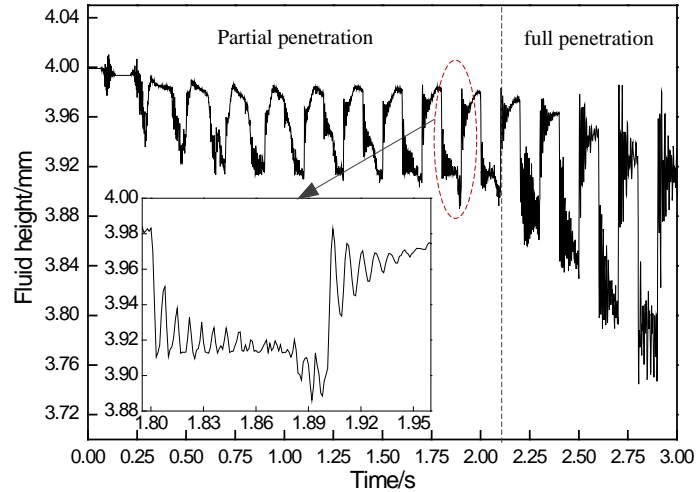


Figure 6-6 Evolution curves of free surface height over time

Figure 6-7 shows the velocity field in the weld pool at different times, where (a) is when the free surface is at the lowest point in the molten pool during peak current, figures (b) to (h) show the velocity field distribution under the action of the base current when the molten pool center height rises to the highest point or falls to the lowest point. It can be seen from the figures that under the action of the base current, the flow direction in the molten pool when the free surface is convex is different from that when the free surface is concave. When the molten pool is convex, the liquid metal flows upward, which forms flow loop from the center to the periphery of the weld pool. However, when the molten pool is concave, the flow direction is opposite to that when the pool is convex.

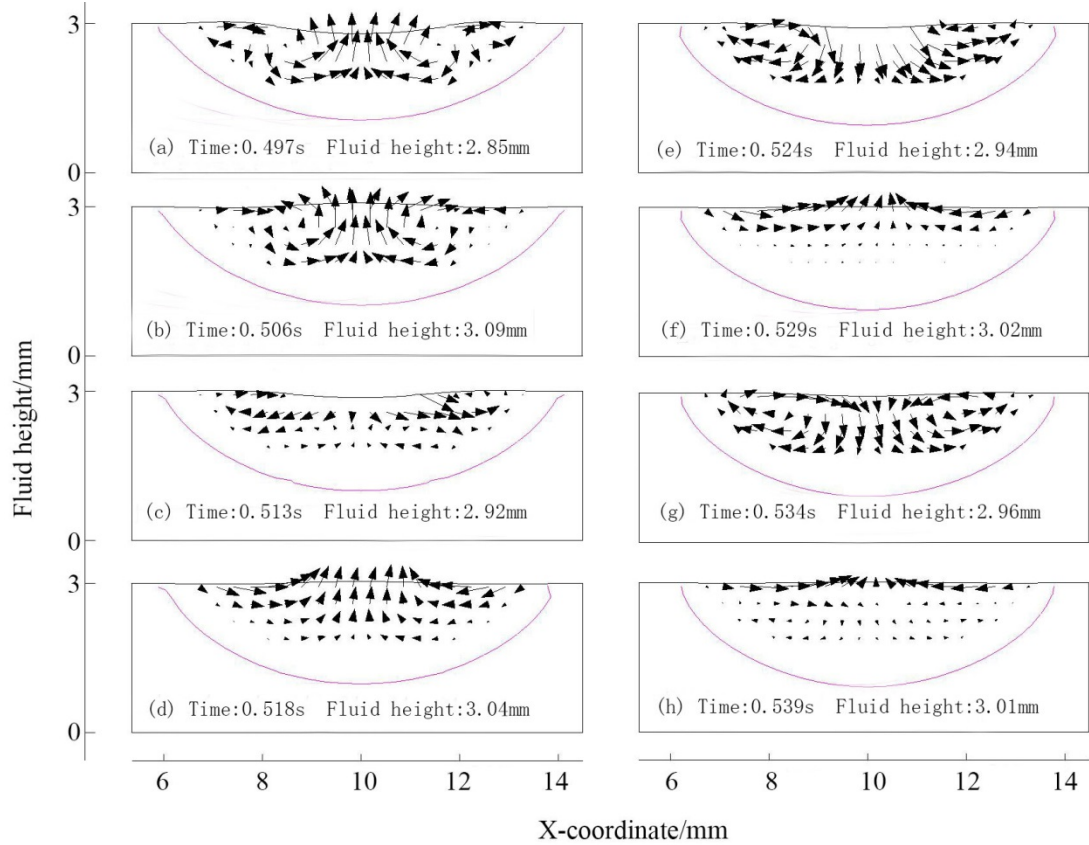


Figure 6-7 The velocity field before full penetration

Figure 6-8 is a bump change of the free surface at different times. As can be seen from the figure, the deformation in the center of the molten pool is the largest, and deformation is smaller farther away from the molten pool. Under the combined actions of the surface tension, arc pressure, electromagnetic force and buoyancy, the amount of concavity in the molten pool increases with the increase in the peak current time, which reaches the maximum (2.851mm) at 0.497s. At the base current, due to the decrease of electromagnetic pinch force and arc pressure, molten pool starts to oscillate upward. At 0.506s, it reaches the highest value of 3.086mm; at 0.513s drops to the lowest, at this time of the molten pool center height of 2.896mm; 0.518s rose to the highest, the highest

value of 3.041mm. From the above data, we can get the oscillation period is 0.012s, and the oscillation frequency is about 83Hz.

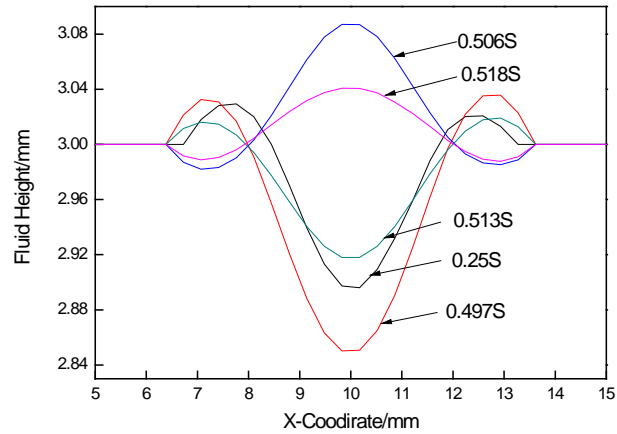


Figure 6-8 Bump change of free surface at different time

2. Full penetration

Figure 6-9 presents the velocity field after full penetration. (a) is the flow field at 1.872s. At this time, the free surface is concave to the maximum before full penetration. In (b), (d) and (f), the free surface is concave to the maximum after full penetration. In other figures, the free surface is convex to the maximum. It can be found that when the weld pool is fully penetrated, the entire weld pool is vibrating up and down.

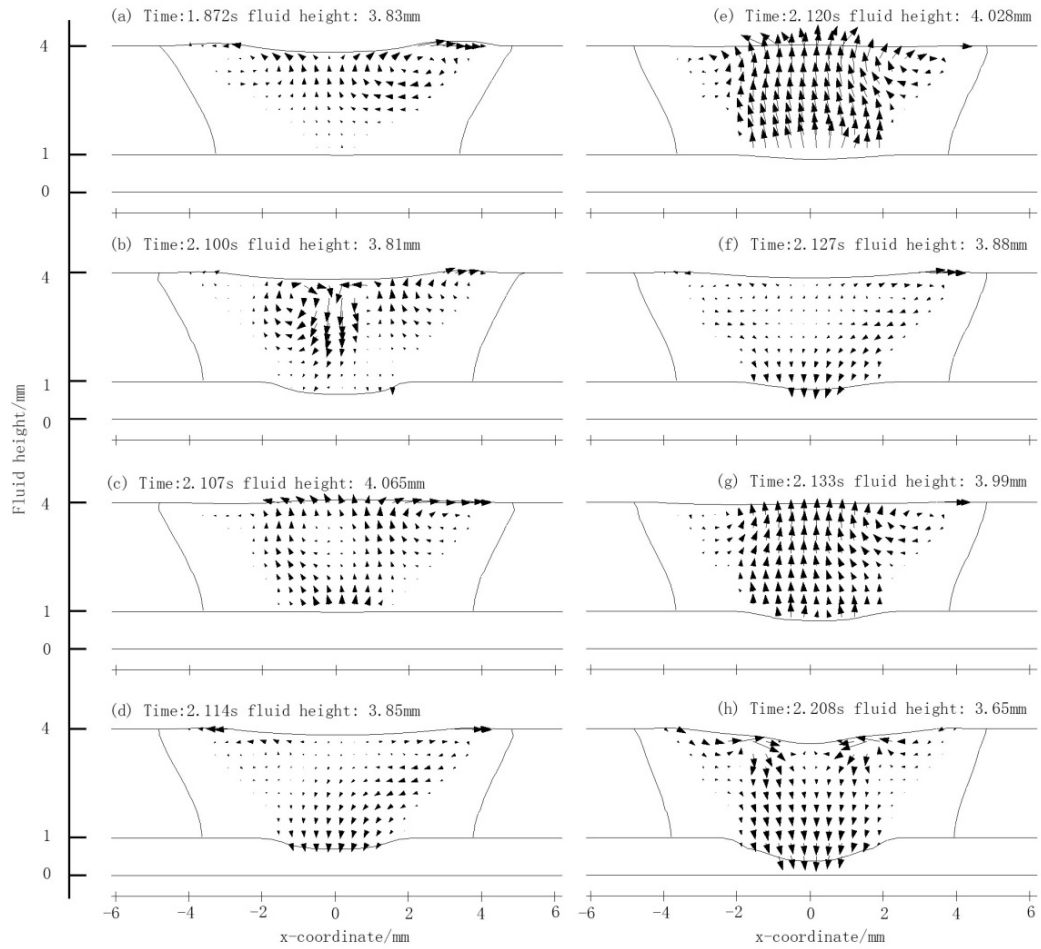


Figure 6-9 The velocity field after full penetration

By calculating the time interval of the adjacent concave or convex surface, we can obtain the oscillation frequency. The calculated data are shown in Figure 6-10. From the figure, it can be concluded that before full penetration, the weld pool oscillation frequency decreases as the welding time increases. At the same time, the penetration depth increases as the welding time increases. After the molten pool reaches full penetration, the oscillation frequency stays the same.

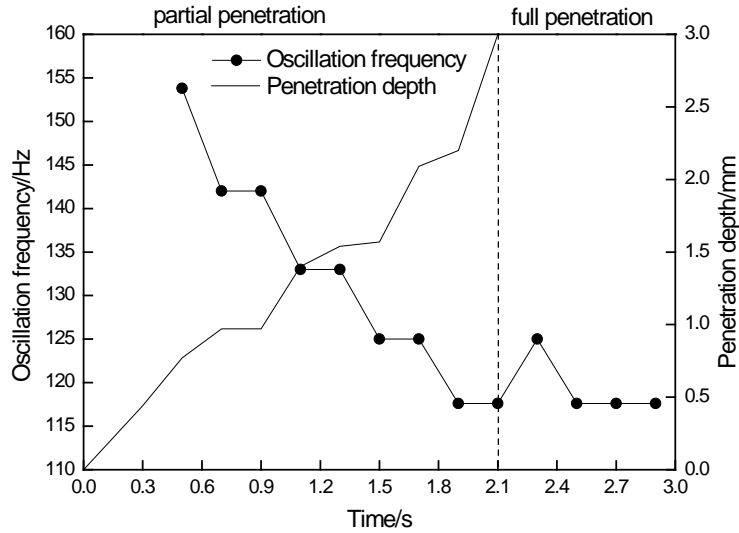


Figure 6-10 Oscillation frequency versus time

6.2.2 Experimental result

Pulsed GTA welding experiment was conducted and compared with simulation. The used weld pool sensing system is the same as in Figure 6-1. The difference is in the torch current. Although both used pulsed current, the peak current in this experiment is 150A, base current is 20A, the pulsed frequency is 5Hz and the duty cycle is 50%.

Figure 6-11 shows images acquired sequentially. From the images, one can clearly see the reflected dots. The pattern has been distorted by the specular weld pool surface. When the weld pool is concave, the dot matrix aggregates; otherwise, the dot matrix diverges as shown in Figure 6-12. By calculating the time interval between two aggregated or diverged picture, the oscillation period in weld pool can be obtained. The oscillation period at different time is shown in Figure 6-13.

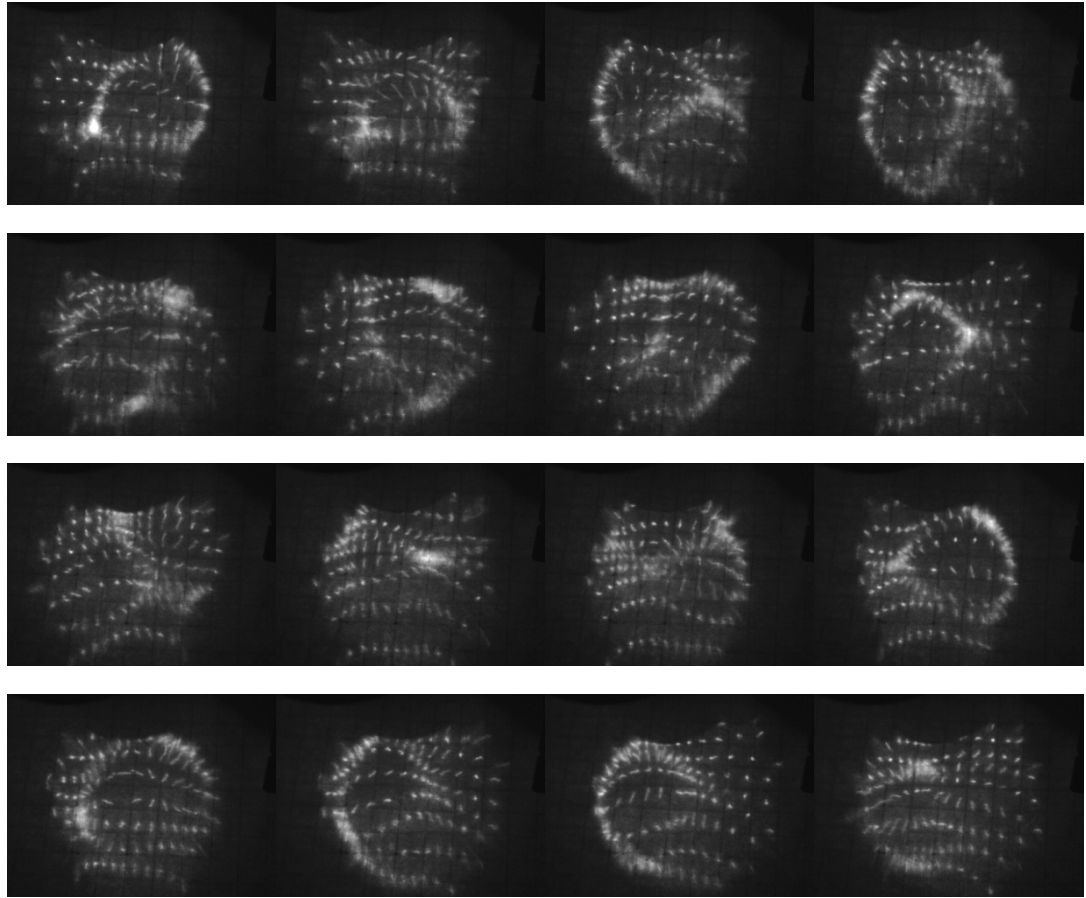


Figure 6-11 Acquired reflected images

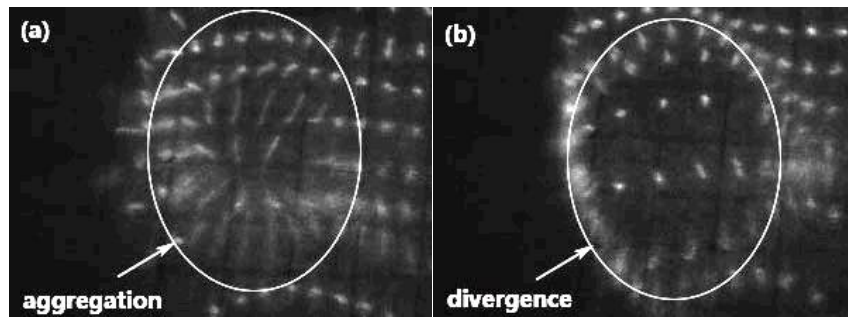


Figure 6-12 Oscillation mode.(a. weld pool is concave; b. weld pool is convex)

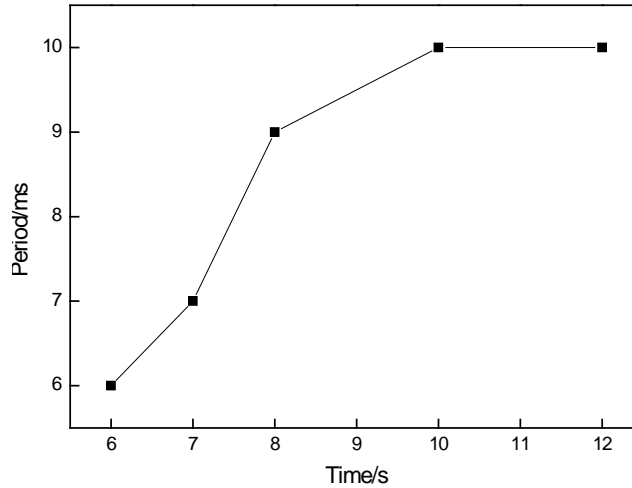


Figure 6-13 Oscillation period at different time

The experiment welding seam is shown in Figure 6-14. The lower row pictures in Figure 6-14 are the back side of the welds, and it is found that the weld pool is not fully penetrated until at 8s.

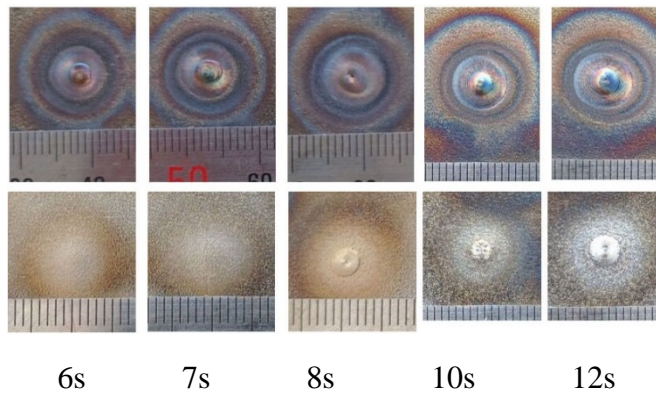






Figure 6-14 Weld morphology at different time

6.2.3 Discussions

Currently, some researchers used mathematic models to study weld pool oscillation. Xiao [20, 22, 29, 32, 61-63] classified the oscillation modes into the axisymmetric mode and the sloshy oscillation mode for partially penetrated weld pools were designated, and the axisymmetric oscillation mode for fully penetrated weld pools. In addition, the

different mathematical models were developed to describe the weld pool oscillation as shown in Table 6-2.

Table 6-2 Mathematical oscillation models for weld pools

				
Maruo-hirata	$f = \frac{1}{2\pi} \sqrt{(gk + \frac{\gamma}{\rho} k^3) \tan(kh)}$		$f = \frac{1}{2\pi} \sqrt{-\frac{2g}{H} + \frac{2\gamma}{\rho H} k^2}$	
	$k = 5.520(D/2)^{-1}$	$k = 3.832(D/2)^{-1}$	$k = 3.832(D/2)^{-1}$	$k = 2.405(D/2)^{-1}$
Xiao-den Ouden	$f = 5.84(\frac{\gamma}{\rho})^{1/2} D_{eq}^{-3/2}$	$f = 3.37(\frac{\gamma}{\rho})^{1/2} D_{eq}^{-3/2}$	$f = \frac{1.08}{D_{eq}} (\frac{\gamma}{\rho H})^{1/2}$	
Hu-den Ouden	$f = \frac{1}{2\pi} (\frac{\gamma}{\rho})^{1/2} (\frac{2N_1}{W_t})^{3/2}$		$f = \frac{1}{2\pi} (\frac{8\gamma}{\rho H})^{1/2} (\frac{N_b}{W_{avg}})$	
Barnett et al	$f = 3.16 \sqrt{\frac{8}{3} \frac{\gamma}{\pi m}}$	$f = 2 \sqrt{\frac{8}{3} \frac{\gamma}{\pi m}}$	Yoo-Richardson	$f = \frac{0.9}{D} (\frac{\gamma}{\rho H})^{1/2}$ $f = \frac{1}{\pi W_t} (2(2-\epsilon)(\frac{W_b}{W_t}) + (\frac{W_b}{W_t})^{-3}) (\frac{\gamma}{\rho H})^{1/2}$

Many researchers studied the weld pool oscillation in pulsed GTA welding. However different scholars obtained different results as shown in Table.3. In the table, the welding parameters and oscillation frequencies acquired by different researchers are listed. Because different researchers used different welding parameters, they obtained different oscillation frequencies. However, from the results, we can find the common trend, that is, when the weld pool changes from partial penetration to full penetration, the oscillation frequency drops dramatically.

Table 6-3 The weld pool oscillation frequency obtained by different researchers

	Sorensen[64]	Aendenroemer[30]	Ju JIANBIN[65]	Shi Yu[25]
Current/A	300/100	160/28	150-240/60-100	144/30-65
Material	A36	Fe360	T304	T304
Base material thickness/mm	9	3	2	3
Partially penetrated frequency/Hz	150-400	230		122-183
Fully penetrated frequency/Hz	38-188	200	15-60	31-62

The relation between the oscillation frequency and the weld pool diameter is illustrated in Figure 6-15. It shows that the oscillation frequency in the weld pool decreases as the weld pool width increases, which is in agreement with the research conducted by many people [63, 65].

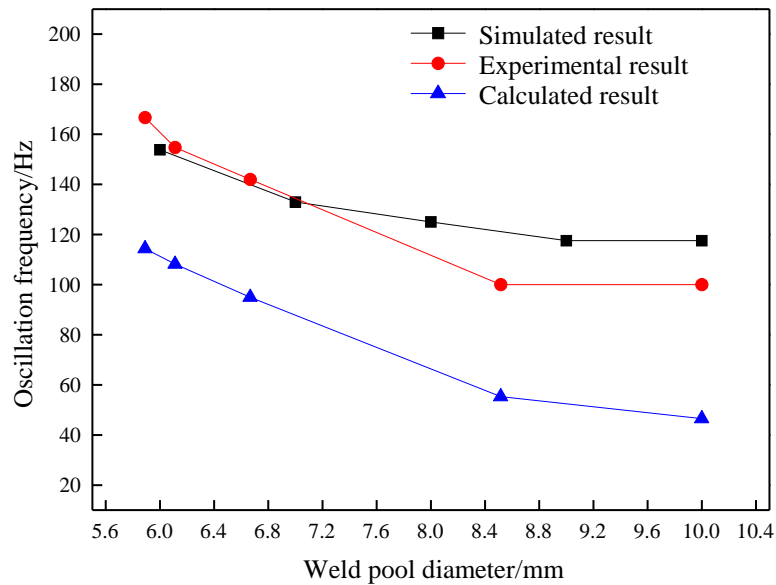


Figure 6-15 The oscillation frequency comparison obtained by theory, experiment and simulation.

6.3 Summary

- (1) The established model agrees well with experimental and theoretical results.
- (2) Before full penetration, the weld pool oscillation frequency decreases as the welding time increases. At the same time, the penetration depth increases with increasing welding time. When the molten pool is fully penetrated, the oscillation frequency stays the same.

(3) When the state of weld pool changes from partial penetration to full penetration, the oscillation frequency decreases rapidly. When the current changes from peak to base or from base to peak, the damping vibration has higher frequency than when the current is constant.

CHAPTER 7 The Grayness Variations of the Laser Dot Images in the Penetration Stages

As discussed in Chapter 2 section 2.3.1, current research is an extension of the vision-based weld pool penetration sensing technique. However, the technique discussed in 2.3.1 is complex and not fault-tolerant. Current research tries to find an alternative approach, but still uses vision sensing to acquire images.

In Chapters 5 and 6, some important characteristics of the weld pool in different penetration stages have been identified: (1). From simulation of the Volume of Fluid (VOF) model, the weld pool oscillation frequency is higher while the oscillation amplitude is lower in partial penetration than in full penetration. (2). It is also found from experiment that the overall shape of the imaged dot matrix light is changing in the two penetration stages. This is explained to be related to the change of the weld pool's curvatures in the two stages. The formation of the curvatures is due to the oscillation of the liquid weld pool. Although correlation between penetration stages and the oscillation characteristics has been found, i.e. oscillation frequency characteristics and the shape changes of the dot image array, this information is not easily utilized for feedback control to be discussed in Chapter 8. The oscillation frequency was obtained through simulation and currently no techniques have been developed to calculate oscillation frequency experimentally. Measuring the shape variations of the dot array images requires the ability to identify individual dots and their relative locations, and is difficult to achieve. Thus, a search for an easier and possibly better method leads to the identification of the

grayness variations of the images which are also caused by the oscillation of the weld pool.

7.1 Experiment Setup

The equipment used and the connections between the devices are the same as in Chapters 5 and 6. The schematic of the setup is shown Chapter 5 (Figure 5-1) and will not be repeated here. The experiment parameters are shown in Table 7-1.

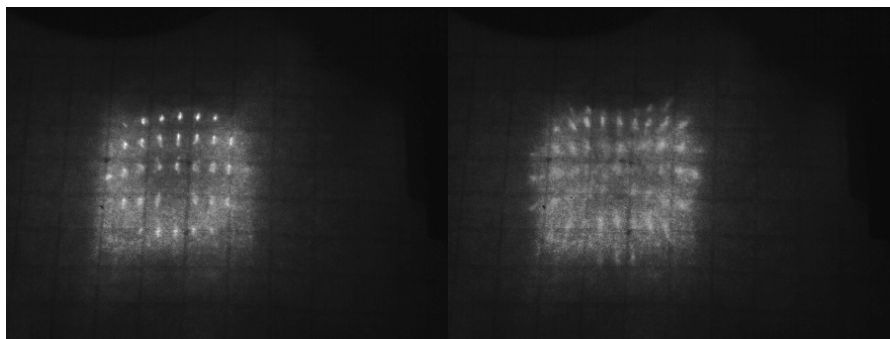
Table 7-1 Welding parameters

Parameter	Value	Unit
Material (Stainless Steel 304)	2	mm
distance from tungsten tip to workpiece	5	mm
Base period time	3-	ms
Base period current	20	A
Peak period time	22	ms
Peak period current	30-120	A
Shielding gas (Ar)	15	CFH
Backside shielding gas (Ar)	30	CFH

7.2 Experiment Approaches

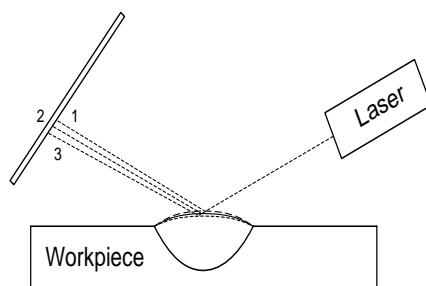
7.2.1 Observation of grayness variations and quantization of the pixel grayness

Experiment was conducted to capture the reflected images in the entire welding process. In this part of the experiment, the peak current is fixed at 80A, and the base current period is fixed at 3ms. By comparing the pictures, it is found that the grayness of the pixels is changing, as can be seen in Figure 7-1. (a) shows the dot matrix image in the early stage of welding when the pool is in partial penetration, while (b) shows the image in a later stage when it is close to full penetration (critical penetration). By comparing the two pictures, we can see that the dot images in (b) become fuzzy. The dots spread, especially those close to the center, and the brightness of each dot decreases.

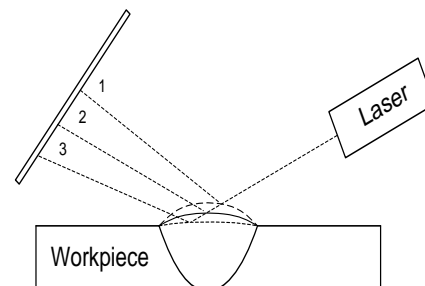


(a)

(b)



(b)



(d)

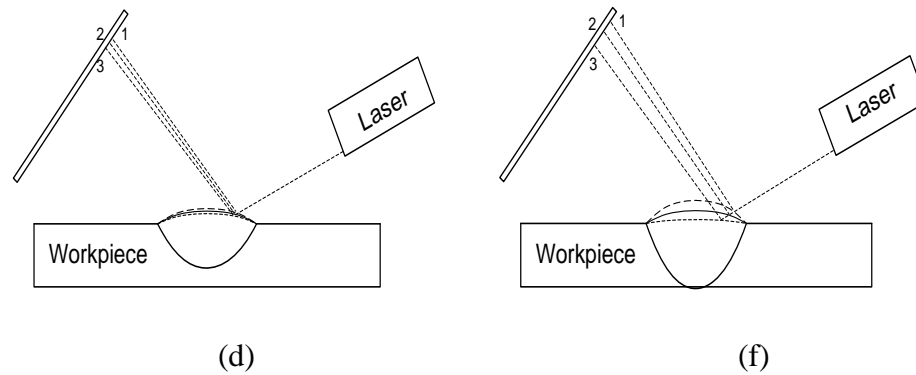


Figure 7-1 Image grayness variations in the different penetration stages and the schematic showing the imaging process while the object is moving

From photographic stand point of view, this could be that the camera moved. However, since the camera is placed on a fixture, this can only be explained by the movement of the weld pool. As discussed in Chapters 5 and 6, pulsed current leads to oscillation of the weld pool. Although oscillation exists in the entire welding process, in the early stage when the pool is only partially penetrated, oscillation is weak (amplitude of the oscillation is small) due to damping caused by the solid bottom of the weld pool. When full penetration is reached or about to be reached, the bottom of the weld pool is softened and can even reach liquid state. Correspondingly, oscillation is no longer hampered by the bottom, and damping is greatly reduced. Oscillation thus becomes stronger, i.e. the amplitude increases to a greater extent. This oscillation explains the fuzziness and the reduction in grayness of the imaged dots, as will be explained in the following paragraph. Figures 7-1(c) and (d) show the imaging process corresponding to one of the central dots in (a) and (b), while Figure 7-1 (e) and (f) correspond to one of the edge dots in (a) and (b).

In Figure 7-1(d) which represents imaging of the center of the weld pool, oscillation amplitude of the pool is fairly large due to full penetration. When the camera shutter just opens and the pool surface is at its highest, the reflected ray hits point 1 on the imaging plane. Then, the surface of the pool depresses as shown in the middle curve, and the same ray now hits on another point on the pool surface and is then reflected on point 2 of the imaging plane. While the shutter is still open, and the pool continues to depress, the ray now hits point 3 on the imaging plane.

Lumen describes the luminous power that a light source can produce in unit time. Since the same laser is used, Lumen (Φ_v) is a fixed quantity. Luminous energy (Q_v) is a product of Lumen and time, in this case, the exposure time:

$$Q_v = \Phi_v \times t \quad (7-1)$$

Because exposure time is fixed in this study (1ms), Q_v is a fixed quantity too. Illuminance is the luminous power incident on a surface of unit area, i.e.

$$E_v = \Phi_v / S \quad (7-2)$$

Where S is the area of the illuminated surface.

Rewrite Equation 7-2 as $\Phi_v = E_v \times S$, and substitute it into Equation (7-1), the following equation is derived:

$$Q_v = E_v \times S \times t \quad (7-3)$$

Since both Q_v and t are fixed, when the illuminated area S is increased, illuminance (E_v) decreases. Illuminance is the quantity that gives the impression of dimness or brightness depending on its values.

When oscillation amplitude increases, the same amount of luminous energy covers a wider area as shown in Figure 7-1 (d) compared to (c). Correspondingly, the illuminance decreases from Equation (7-3), and the brightness of the image decreases. This explains why the imaged dots in Figure 7-1(b) look dimmer than in (a). In addition, since the original laser dot light now spans on a wider area when it is reflected on the imaging plane, the image also looks fuzzier. In Figure 7-1(c), although we also see that the ray is reflected on an interval in the 2-D sketch rather than one point on the imaging plane, the interval it covers is much smaller than in (d), and thus the imaged dots are still fairly clear as shown in (a).

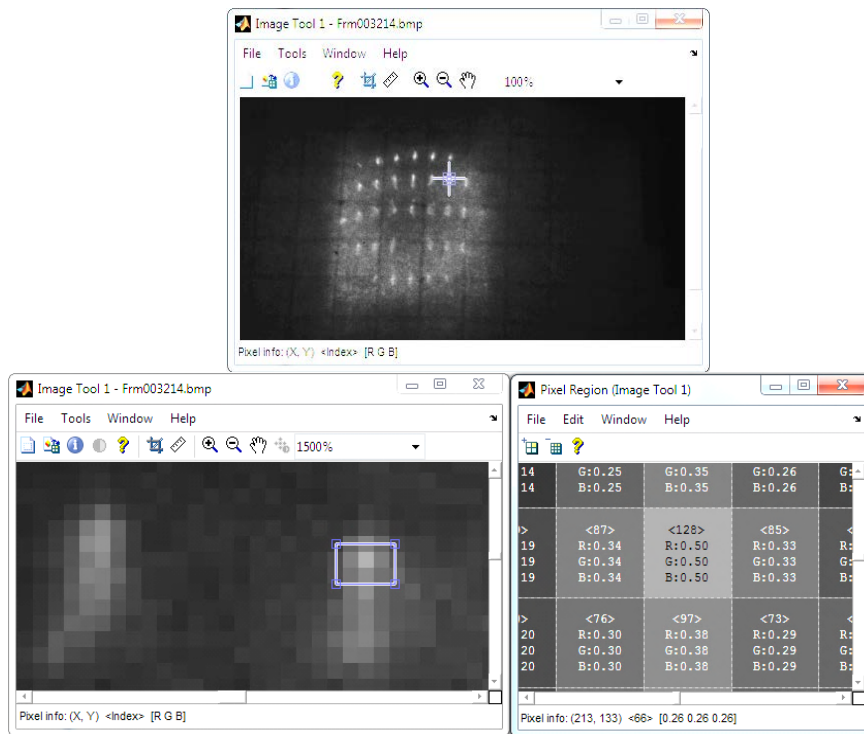
The edge of the pool is not affected as much as the center area. However, the edge of the pool is not fixed either; it oscillates with smaller amplitude. Figure 7-1(e) and (f) show the imaging process at the edge of the pool.

From the observation and the analysis, it appears that the grayness information of the reflected laser dot images is useful in identifying the penetration stages. However, to make use of it, method has to be found to quantify the grayness information.

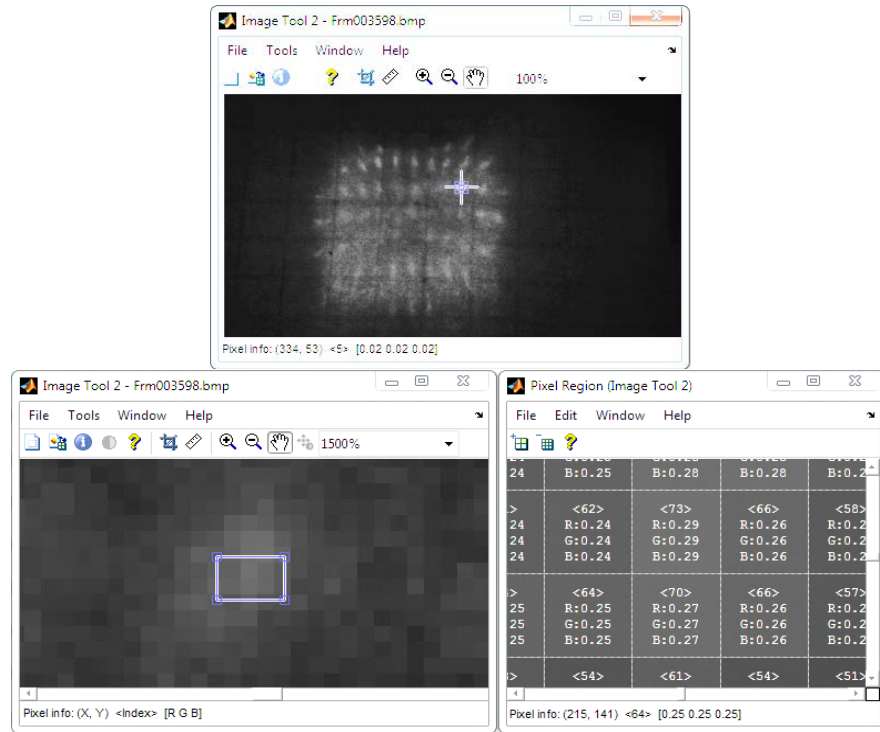
A picture is composed of many pixels. A pixel has its pixel value which describes how bright the pixel is. In black-and-white pictures, a pixel has only the grayness value which is an 8-bit integer in the range from 0 to 255. In colored pictures, a pixel has three components, red, green and blue. Each component has a value in the range from 0 to 255.

In this study, all pictures are black-and-white, and thus it considers only the grayness value.

In order to quantize the variations of the grayness information, the Imagetool package of Matlab is used to identify the grayness values of individual pixels, as can be seen in Figure 7-2.



(a) Partial penetration



(b) Critical penetration

Figure 7-2 Reflected dot images and their individual pixel's grayness value

In Figure 7-2(a), the top picture is the same as that in Figure 7-1(a). A dot image that is close to the center is highlighted by the crossbar. At the bottom, the left picture is the same as above, but is magnified so the highlighted dot image can be easily seen, which is composed of a few pixels. On the right picture, the pixel value arrays in the middle column are from those highlighted and shown on the left picture. We can see that the one pixel has highest grayness value than the neighboring pixels, with a value 128. The next highest value is 97. The other neighboring pixels have much lower grayness values. This agrees with visual observations on the left picture. The grayness variation information related with pool penetration and the ability to quantize the pixel grayness opens up new a direction to identify full penetration.

7.2.2 Quantization of the image grayness variations during welding

As discussed in the previous section, the grayness of the pixels that compose the imaged laser dots decreases as the weld pool is close to or is in full penetration. To make use of the information, we need to see how the grayness varies in the whole welding process, so that it can be used for later development of a feed-back control system.

In order to achieve this, a series of experiments are designed for different penetration stages and to obtain images. The only variable in these experiments is the welding times, which are 1s, 2s and 3s, respectively. Figure 7-3 shows the finished workpiece.



(a) Front view



(b) Back view

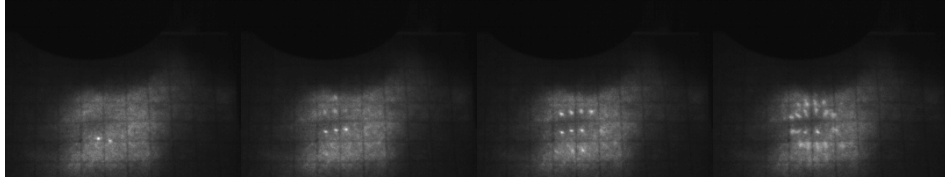
Figure 7-3 Surface appearances of the finished welds with 1s, 2s and 3s welding time

From Figure 7-3, it can be seen that with 1s welding time, full penetration is not reached since the bead is not visible on the back side of the weld. With 2s, full

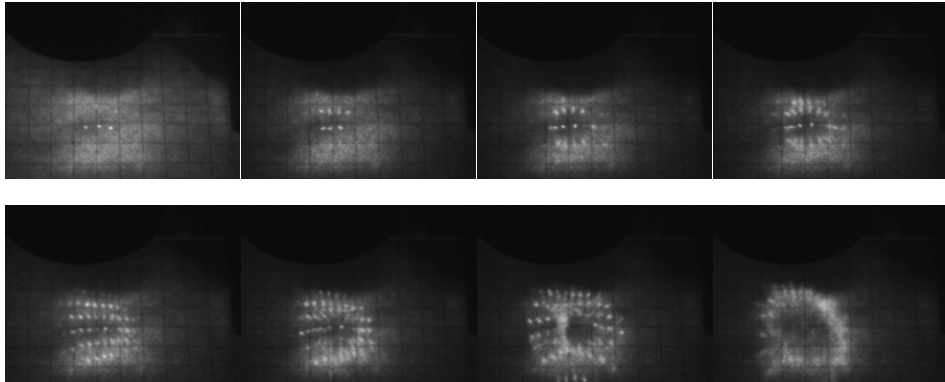
penetration is reached, and bead size is just right. With 3s, over penetration is reached since the bead size is a bit large.

For taking pictures of the reflected laser dots, camera exposure time is set to 1ms. The base current period is the time when pictures are taken. Base current is low (20A) as shown in Table 7-1 so that there is no strong arc light to interfere with taking pictures. The base current cycle is 3ms which allows three pictures to be taken in each pulsed current period. The total pulse current period is 25ms. In 1-second welding, $3 \times (1000/25) = 120$ pictures will be taken in base current period time. 2-second welding will allow 240 pictures and 3-second will result in 360 pictures in base period time. With so many of them, it is a waste of space to show them all. To show the welding process in terms of imaging, one is selected of each 10 continuous periods, and the result is shown in Figure 7-4.

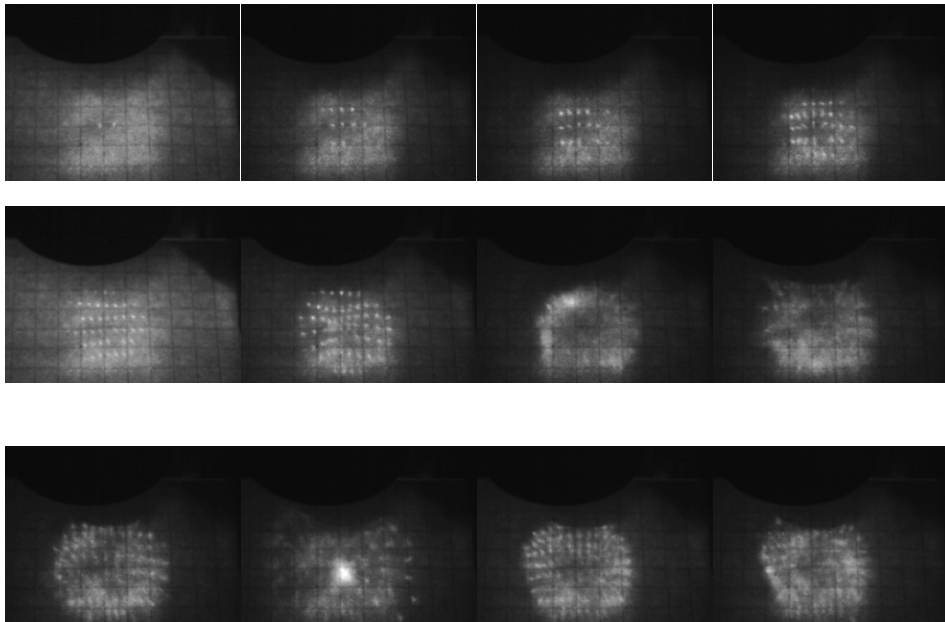
From these pictures, we can identify the evolution and oscillation of the weld pool through the change of the imaged laser matrix dots. During early stages of welding when the weld pool just forms, only few laser dots are reflected on the image plane. As welding continues, the weld pool becomes larger, and more imaged dots are visible. This is true for all three experiments. Another phenomenon is that in later stages of welding, the arrays of laser dots are curved. However, the curvature is more pronounced in 2s and 3s welding than the 1s welding, since oscillation amplitude increases as the size of the weld pool increases. Another observation is that when full penetration is reached, some of the pictures show one very large and bright spot, as can be seen in (c). This can be explained in Figure 7-5.



(a) 1-second welding



(b) 2-second welding



(c) 3-second welding

Figure 7-4 Captured images displaying the evolution of welding

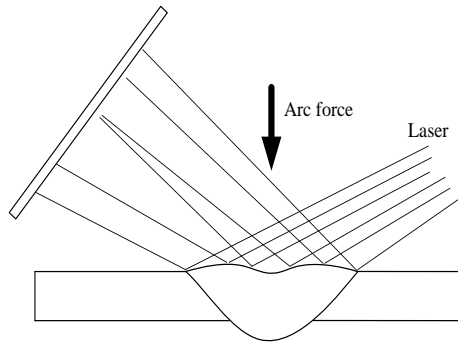


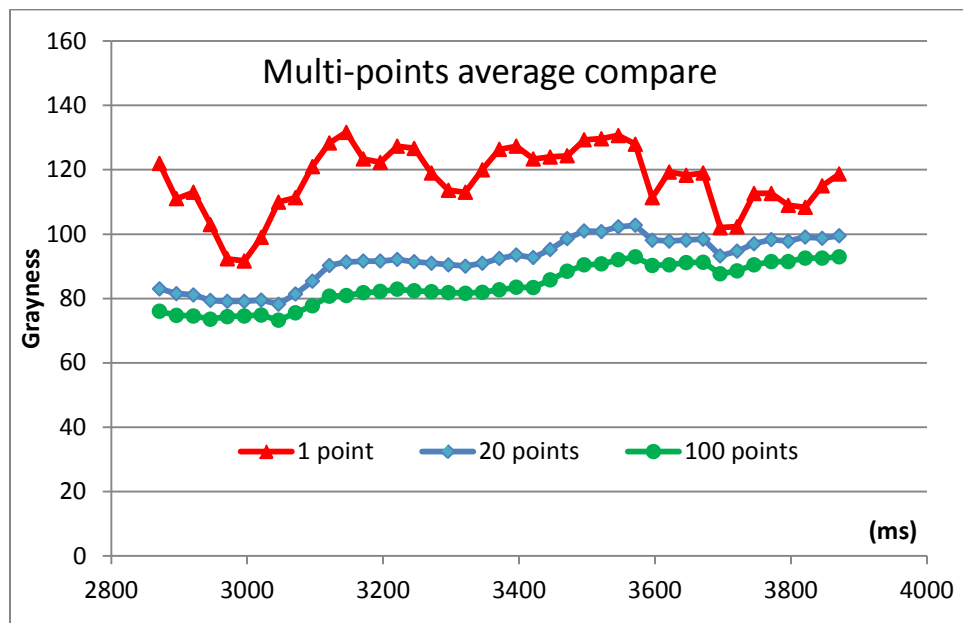
Figure 7-5 Concavity of the weld pool surface in full penetration leads to convergence of the laser rays

As shown in Figure 7-5, after full penetration is reached, the bottom of the weld pool is no longer supported by solid back, some areas of the pool surface can depress more, which leads to the concave sub-region. When a few laser rays hit the concave region, and are reflected, these rays converge and can form one big bright spot on the image plane. This is why such a bright spot is observed in the 3-second welding. As long as full penetration is reached, and the welding time is long enough, concavity of the pull surface will be reached at some point due to oscillation. Thus, the large bright spot will be formed. When the surface changes shape, the spot will disappear. When a large bright spot appears, it usually indicates over penetration, as is the case in this experiment, where 3-second welding causes over penetration.

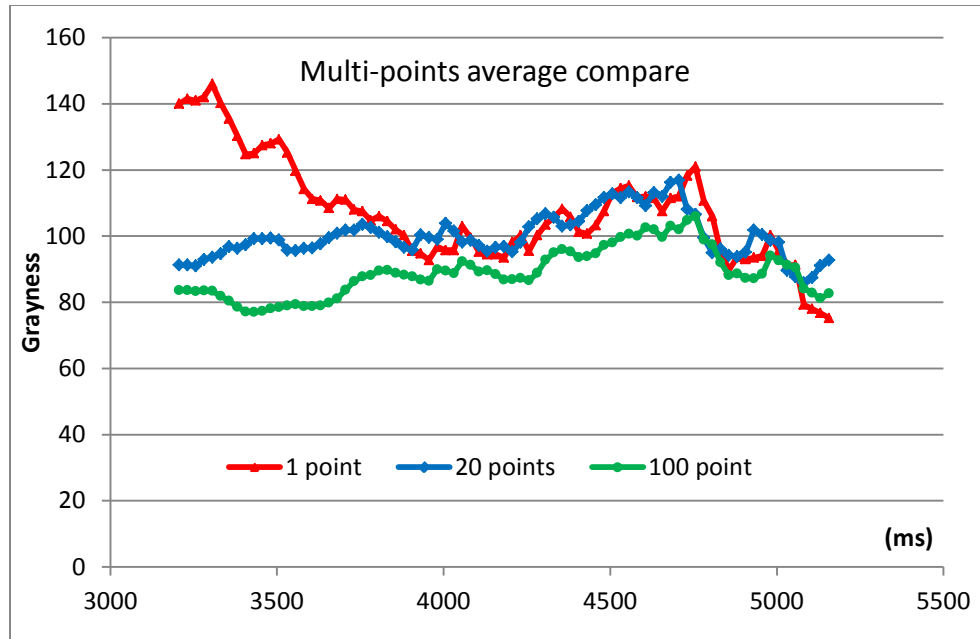
The above analysis indicates that if we capture the evolution of the image grayness, it is likely to be able to identify when full penetration is reached. In order to do this, we can use the pixel value that is the largest of all pixels in each picture to represent the grayness in that welding instant, or we can average the grayness of the first few brightest pixels and use it to represent the grayness. The first instinct is that using only one pixel value is

not a good representation of the grayness at any instant. This is because like any experiment, welding process has variations. Using one point to represent the whole picture is likely to miss a lot from reality. The simplest common practice in doing experiment is usually to average from many data points. However, averaging all pixel grayness values of a picture is not a wise choice either. This is because the camera's exposure time is fixed, and thus the lumen that enters the camera is fixed regardless of whether the pool is fully penetrated or not. If we average over all pixels, we will get a flat line, i.e., there is no variation in grayness in the entire welding process.

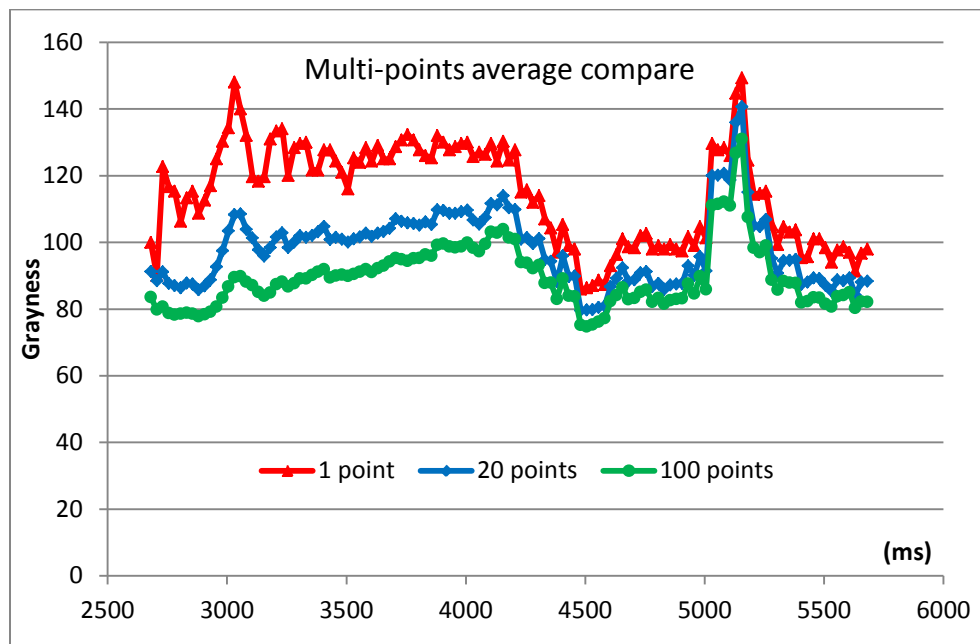
In finding the best representation of the image grayness at any instant, experiment is carried out to vary the number of points used for averaging, and these include 1 point, 20 points and 100 points. The results are shown in Figure 7-6. Figures (a), (b) and (c) correspond to 1-second, 2-second and 3-second welding, respectively.



(a) 1-second welding



(b) 2-second welding



(c) 3-second welding

Figure 7-6 Grayness variations with welding time with different number of pixels for averaging

As can be seen in all three sub-figures, when using only one pixel value to represent the whole image at one instant, the variation is quite large and the overall line is above the others. The large variation cannot represent the evolution of the weld pool. As we can see from Figure 7-4, as welding is in early stage, there are only a few imaged dots, and the overall grayness is small. As welding continues, weld pool expands, and grayness increases too. When the weld pool is close to full penetration (critical penetration), the overall grayness is decreased due to the strong oscillations. Thus, the grayness plot over welding time should show slow increase during partial penetration and then an obvious decrease when critical penetration is reached. Using one point to represent the entire image, we see a lot of ups and downs in the plotted curve, which cannot represent the observed phenomenon.

When using 100 points for averaging, the curves look rather flat, which can be understood from previous explanation, i.e., the total amount of luminous energy is fixed regardless of which penetration stage the pool is in.

When using 20 points for averaging, it captures the behaviors well. Grayness starts to increase over a long period of time, when the first peak is reached, it starts to decrease more abruptly. After a certain amount of decrease, the curve can become irregular, meaning that it can have sharper peaks (large grayness), or sharper valleys at any time. This irregularity is due to the fact that over-penetration is reached. When the weld pool is in over-penetration, its surface is more freely to move without the constraint at the bottom. Correspondingly, its surface can reach higher concavity or convexity during oscillation than in partial penetration. When the surface is much concave and the area is larger, more light rays hit the concave surface, reflected and converged on a large spot on

the image plane. This leads to a very bright spot in the image, as shown in Figure 7-4 (c). On the contrary, when the surface is much convex, light arrays are scattered over a wider area on the image plane. The overall effect is that the image looks dimmer. Selecting and averaging the pixel grayness values will end in a lower grayness value, thus a sharp valley.

When comparing the 20-point averaging results in Figure 7-4(a), (b) and (c), it can be seen that with 1-second welding, since full penetration is not reached, no sharp decrease in grayness is observed. With 2-second welding, the sharp decrease in grayness is visible. With 3-second welding, not only is there the first sharp decrease following the continuous slow increase in grayness, there are sharp increases and decrease after the first one. This grayness evolution information can be used for the feedback control system design that will be discussed in the next chapter.

7.3 Ranges of Applicability

The applicability ranges of the image grayness method refer mainly to the current ranges, in terms of both the peak current values and the base current period. The applicability ranges of other parameters are considered in this study since current is the most important and has the biggest impact on the welding process.

As discussed earlier, the grayness method takes advantage of the image grayness patterns that is generally repeatable in the welding process. Specifically, the grayness increases in the early stages of welding until it encounters the first peak. After that, it starts to decrease. The first peak value should be considerably larger than the subsequent valley to be considered a real first peak. After the first peak, the grayness can have a few

peaks, but are usually irregular. These later stage irregular peaks are associated with the formation of concave pool surface when the pool is fully penetrated. This can occur very randomly, which accounts for the irregularity of the peaks both in terms of the shape and in terms of time. However, this irregularity that occurs in full penetration is not of particular interest in this study. The focus is on the detection of the first peak, since that is an indication that critical penetration is about to occur.

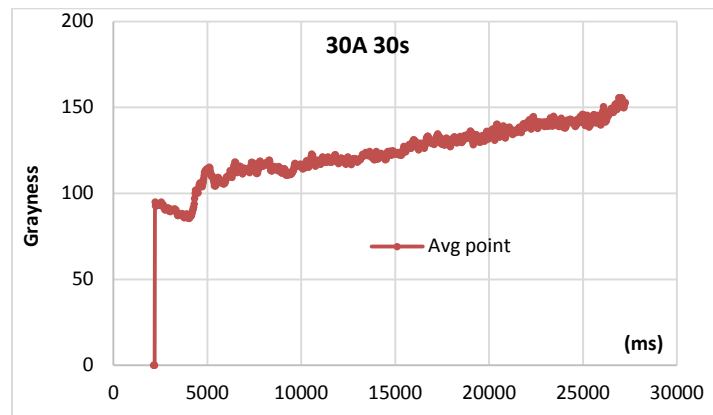
In order to find that under what peak current range the first peak can occur, experiment is conducted by varying the peak current values. As shown in Table 7-1, peak current ranges from 30A to 120A. The grayness results are shown in Figure 7-7. In (a), with a peak current of 30A, the first peak never occurs during the entire welding time. This indicates that full penetration never occurs in this case. It is possible that given enough time, full penetration will eventually appear. However, if the heat absorbed by the workpiece from the welding torch is equivalent to the heat dissipated, weld pool may not grow large enough to reach full penetration. Thus, a current of 30A is not enough.

As the peak current is increased to 40A, the first grayness peak occurs with a value of 155 at the welding time of 10s. With subsequent increases in peak current, the first grayness peaks are more pronounced.

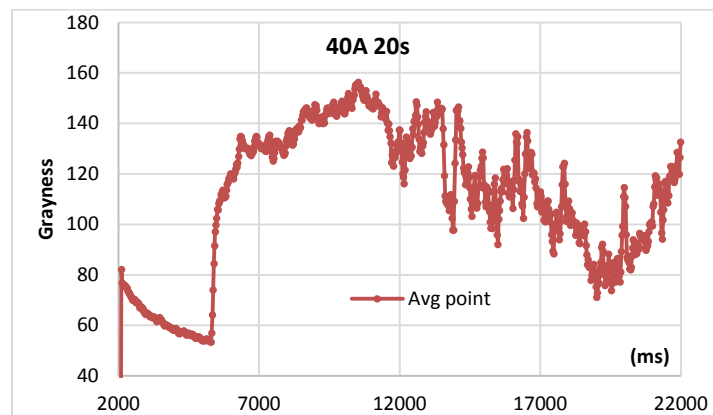
When the peak current reaches 120A, the first peak that indicates the partial penetration (which is close to critical penetration) does not occur. Separate experiment has shown that under such high peak current, full penetration occurs at about 2.5s. However, from Figure 7-7 (j) there is no observable peak at 2.5s. Since it is hard to

identify the first peak at this current, the grayness evolution cannot be used for further dynamic control of the welding process.

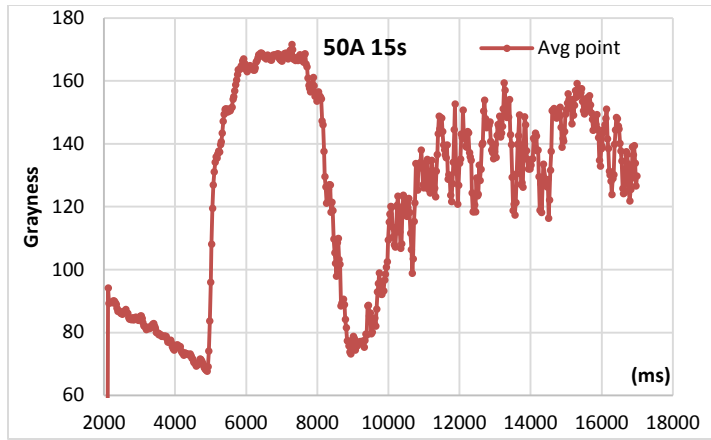
From the results and analysis, image grayness is greatly affected by welding current. With too low or too high current, the normally observed peak pattern disappears. Thus, in this study, the range of peak current has to be limited to between 40A to 110A.



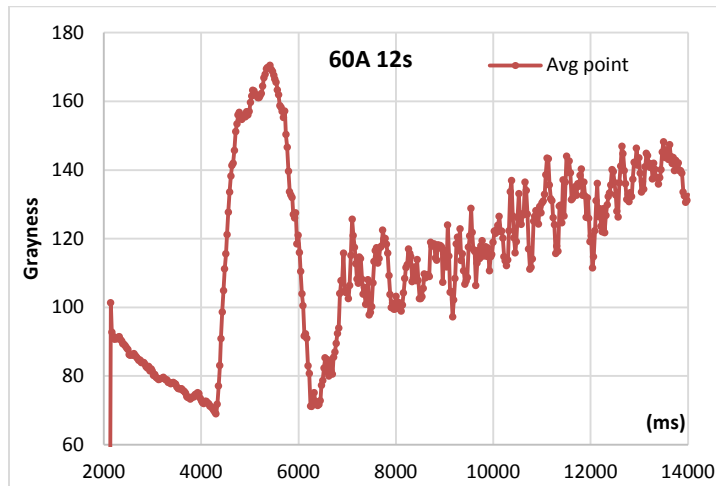
(a) Peak current = 30A



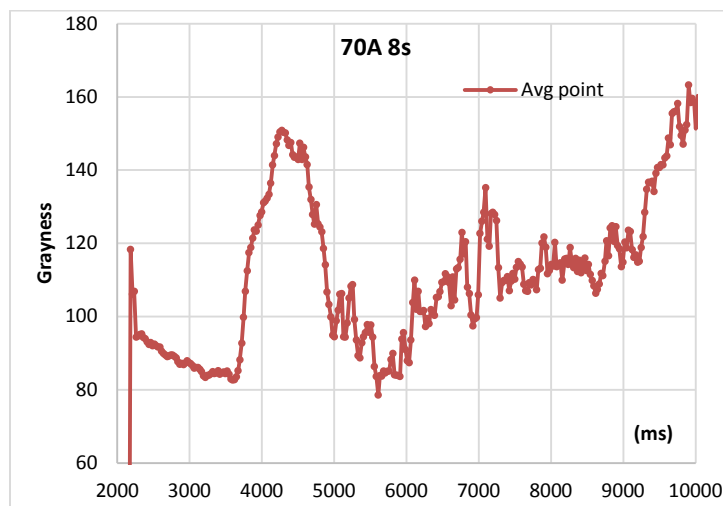
(b) Peak current = 40A



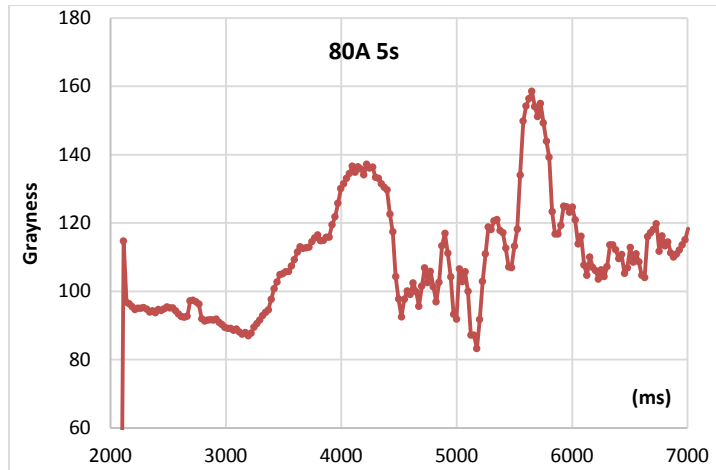
(c) Peak current = 50A



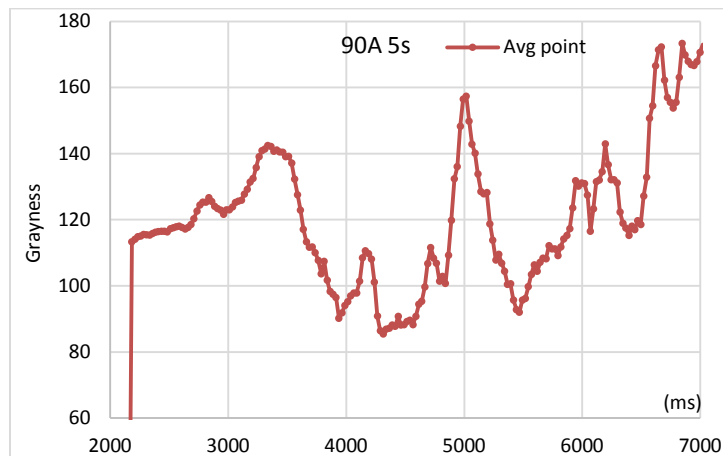
(d) Peak current = 60A



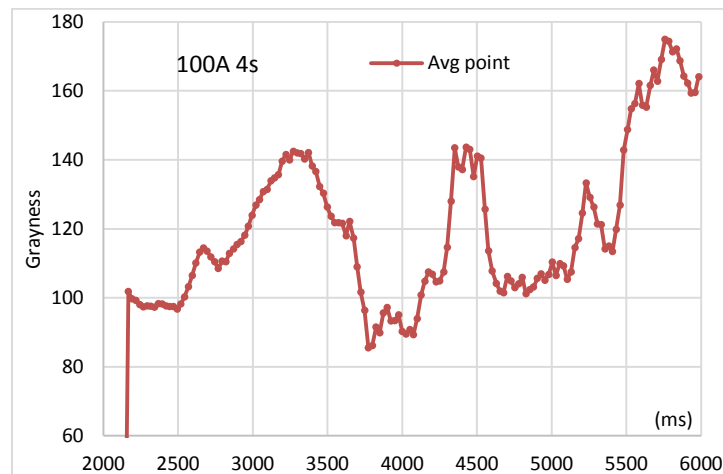
(e) Peak current = 70A



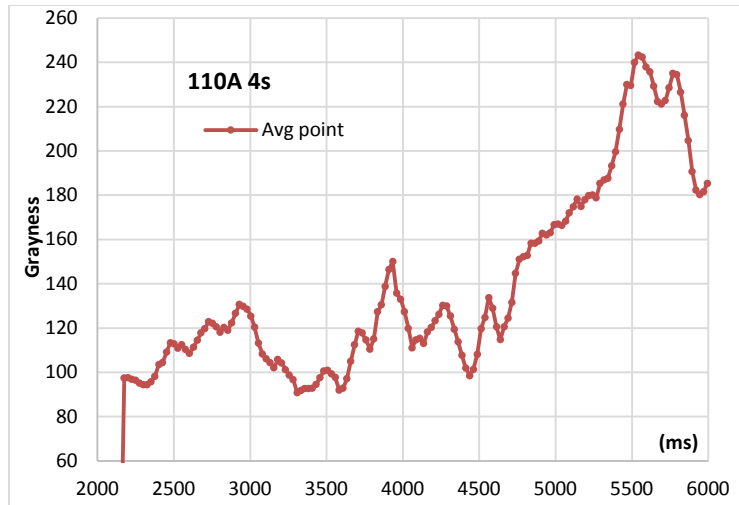
(f) Peak current = 80A



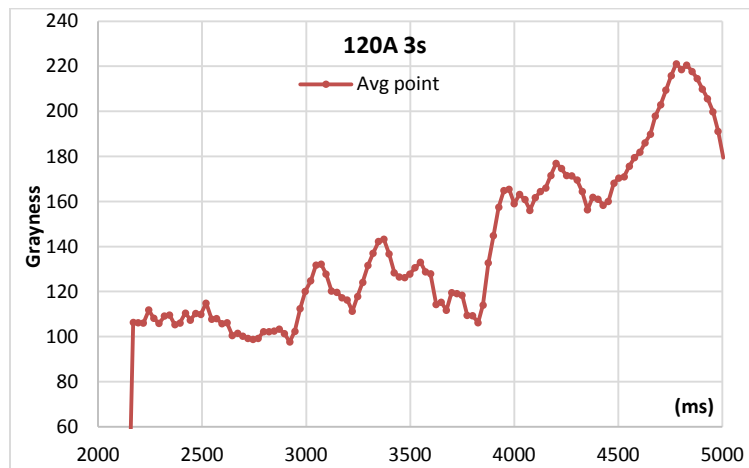
(g) Peak current = 90A



(h) Peak current = 100A



(i) Peak current = 110A



(j) Peak current = 120A

Figure 7-7 Comparison of the grayness variations between different peak welding current.

The base current period also affects the grayness pattern. This is because the used camera can take only one picture per mini-second. This basically sets lower end of the base current period, which is 3ms. During the 3ms period, three pictures can be taken. However, when the first picture is taken, instruction has just been sent to lower power supply. During this gray period, the torch current may still be high. As we know, high

torch light interferes with imaging. On the other hand, when the third picture is being taken, instruction is also sent to increase torch current. During this time, torch light can become strong, and thus affect the picture taken.

Generally speaking, longer base period time does not adversely affect imaging. However, setting a too long base period makes welding too slow, which is not efficient. Overall, base current period cannot be lower than 3ms, but can be as long as desired.

7.4 Summary

(1) The weld pool penetration stages can be identified from the evolution of the image grayness.

(2) In early stages of welding, the weld pool is small, and only a few laser dots are reflected specularly. The overall grayness of the image is small.

(3) When the pool size increases significantly, but critical penetration has not been reached, and thus oscillation is small. There are many reflected laser dots, but due to the small oscillation, each reflected dot is bright and clear. The overall image grayness is high.

(4) When critical penetration is reached, oscillation is much stronger. Correspondingly, the reflected dots are spread, dim and fuzzy. The overall image grayness decreases.

(5) When full penetration is reached, oscillation is very strong and irregular. Correspondingly, very large and bright spot can form on the imaging plane, or the entire image can become dim.

(6) The ranges of the applicability of the grayness method are 40A to 110A for the peak current. For the base current period, it only has a lower limit of 3ms.

CHAPTER 8 Feed-Back Control Using Grayness

Variations of the Laser Dot Image

As has been discussed in Chapter 7, the grayness evolution during welding contains information about partial penetration, critical penetration and full penetration. If this information is used in designing a feedback system to control welding process, issues such as under-penetration and over-penetration can be avoided. This is the purpose of this chapter.

8.1 The simple feedback control system design

From Figure 7-6(c) in Chapter 7, we observed that before critical penetration is reached, the grayness increases to a peak value. After the peak, grayness reduces at a faster speed than the increase. From experiment, at about 20-30% decrease, the critical penetration is reached. From that time on, the grayness variation becomes irregular. This information will be used in designing a feedback control system.

Designing such a system involves writing a computer program that can detect the peak, and then find out the 25% reduction from the peak. When that point is identified, the program determines how long welding current will continue to be supplied until it turns off the current. As a first attempt, the feedback control is run only for stationary welding, i.e. there is only one spot on the workpiece to be welded. If this proves to be effective, the feedback control can be improved to run on traveling welding, i.e. welding is continued

on a series of continuous locations on the workpiece. Figure 8-1 is the flow chart of such a feedback control.

Before welding starts, the program sets the welding and the camera parameters. The welding parameters are the same as in Chapter 7 Table 7-1. The camera parameters include the exposure time (1ms) and the size of an image (384x288 pixels). The selected image size is on the lower range of the available sizes in order to ensure that the time spent on transferring the images to the computer is as short as possible. Indirectly, it also allows smaller exposure time, which is desirable. However, the minimum available size is not selected, because a too small size cannot guarantee that the entire laser dot matrix can be imaged on the imaging plane.

After the camera and the welding parameter setting, the program starts the welding current. Since peaks and valleys (base) of the pulsed welding current as well as their elapsed time are controlled by the program, it knows when the pulsed current is at its base value. Thus, when the pulsed current enters its base period, it starts the camera, and then collects images from the camera. When pulsed current is high again, the program starts image processing. This process repeats until full penetration is reached.

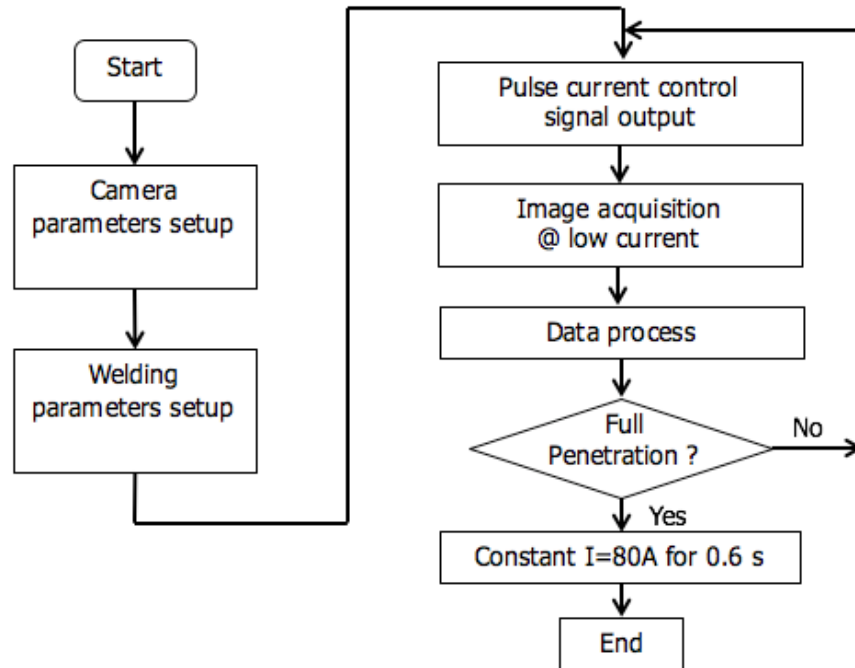


Figure 8-1 Flowchart of the feedback control for stationary welding

For each image collected, the program sorts all the pixels in terms of their grayness in descending order, select the first 20 pixels with the highest grayness values, and average these pixels as the grayness of this image. In order to further reduce noise, the grayness values of every five continuous images are averaged again as one grayness point on the grayness vs time curve. For example, if there are 10 grayness values from 10 images (1,2,3,4,5,6,7,8,9,10 represents the ordered images), grayness values of images 1 to 5 are averaged as one grayness point, then grayness values of images 2 to 6 are averaged as one grayness point, grayness values of images 3 to 7 are averaged as one grayness point, and so on.

After the program calculates one grayness point, it compares it with the previously selected peak grayness point, if the current grayness value is greater than the peak value, the current becomes the peak; otherwise, the peak stays the same. In addition, it also

checks if the current grayness is 25% smaller than the peak. If it is, then it considers that the critical penetration point has been reached. Usually for grayness points that occur after the first observed peak, it will take 10 to 20 grayness points to reach the 25% decrease, that is, 10 to 20 images. After the critical penetration point is found, the program switches the pulsed current to a constant current that has the same value as the peak value of the pulsed current. The constant current stays on for 600ms to ensure that full penetration is reached.

Figure 8-2 shows the variation of the grayness with welding time. The peak point has a grayness value of about 135, and the critical penetration point at the end of the curve has a value of 101.2. Unlike Figure 8-6(c), the curve ends at the threshold point. This is because no image is taken after the threshold point since the current is switched to constant current (peak value in pulsed current) and strong arc light due to the constant current overshadows the laser dot matrix light.

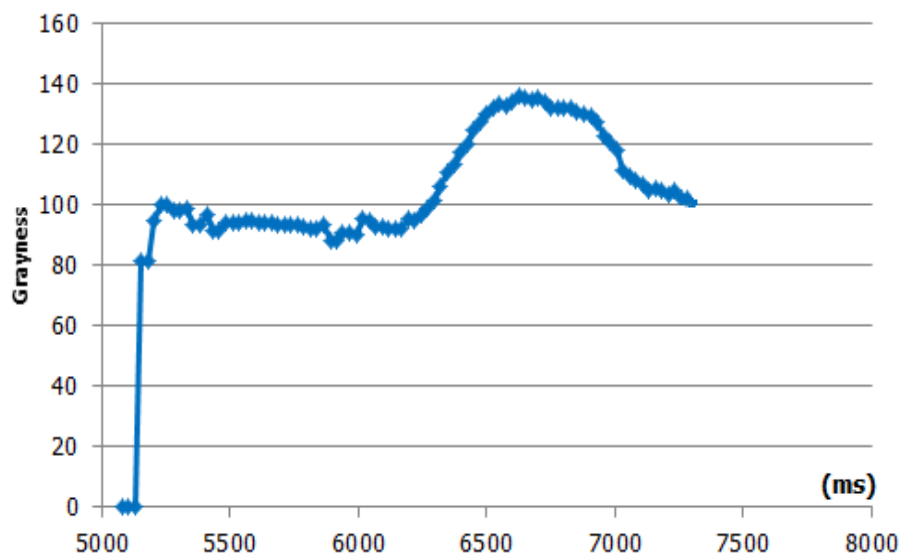


Figure 8-2 Grayness variations with time using the simple feedback control

The raw point is the calculated grayness value for each image, and the averaged point is the averaged grayness values of five continuous images, as explained previously. As can be seen, averaging reduces the noises in the curve plotted with raw points.

Figure 8-3 compares the front and back of the finished workpiece between the controlled welding and non-controlled welding. The bead surface pictures for non-controlled welding are from Figure 8-3 where welding was performed one second and three seconds. As we can see, with uncontrolled welding (a) and (c), the weld pool either reaches partially penetrated only or is over-penetrated. It takes trial-and-errors to obtain the perfect full penetration, which is not desirable. With a feedback control system, no trial-and-errors are needed to find the right penetration, as can be seen in (b): the weld pool reaches full penetration, but it is not overly penetrated. Another disadvantage with non-controlled welding is that if the welding parameters are changed (e.g., peak current value, peak current period), another set of trial-and-errors have to be attempted to find the right penetration.

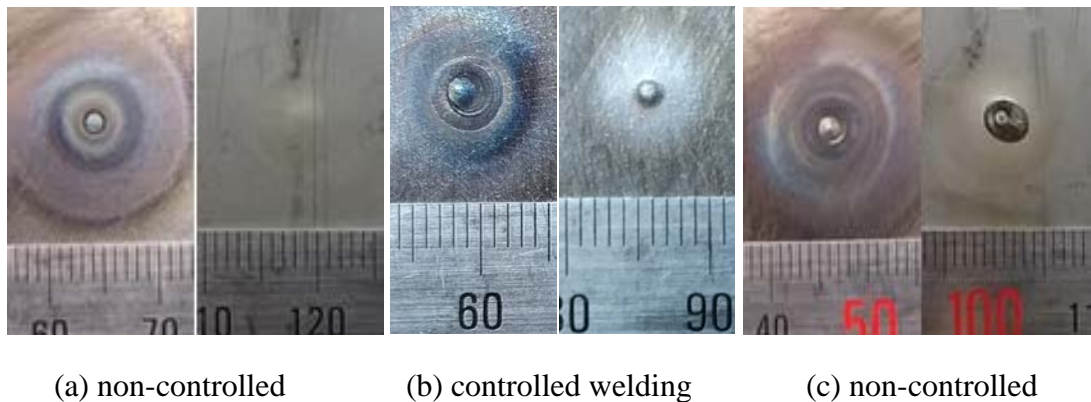


Figure 8-3 Weld beads comparison between controlled and non-controlled welding

With the desirable results from the first attempt to use feedback control, it looks like that using feedback is the right approach. To improve on this, the control system can be optimized to take into account continuous welding, and this involves in only slight change in the control system from above. Continuous welding is how welding is usually performed. The flow chart for continuous welding is shown in Figure 8-4.

The flow chart for continuous welding is very similar to that of stationary welding. The difference is that when one spot is finished, the control system instructs the robotic arm to move the welding torch to the next location. At the same time, the control adjusts the torch current to the base value, i.e. 20A and holds it for 1s to ensure that welding will not start until the torch has been move to above the new location. For simplicity, the flow chart in Figure 8-4 does not take into account the number of welding spots to be welded, and thus no decision block to show when the process will finish.

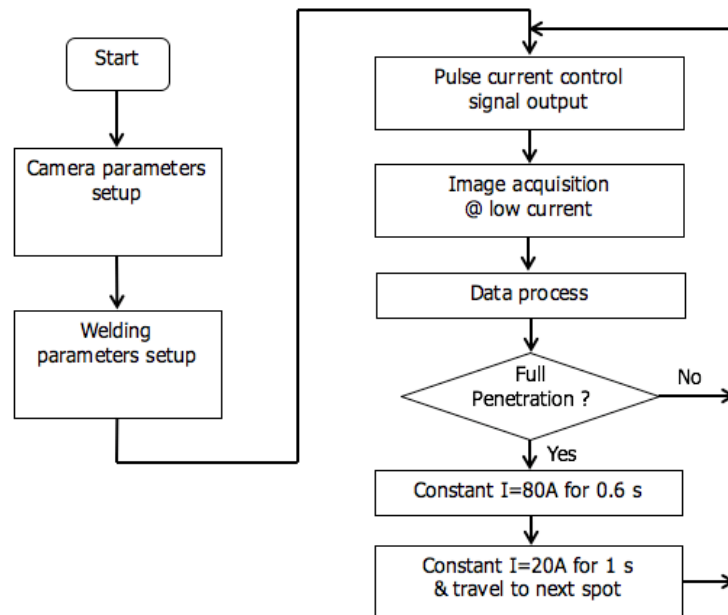


Figure 8-4 Flow chart of the feedback control in continuous welding

Figure 8-5 is the plot of the grayness over welding time. The real peak is where the first peak occurs while welding each spot. The T-point is the threshold point where the critical penetration is reached.

When welding just starts, the weld pool is far from formed, so there is no mirror-like surface to induce specular reflection of the laser matrix dot light on the workpiece. Reflection is diffused, and the reflected light on the image plane is uniform and overall dim. This accounts for the flatness of the curve and the low grayness values from about 3000ms to about 4300ms. From 4300ms on, the weld pool is formed, but it is still small at first. As the weld pool increases in size, more laser dots are reflected, and thus the grayness starts to increase. At the peak grayness, most laser dots are reflected and imaged. After that, due to increased oscillation, grayness starts to decrease until it reaches the threshold value which indicates that the critical penetration is reached. From that point on, current is low, so welding is temporarily stopped in order for the torch to travel to the next location.

In continuous welding, a weld bead is required to overlap with its neighboring beads to make sure the stress is uniformly distributed and the seam has enough strength. Non-uniform stress in the finished workpiece can cause crack and other issues. However, overlapping has its problems as can be seen in Figure 8-5. Figure 8-5 shows seven peaked regions corresponding to the seven spots that are welded. The first region is very much like the stationary welding result as shown in Figure 8-2. It shows the grayness variations associated with the first spot welded. For the rest of the regions, the starting points (e.g. B, C, D, E, F and G) are usually much higher than the starting point (point A) of the region corresponding to the first welded spot. The much higher values of these starting points

are thought to be related to the fact that the rest spots are welded by overlapping with the previous spots. More detailed explanation can be seen from Figure 8-6, as well as from the following paragraph.

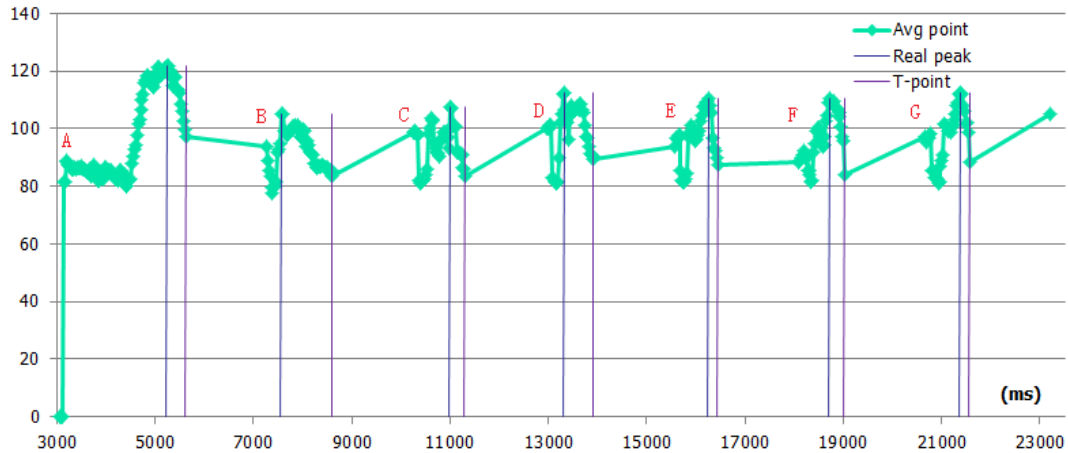


Figure 8-5 Variations of grayness over welding time in continuous welding

As shown in Figure 8-6 (a), after the previous spot (i.e. the pool shaped area in (a), and also the left ones in (b) and (c)) is finished welding, the torch travels to the next spot. The pool in the previous spot starts to solidify. At the same time, there is still base current applied on the torch. Although much lower than the peak current value, it still has some effect on the weld pool of the previous spot. The dotted line that starts from the torch and ends on right corner of the previous spot represents the arc exerted by the base current. The arc, although not as strong as the peak current arc, can keep part of the previous spot in liquid state. However, pool oscillation in the previous spot is not as strong as before, and thus laser matrix dots reflected by it are imaged clearly (not fuzzy) on the imaging plane. This explains the higher starting grayness values in the rest of the welding spots.

In Figure 8-6(b), the peak current is now applied on the torch again, and the pool on the current spot will begin to form. The previous pool in the overlapped region flows to

the current spot, and this causes oscillation. The oscillation leads to decrease in grayness of the imaged laser dots. After a while (Figure 8-6 (c)), the effect from the previous pool disappears, the grayness variation is like in the stationary welding again.

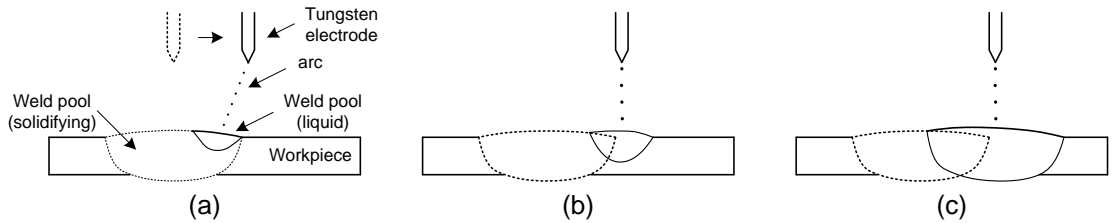


Figure 8-6 Explanation of the grayness variation behaviors in continuous welding

Although there are oscillations (a few ups-downs in the peaked regions in Figure 8-5 after the first one) in the grayness curve in the rest of the peaked regions in the continuous welding, the simple feedback control can still detect the real peaks and the subsequent threshold points (as marked with vertical lines). Consequently, in continuous welding the simple feedback control performs well, as can be seen in Figure 8-7. In Figure 8-7, the bead is uniform on both the front and back sides. There is no partial penetration, or over-penetration.

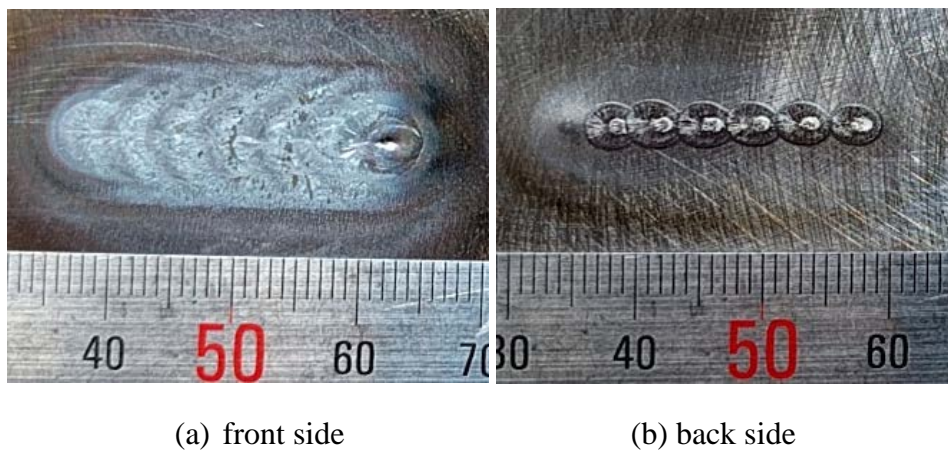


Figure 8-7 The bead surface appearance in continuous welding

Although the simple feedback control works well in both stationary and continuous welding, it has no control on how long the welding process can take. It passively detects the threshold point after the first peak at each welding spot. Only when the threshold point is identified, it then regains control on how long the process can continue on the current welding spot; it uses a fixed amount of time for attaining full penetration.

In order to have more control over the welding process, a better control method has to be found. This is how the Model Predictive Control method is considered. More detailed discussion about designing the feedback control system in this research using this advanced method is in Section 7.2.

8.2 The Model-Predictive-Control feedback system design

8.2.1 Review of model predictive control

Model predictive control (MPC) is an advanced method of process control that has been in use in industries since 1980s. It builds dynamic models of the process, and the models are often in linear mathematic forms obtained by system identification. Its main advantage is that it allows the current timeslot to be optimized, and at the same time keeps future timeslots into account. It does this by optimizing a finite time-horizon, but only implementing the current timeslot. The basic idea of MPC can be summarized in the following steps:

1. Deciding on the type of the dynamic incremental model to be used, most often a linear model will satisfy the needs.

2. Predicting the system outputs k -steps ahead ($k=1,2,\dots,N$) using the dynamic incremental model.
3. Creating desired trajectories for the output signal(s) of the system to transmit from their current values to the desired values.
4. Deciding on a cost function using the squared differences between the predicted output and the desired output for N steps in the future.
5. Solving for the parameters of the model by minimizing the cost function.
6. Using the model in the feedback control to achieve the desired result.

8.2.2 MPC model development

One of the purposes of this research is to achieve full penetration in a pre-specified welding time. Thus, this welding time is a variable that can be changed to suit the user's needs. The feedback control designed in section 7.1 cannot fulfill this requirement since it has no control of when the critical penetration is reached. With MPC, it can set up a goal (the desired result) and adjust the input (in this case the welding current) to approach the desired result. Thus, using MPC is a good choice in achieving this purpose. Figure 8-8 illustrates how MPC works.

A desired output (Y_d) is specified. A model is built that takes the desired output and the measured output as inputs, and minimizes the difference between the desired output and the measured output: A cost function is set up in the model. By minimizing the cost function, the model calculates the input ($u(t)$) that satisfies this. This input becomes the new input to the real system. The important part in building the MPC feedback control system is to create the model, and this is what's going to be discussed next.

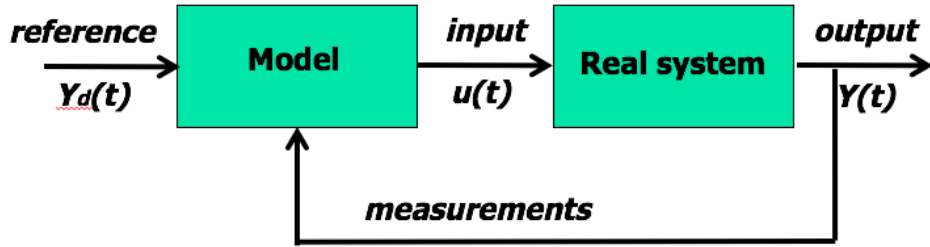


Figure 8-8 Schematic of MPC

1. Calculation of the system output

In this research, since the region that needs to be modeled is only the one after the peak in the grayness plot, and there is only one input (the welding current) and one output (image the grayness) in the process, a simple linear one-input-one-output model can satisfy the needs. The mathematic equation of the model is,

$$y[k + 1] = a \cdot y[k] + b \cdot u[k] \quad (8-1)$$

where $y[k+1]$ is the output at step $k+1$, $u[k]$ is the input at step k , a and b are constant parameters that need to be determined.

To predict one step ahead from the current step (e.g. k), the equation can be rewritten as:

$$y[k + 1|k] = a \cdot y[k] + b \cdot u[k] \quad (8-2)$$

To predict two steps ahead from k ,

$$y[k + 2|k] = a \cdot y[k + 1|k] + b \cdot u[k + 1] \quad (8-3)$$

where $u[k+1]=u[k]$ since it is desirable to keep the input current constant.

Substituting Equation (8-2) into (8-3),

$$y[k + 2|k] = a \cdot (a \cdot y[k] + b \cdot u[k]) + b \cdot u[k]$$

$$y[k + 2|k] = a^2 y[k] + (a \cdot b + b) u[k] \quad (8-4)$$

To predict three steps ahead from k,

$$y[k + 3|k] = a^3 y[k] + (a^2 + a + 1) \cdot b \cdot u[k] \quad (8-5)$$

To predict N steps ahead from k,

$$y[k + N|k] = a^N y[k] + (a^{N-1} + \dots + a + 1) \cdot b \cdot u[k] \quad (8-6)$$

Combine these equations together into a vector form,

$$\hat{Y} = \begin{bmatrix} \hat{y}[k + 1|k] \\ \hat{y}[k + 2|k] \\ \dots \\ \hat{y}[k + N|k] \end{bmatrix} = \begin{bmatrix} a \\ a^2 \\ \dots \\ a^N \end{bmatrix} \cdot y[k] + \begin{bmatrix} 1 & 0 & 0 & \dots & 0 \\ 1 & 1 & 0 & \dots & 0 \\ \dots & \dots & \dots & \dots & \dots \\ 1 & 1 & 1 & \dots & 1 \end{bmatrix} \cdot \begin{bmatrix} 1 \\ a \\ \dots \\ a^{N-1} \end{bmatrix} \cdot b \cdot u[k] \quad (8-7)$$

$$\text{Let } F_N = \begin{bmatrix} a \\ a^2 \\ \dots \\ a^N \end{bmatrix} \text{ and } H_N = \begin{bmatrix} 1 & 0 & 0 & \dots & 0 \\ 1 & 1 & 0 & \dots & 0 \\ \dots & \dots & \dots & \dots & \dots \\ 1 & 1 & 1 & \dots & 1 \end{bmatrix} \cdot \begin{bmatrix} 1 \\ a \\ \dots \\ a^{N-1} \end{bmatrix} \cdot b = \begin{bmatrix} b \\ b + a \\ \dots \\ b + ab + \dots + a^{N-1}b \end{bmatrix}$$

Equation (8-7) can be rewritten as,

$$\hat{Y} = F_N \cdot y[k] + H_N \cdot u[k] = \overline{F_N} + H_N \cdot u[k] \quad (8-7)$$

2. Finding the desired system input

In order for the real output to approach the desired output, a cost function is set up in the model that takes into account both the calculated (real) output and the desired output. By minimizing the cost function, the desired input to the system is found. The following mathematic derivations show how to find such input.

The cost function is defined as:

$$J = \sum_{j=1}^n (y[k+j] - y_d[k+j])^2 + \lambda(u[k] - u[k-1])^2 \quad (8-8)$$

where $y[k+j]$ is the calculated output at step j from the current step (k), and $y_d[k+j]$ is the desired output at step j from current, λ is the penalty coefficient, $u[k]$ and $u[k-1]$ are the current and the previous inputs.

Let $L = \begin{bmatrix} y_d[k+1] \\ y_d[k+2] \\ \dots \\ y_d[k+N] \end{bmatrix}$, and J can be rewritten in terms of the matrices and vectors:

$$J = [(F_N - L) + H_N \cdot u[k]]^T \cdot [(F_N - L) + H_N \cdot u[k]] + \lambda \cdot (u[k] - u[k-1])^2$$

Rewrite the above equation, we get:

$$J = (F_N - L)^T \cdot (F_N - L) + 2 \cdot (F_N - L)^T \cdot H_N \cdot u[k] + H_N^T \cdot H_N \cdot u^2[k] + \lambda \cdot (u[k] - u[k-1])^2 \quad (8-9)$$

In order to minimize the cost, find the derivative of J with respect to the input, and set it to 0:

$$\frac{\partial J}{\partial u[k]} = 0 \quad (8-10)$$

Substitute equation (8-9) into (8-10),

$$\frac{\partial J}{\partial u[k]} = 2 \cdot (F_N - L)^T \cdot H_N + 2 \cdot H_N^T \cdot H_N \cdot u[k] + \lambda(u[k] - u[k-1]) = 0 \quad (8-11)$$

From equation (8-11), the desired input at step k is:

$$u[k] = \frac{\lambda u[k-1] - (F_N - L)^T \cdot H_N}{\lambda + H_N^T \cdot H_N} \quad (8-12)$$

At this point, the input has been found and the model is considered built up. However, the vector F_N is dependent on the parameter a, H_N is dependent on the parameter b. Both parameters are unknown (they appear in Equation 8-1) and need to be found.

3. Calculation of model parameters using least square method

Least square method is a form of mathematical regression analysis that finds the line of best fit for a dataset, providing a visual demonstration of the relationship between the data points. Each data point is representative of the relationship between a known independent variable and an unknown dependent variable.

In order to solve for the model parameters a and b using least square method, a series of stationary welding experiments were conducted to get the grayness values vs. welding time. In each experiment, the only experiment parameter that was changing is the input current, i.e. 70A, 75A, 80A, 85A and 90A. This will create five grayness vs time plots. The purpose of using these welding currents is to make sure that the created model works well in this current range. The process for calculating the model parameters is as follows.

On each of the plot, identify the first real peak. From that point on, select 25 grayness values. These are the real $y[k]$ values. The model equation (8-1), which will be used for deriving the model parameters, is repeated below:

$$y[k] = a \cdot y[k - 1] + b \cdot u[k - 1] \quad (8-1)$$

$u[k-1]$ is the current at step $k-1$. In the five experiments, the current is fixed for each one, thus, $u[k] = u[k-1] = \dots = u[1]$.

Let $\phi[k] = [y[k-1] \quad u[k-1]]$, and $\theta = \begin{bmatrix} a \\ b \end{bmatrix}$. Equation 8-1 can be rewritten as:

$$y[k] = \phi[k] \cdot \theta \quad (8-13)$$

With the five sets of data and 25 data points in each data set, this forms a 125x1 vector

Y. Put the 125 equations together, we get:

$$\begin{bmatrix} y[1] \\ y[2] \\ \dots \\ y[125] \end{bmatrix} = \begin{bmatrix} \phi[1] \cdot \theta \\ \phi[2] \cdot \theta \\ \dots \\ \phi[125] \cdot \theta \end{bmatrix} = \begin{bmatrix} \phi[1] \\ \phi[2] \\ \dots \\ \phi[125] \end{bmatrix} \cdot \theta \quad (8-14)$$

Let $Y = \begin{bmatrix} y[1] \\ y[2] \\ \dots \\ y[125] \end{bmatrix}$ and $\Phi = \begin{bmatrix} \phi[1] \\ \phi[2] \\ \dots \\ \phi[125] \end{bmatrix}$, we can solve for θ :

$$\theta = (\Phi^T \cdot \Phi)^{-1} \cdot \Phi^T \cdot Y \quad (8-15)$$

Since Φ and Y are known, θ can be calculated, which means that a and b can be found.

Solving the matrix equation (8-15) is done in Matlab, and the calculated a and b are shown in Table 8-1.

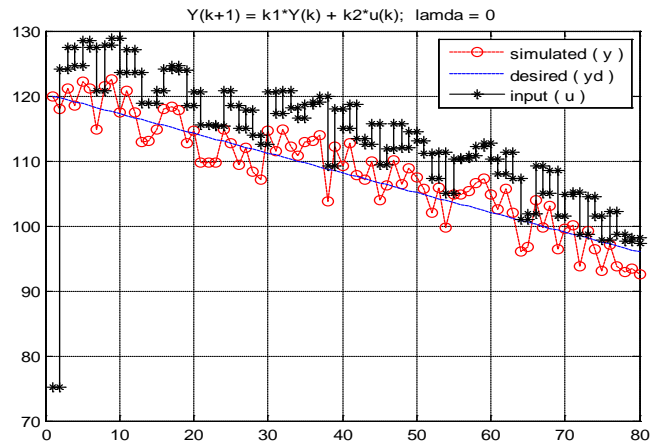
Table 8-1 Calculated MPC model parameters

Parameter	Value
a	1.06
b	-0.098

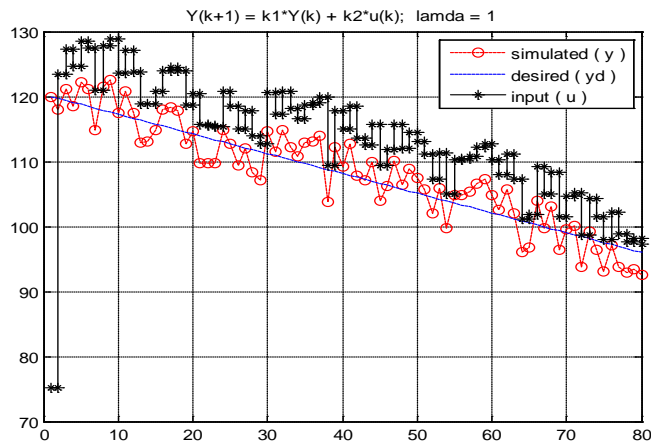
With the model parameters determined, the model built is considered complete. The model equation can now be written as:

$$Y(k + 1) = 1.06 * Y(k) - 0.098 * u(k) \quad (8-16)$$

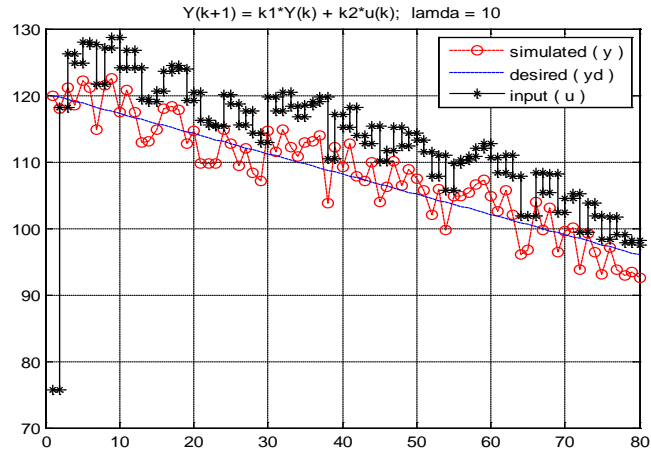
The next step is to simulate the output under the model's control, and by comparing it with the desired output, evaluate the effectiveness of the model. The simulated and the desired output are plotted in Figure 8-9.



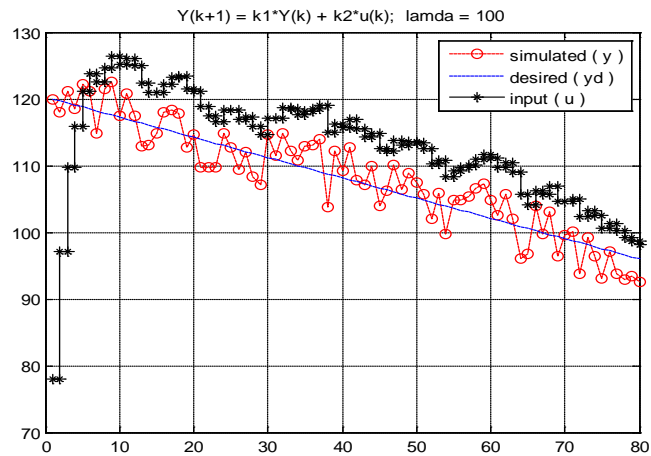
$\lambda = 0$



$\lambda = 1$



$\lambda = 10$



$\lambda = 100$

Figure 8-9 Grayness comparison between the simulated (model) data and the real data.

In order to find out how the calculated input responds to the simulated output, a small random variation is added to the simulated output. By doing this, not only can we see the variation of the input, but we can also see that the simulated output fluctuates. This better shows the real welding process. The variation of the input is in response to the output variations, which shows that the model works as desired. In addition, although the simulated output varies a lot, it only fluctuates around the desired input.

The four plots in Figure 8-9 have different penalty coefficient (λ) values. As shown in equation (8-9), the last term on the right side is the penalty. When the cost function J and the first three terms on the right hand side are fixed, penalty is fixed. Since λ is inversely proportional to $\Delta u[k]$ ($u[k]-u[k-1]$), when λ is increased, $\Delta u[k]$ decreases. This is especially obvious by comparing Figure 8-9(a) with the Figure 8-9(d). With a λ value of 0, input current u varies much more prominently in (a) than in (d) which has a large λ (100).

Ideally, we would like the input current variation to be small. This is because large input current variation causes large electromagnetic force acting on the weld pool. This can cause large oscillations which is not desirable. However, too small a λ value can lead to slow response of the feedback control system. Therefore, a compromise between these two conditions is to use a λ that is neither too small nor too large.

8.2.3 Experiment results using MPC feedback control

In this section, the MPC feedback control is applied to both the stationary welding and the continuous welding, and experiment results show that MPC is effective in controlling both the welding time and in achieving full penetration.

Experiment parameters used are the same as in Chapter 7. However, since the MPC control requires adjusting the input current, the current now varies, i.e., $80A \pm 15A$. The pre-specified welding time starting at the peak grayness is set to 2s. This is equivalent to 80 cycles, since the pulsed current period is 25ms: $25ms * 80 = 2000ms = 2s$.

Figure 8-10 shows the grayness variations as well as the current variations with welding time in stationary welding. MPC_current is the calculated current, while the

I_{weld} is the real input current supplied to the torch. In this experiment, control is set such that when the real input current is below 65A or above 95A, no adjustment is made to the current. This is to make sure that current variations are not too large. In Figure 8-10, such no adjustment can be seen in a small time period from 3800ms to 4000ms. The time when MPC control starts is at about 2500ms. Control finishes at about 4800ms. At that time, current is cut off and welding is complete.

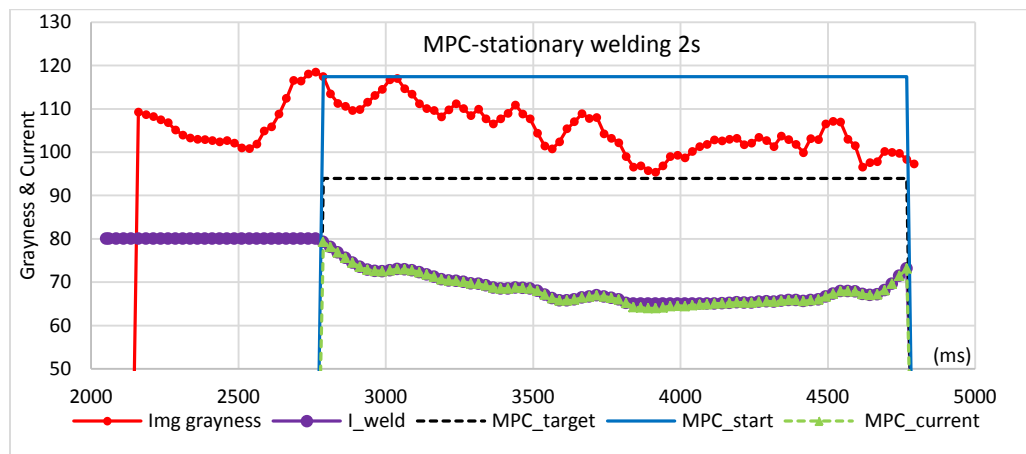


Figure 8-10 Grayness and input current variations with time using stationary welding and MPC feedback control.

Figure 8-11 is the surface appearance of the finished workpiece. Full penetration is achieved as can be seen on the backside. This demonstrates that using MPC control on stationary welding is effective.



Figure 8-11 Surface appearance of the finished workpiece using stationary welding and MPC feedback control.

When MPC control is applied on continuous welding, special care is taken to reduce the adverse effect of previous unsolidified pool on the current (present) welding spot. As discussed in section 8-1, the previous unsolidified pool causes strong reflection at the current welding spot, which leads to high grayness values at the start of the welding on the current spot. The grayness can subsequently have a few peaks, but those are not real peak that indicates the partial to full penetration on the current spots. The strategy taken to avoid this effect is to use a large value (1000) of λ (the penalty coefficient as discussed previously), small current (I) adjustment range of $\pm 0.5A$ for one pulse current period (25ms), and a total current adjustment of $\pm 15A$.

Figure 8-12 is the grayness and current curves obtained from continuous welding. The end of the black lines (MPC_Target) indicates the desired grayness at the end of each welding cycle. The welding cycle is different from the pulse current cycle (period). One welding cycle is the time spent on one welding spot, and one welding cycle takes 40 pulse current cycles (1s) in this experiment. The first welding cycle (3s) is set to be three times longer than subsequent cycles. This is due to the fact that at the start of welding, the workpiece is cold and need time to warm up.

Generally speaking, the real grayness is close to the target grayness or is approaching the target. There are a few cases that the real grayness drops below the target at the end of a welding cycle, and also a few cases that the real grayness is still above target when a welding cycle finishes. As shown in Equation (7-16), the grayness and the current have a linear relationship. However, Figure 8-12 indicates that there is a deviation to this relationship, as can be seen on the second and fifth welding cycles. In the second cycle, the real grayness does not drop enough to meet the target, while in the fifth cycle the real

grayness drops below the target. However, the current adjustment is in the right track. For example, in the second welding cycle, the welding current does increase according to Equation 8-16 to make the grayness drop. But the current increase is not large enough for the real grayness to meet the target. In this case, increasing current has more impact on the weld pool which leads to even stronger oscillation. As another example, in the fifth welding cycle, the grayness drops very sharply. In order to reduce the rate of decrease, the current is reduced too, as shown in Equation 8-16. But because the current reduction is not large enough, the final grayness does not meet the target. Although it looks like that current should be reduced more in order to have better control of the grayness variation, too much reduction in current drop has other undesirable effect which may cause more problems than meeting the grayness target. Thus, tight restrictions are set on the current adjustment range, as discussed earlier in this section. To have a better control system, more research work is needed to develop a better model and also to study the grayness evolution pattern in more detail.

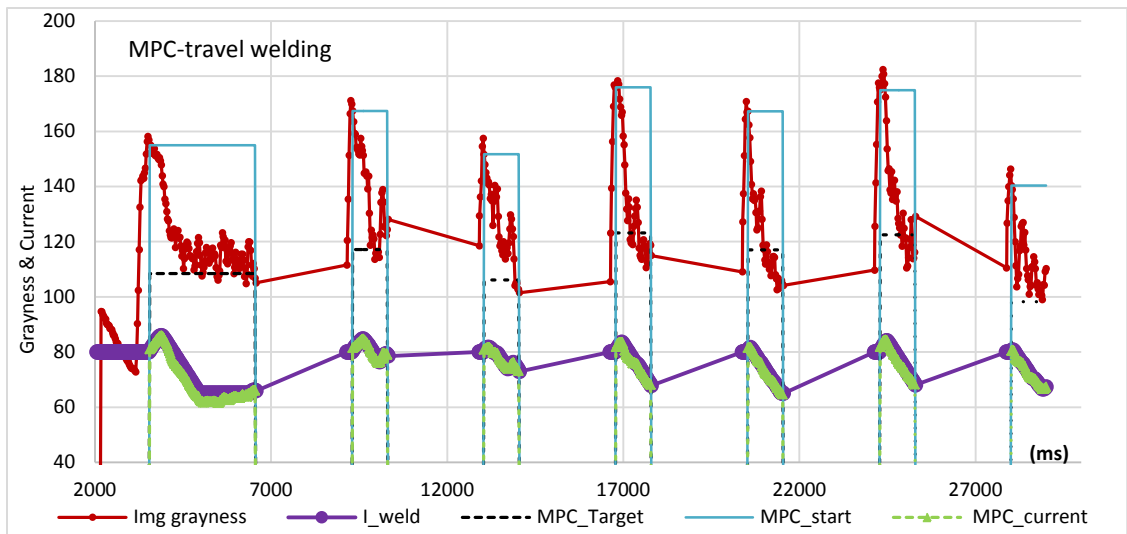
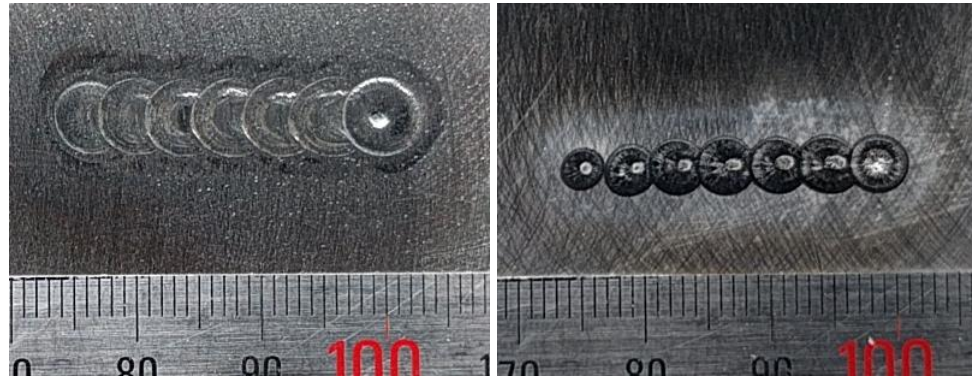


Figure 8-12 Grayness and input current variations with time using continuous welding and MPC feedback control.

Figure 8-13 is the surface appearance of the finished workpiece. As can be seen from the backside, the beads are overall uniform, despite the fact that control is not perfect.



(a) Front side

(b) Back side

Figure 8-13 Surface appearance of the finished workpiece using continuous welding and MPC feedback control

8.3 Summary

(1) Two MPC feedback control systems are developed based on the image grayness evolution during welding.

(2) The simple method finds the first real peak in the grayness evolution curve and then the subsequent 25% grayness reduction point as the critical penetration point. After that, it switches the pulsed current to a constant current for specified amount of time to make sure that full penetration is reached. Experiment results show that this method is effective in reaching full penetration.

(3) The model predictive control method first builds a model based on experiment data. Then the model is used to control the welding process. It works well on stationary welding, but needs improvement in continuous welding.

CHAPTER 9 Conclusions and Future Work

This chapter draws conclusions from previous chapters and outlines future work for improvement.

9.1 Conclusions

Weld pool penetration has been studied extensively. Many approaches have been found that can identify the penetration stages, especially full penetration. These approaches include vision-based sensing, voltage variation-based sensing, infrared-based sensing, and ultrasonic-based sensing, among others. Current research is based on vision-based sensing. However, unlike previous approaches, the current research is not focused on reconstructing the pool's shapes, but uses the image's overall grayness as indication of the penetration stage. This approach is simple and robust. It is simple because, for an image, it only needs to sort the pixels' grayness and select the first 20 with the highest grayness, and then average the 20 grayness values to represent the grayness of the image. It is robust, because experiment results show that grayness evolution behavior is highly repeatable.

With the observation, feedback control systems are built to ensure that in welding full penetration is reached, but not over-penetration. The first control system is simple. It identifies the first real peak and subsequently the point where the grayness decreases by 25% of the peak value. This point is the critical penetration point. When welding reaches this point, the control switches the pulsed current to a constant current and maintains it

for fixed time to make sure full penetration is reached. Results show that this simple method is effective. However, it has no control of when welding can finish.

To solve the issue in the simple control system, a MPC control system is developed. From experiment data, the model parameters are calculated. The model is then used to control stationary welding and continuous welding, with specified welding time. In stationary welding, the control works well. In continuous welding, due to the effect of the previous unsolidified pool, oscillation is still strong on the current welding spot. This leads to the grayness starts at a higher value than in the stationary welding. This leads to the model not able to predict the grayness variations well. Consequently, a good control is hard to obtain. However, the finished weld beads still have a fairly good quality, that is the uniformity of the beads. More research is underway to improve this model.

In addition to identifying image grayness as the key factor in tracking the weld pool penetration stages, work is also done in building a model of the dynamic weld pool. This model reveals some characteristics of the oscillation of the weld pool. Moreover, experiments are conducted that reveals the three oscillation mode, i.e. symmetrical oscillation for partial penetration, sloshing oscillation for critical penetration, and symmetrical oscillation for full penetration.

9.2 Future Work

As discussed in early chapters, the proposed grayness method to identify weld pool penetration stages is simple and robust; the developed feedback control systems generally can meet requirements. However, there is room for improvement:

1. As discussed and shown in Chapter 8, MPC control does not work very well in continuous welding due to the interference of the previous unsolidified weld pool. The future work will be conducted in improving this model. This may involve building a more sophisticated higher order model.
2. Currently the camera speed is not very high. It can take only three pictures in the base current period. If we assume that the oscillation has the shape of a sine wave, we do not have control on where the image taken corresponds to on the wave form. Lacking this knowledge means that we do not know exactly which oscillation state the image taken is from; for example we do not know if the image is from when the pool is oscillating upward or downward, how much upward, how much downward. Thus, future work is needed to increase the camera speed.
3. At this time, the camera cannot work for long period of time. The camera cannot be turned on and off repeatedly due to the lag in changing the camera state (on and off). Since the camera has only limited memory, when it is always on during welding, it takes too many pictures that are not useful and at the same time it significantly reduces the working time of the camera. In the future, work should be done to manipulate the camera so that it can switch on and off much faster.

REFERENCES

1. Connor, L.P., R.L. O'Brien, and A.W. Society, *Welding Handbook: Welding processes*. 1991: American Welding Society.
2. Cary, H.B. and S.C. Helzer, *Modern Welding Technology*. 2005: Pearson/Prentice Hall.
3. Zhang, Z.Z. and C.S. Wu, *Effect of fluid flow in the weld pool on the numerical simulation accuracy of the thermal field in hybrid welding*. *Journal of Manufacturing Processes*, 2015. **20**: p. 215-223.
4. Wu, C.S., et al., *Plasma arc welding: Process, sensing, control and modeling*. *Journal of Manufacturing Processes*, 2014. **16**(1): p. 74-85.
5. Liu, Z.M., et al., *Keyhole Behaviors Influence Weld Defects in Plasma Arc Welding Process*. *Welding Journal*, 2015. **94**(9): p. 281S-290S.
6. Chen, S.B. and N. Lv, *Research evolution on intelligentized technologies for arc welding process*. *Journal of Manufacturing Processes*, 2014. **16**(1): p. 109-122.
7. Bahrami, A., D.K. Aidun, and D.T. Valentine, *Interaction of Gravity Forces in Spot GTA Weld Pool*. *Welding Journal*, 2014. **93**(4): p. 139S-144S.
8. Ahsan, M.R.U., et al., *Cold Metal Transfer (CMT) GMAW of Zinc-Coated Steel*. *Welding Journal*, 2016. **95**(4): p. 120S-132S.
9. Bahrami, A. and D.K. Aidun, *Modeling of Carbon Steel-Duplex Stainless Steel GTA Weld Pool*. *Welding Journal*, 2014. **93**(7): p. 262S-270S.
10. Kotecki, D., D. Cheever, and D. Howden, *Mechanism of ripple formation during weld solidification*. *WELD J*, 1972. **51**(8): p. 368.

11. Yudodibroto, B., et al., *Influence of filler wire addition on weld pool oscillation during gas tungsten arc welding*. Science and Technology of Welding & Joining, 2013.
12. Tewari, S., *Effects of oscillation on impact property of weldments*. ISIJ international, 1999. **39**(8): p. 809-812.
13. Methong, T. and B. Poopat. *The effect of ultrasonic vibration on properties of weld metal*. in *Key Engineering Materials*. 2013. Trans Tech Publ.
14. Kägeler, C. and M. Schmidt, *Frequency-based analysis of weld pool dynamics and keyhole oscillations at laser beam welding of galvanized steel sheets*. Physics Procedia, 2010. **5**: p. 447-453.
15. Jose, M., S.S. Kumar, and A. Sharma, *Vibration assisted welding processes and their influence on quality of welds*. Science and Technology of Welding and Joining, 2016. **21**(4): p. 243-258.
16. Huang, C. and S. Kou, *Liquation cracking in partial-penetration aluminum welds: Effect of penetration oscillation and backfilling*. WELDING JOURNAL-NEW YORK-, 2003. **82**(7): p. 184-S.
17. Hermans, M. and G. Den Ouden, *Process behavior and stability in short circuit gas metal arc welding*. WELDING JOURNAL-NEW YORK-, 1999: p. 137-s.
18. Dowden, J. and P. Kapadia, *Oscillations of a weld pool formed by melting through a thin work piece*. Lasers in Engineering(UK), 1999. **8**(4): p. 311-318.
19. Cho, J., et al., *Numerical analysis of weld pool oscillation in laser*

welding. Journal of Mechanical Science and Technology, 2015. **29**(4): p. 1715-1722.

20. Xiao, Y. and G. Den Ouden, *A study of GTA weld pool oscillation*. Weld. J., 1990. **69**(8): p. 289.

21. Xiao, Y. and G. Den Ouden, *Direct Observation of GRA Weld Pool Oscillation*. International Trends in Welding Science and Technology, 1992: p. 423-426.

22. Xiao, Y. and G.d. Ouden, *Weld pool oscillation during GTA welding of mild steel*. Welding Journal (Miami);(United States), 1993. **72**(8).

23. Shi, Y., et al. *Weld pool oscillation frequency in pulsed gas tungsten arc welding with varying weld penetration*. in *2015 IEEE International Conference on Automation Science and Engineering (CASE)*. 2015. IEEE.

24. Shi, Y., et al., *Laser-Vision-Based Measurement and Analysis of Weld Pool Oscillation Frequency in GTAW-P*. Welding Journal, 2015. **94**(5): p. 176s-187s.

25. Yu, S., et al., *Frequency characteristics of weld pool oscillation in pulsed gas tungsten arc welding*. Journal of Manufacturing Processes, 2016. **24**: p. 145-151.

26. Tarn, A. and D. Hardt, *Weld pool impedance for pool geometry measurement: stationary and non-stationary pools*. Journal of dynamic systems, measurement, and control, 1989. **101**: p. 545-553.

27. Kovacevic, R., Y. Zhang, and L. Li, *Monitoring of Weld Joint Penetrations Based on Weld Pool Geometrical Appearance*. Welding Journal-

Including Welding Research Supplement, 1996. **75**(10): p. 317-329.

28. Joshi, Y., et al., *Nonaxisymmetric convection in stationary gas tungsten arc weld pools*. Journal of heat transfer, 1997. **119**(1): p. 164-172.

29. Andersen, K., et al., *Synchronous weld pool oscillation for monitoring and control*. IEEE Transactions on Industry Applications, 1997. **33**(2): p. 464-471.

30. Aendenroomer, A. and G. Den Ouden, *Weld pool oscillation as a tool for penetration sensing during pulsed GTA welding*. WELDING JOURNAL-NEW YORK-, 1998. **77**: p. 181-s.

31. Renwick, R. and R. Richardson, *Experimental investigation of GTA weld pool oscillations*. WELDING J., 1983. **62**(2): p. 29.

32. YOO, C.D. and R.W. Richardson, *An Experimental Study on Sensitivity and Signal Characteristics of Welds Pool Oscillation*. Transactions of the Japan Welding Society, 1993. **24**(2): p. 54-62.

33. Ramos, E.G., G.C.d. Carvalho, and S.C.A. Alfaro, *Analysis of weld pool oscillation in P-GMAW by Means of Shadowgraphy Image Processing*. Soldagem & Inspeção, 2013. **18**(1): p. 39-49.

34. MATSUDA, F., et al., *Effects of current pulsation on weld solidification structure of aluminum alloys*. Transactions of JWRI, 1978. **7**(2): p. 287-289.

35. Yamamoto, H., et al., *Beneficial effects of low-frequency pulsed MIG welding on grain refinement of weld metal and improvement of solidification crack susceptibility of aluminium alloys: Study of low-frequency pulsed MIG*

welding. *Welding international*, 1993. **7**(6): p. 456-461.

36. Zacksenhouse, M. and D. Hardt, *Weld pool impedance identification for size measurement and control*. *Journal of Dynamic Systems, Measurement, and Control*, 1983. **105**(3): p. 179-184.

37. Renwick, R.J., *Real Time Control of GTA Weld Size by Controlling Pool Oscillation Frequency*. 1983.

38. Chen, S.-B., et al., *Fuzzy-neural network modelling and control of pool dynamic process in pulsed GTAW*. *Acta Automatica Sinica*, 2002. **28**(1): p. 74-82.

39. Chen, S.-B., et al., *Welding robotic systems with visual sensing and real-time control of dynamic weld pool during pulsed GTAW*. *International Journal of Robotics and Automation*, 2004. **19**(1): p. 28-35.

40. Liangqiang, Z., W. Jifeng, and L. Tao, *Analysis of aluminum GTAW pool oscillation model*. *Journal of Shanghai Jiaotong University*, 2010. **44**(Suppl 1): p. 92-94.

41. Shi, Y., et al., *Laser vision based detection and analysis of weld pool oscillation for pulsed GTAW*. *Jixie Gongcheng Xuebao*(Chinese Journal of Mechanical Engineering), 2012. **48**(24): p. 28-32.

42. Fan, H., Y. Shi, and S. Na, *Numerical analysis of the arc in pulsed current gas tungsten arc welding using a boundary-fitted coordinate*. *Journal of Materials Processing Technology*, 1997. **72**(3): p. 437-445.

43. Traidia, A. and F. Roger, *Numerical and experimental study of arc and weld pool behaviour for pulsed current GTA welding*. *International journal of*

heat and mass transfer, 2011. **54**(9): p. 2163-2179.

44. Wu, C., *ANALYSIS OF DYNAMIC DEVELOPMENT OF SURFACE DEPRESSION IN FULL-PENETRATED WELDPPOOL*. Acta Metall Sin, 2006. **42**(8): p. 865-869.

45. Wu, C., W. Zheng, and L. Wu, *Numerical simulation of TIG weld pool behavior under the action of pulsed current*. ACTA METALLURGICA SINICA-CHINESE EDITION-, 1998. **34**: p. 416-422.

46. Zhao, M., C. Wu, and Q. Hu, *Numerical simulation of penetrated weld pool geometry and surface deformation in TIG welding*. Jixie Gongcheng Xuebao(Chinese Journal of Mechanical Engineering), 2006. **42**(10): p. 203-208.

47. Ohji, T. and K. Nishiguchi, *Mathematical modelling of a molten pool in arc welding of thin plate*. Technology Reports of the Osaka Univ, 1983. **33**(1688): p. 35-43.

48. Wu, C. and L. Dorn, *Prediction of surface depression of a tungsten inert gas weld pool in the full-penetration condition*. Proceedings of the Institution of Mechanical Engineers, Part B: Journal of Engineering Manufacture, 1995. **209**(3): p. 221-226.

49. Cao, Z., Y. Zhang, and R. Kovacevic, *Numerical dynamic analysis of moving GTA weld pool*. Journal of manufacturing science and engineering, 1998. **120**(1): p. 173-178.

50. Fan, H., H.-L. Tsai, and S. Na, *Heat transfer and fluid flow in a partially or fully penetrated weld pool in gas tungsten arc welding*. International Journal of Heat and Mass Transfer, 2001. **44**(2): p. 417-428.

51. Karunakaran, N. and V. Balasubramanian, *Effect of pulsed current on temperature distribution, weld bead profiles and characteristics of gas tungsten arc welded aluminum alloy joints*. Transactions of Nonferrous Metals Society of China, 2011. **21**(2): p. 278-286.
52. Song, H. and Y. Zhang, *Measurement and analysis of three-dimensional specular gas tungsten arc weld pool surface*. WELDING JOURNAL-NEW YORK-, 2008. **87**(4): p. 85.
53. Chen, W. and B. Chin, *Monitoring joint penetration using infrared sensing techniques*. Welding Journal, 1990. **69**(4): p. 181s-185s.
54. Graham, G.M. and I.C. Ume, *Automated system for laser ultrasonic sensing of weld penetration*. Mechatronics, 1997. **7**(8): p. 711-721.
55. Garasic, I., Z. Kozuh, and M. Remenar, *Sensors and their classification in the fusion welding technology/Senzori i njihova podjela u tehnologiji zavarivanja*. Tehnicki Vjesnik-Technical Gazette, 2015. **22**(4): p. 1069-1075.
56. Song, H. and Y. Zhang. *An image processing scheme for measurement of specular weld pool surface*. in *2007 2nd IEEE Conference on Industrial Electronics and Applications*. 2007. IEEE.
57. Kothe, D. and R. Mjolsness, *Ripple: a new model for incompressible flows with free surfaces*. 1991, Los Alamos National Lab., NM (United States).
58. Bag, S. and A. De, *Probing reliability of transport phenomena based heat transfer and fluid flow analysis in autogeneous fusion welding process*.

Metallurgical and Materials Transactions A, 2010. **41**(9): p. 2337-2347.

59. Wu, C.S., *Welding thermal processes and weld pool behaviors*. 2010: CRC Press/China Machine Press.

60. McNallan, M.J. and T. Debroy, *Effect of temperature and composition on surface tension in Fe-Ni-Cr alloys containing sulfur*. Metallurgical and Materials Transactions B, 1991. **22**(4): p. 557-560.

61. Hartman, D., et al. *A neural network/fuzzy logic system for weld penetration control*. in *Trends in Welding Research, Proceedings of the 5th International Conference, Pine Mountain, GA*. 1998.

62. Hu, B. and G. Den Ouden. *Weld penetration sensing and control during GTA welding using weld pool oscillation*. in *5 th International Conference: Trends in Welding Research*. 1998.

63. Maruo, H. and Y. Hirata, *Natural frequency and oscillation modes of weld pools. 1st Report: Weld pool oscillation in full penetration welding of thin plate*. 1993.

64. Sorensen, C.D. and T.W. Eagar, *Digital signal processing as a diagnostic tool for gas tungsten arc welding*. 1985, Citeseer.

65. Jianbin, J., H. Hasegawa, and Y. Suga, *Oscillation of molten pool by pulsed assist gas oscillating method and penetration control using peculiar frequency*. Journal of High Temperature Society, 2005. **30**: p. 263-269.

VITA

Jinsong Chen was born in SiChuan, China.

Education:

M.S. in Electrical Engineering, University of Kentucky May. 2009

M.S. in Electrical Engineering, University of Electronic Science and
Technology of China

B.S. in Electrical Engineering, Harbin Institute of Technology

Publications:

1. Lu, Yi, Jinsong Chen, and YuMing Zhang. "Dynamic Model of Consumable Double-Electrode Submerged Arc Welding Process." *Journal of Manufacturing Science and Engineering* 137, no. 2 (2015): 021001
2. Lu, Yi, JinSong Chen, YuMing Zhang, and Lee Kvidahl. "Predictive control based double-electrode submerged arc welding for fillet joints." *Journal of Manufacturing Processes* 16, no. 4 (2014): 415-426.
3. Lu, Yi, ShuJun Chen, Yu Shi, Xiangrong Li, Jinsong Chen, Lee Kvidahl, and Yu Ming Zhang. "Double-electrode arc welding process: principle, variants, control and developments." *Journal of Manufacturing Processes* 16, no. 1 (2014): 93-108.
4. Chen, JinSong, Y. Lu, X. R. Li, and Y. M. Zhang. "Gas tungsten arc welding using an arcing wire." *Welding Journal* 91, no. 10 (2012): 261-269.
5. Li, K. H., JinSong Chen, and YuMing Zhang. "Double-electrode GMAW process and control." *WELDING JOURNAL-NEW YORK-* 86, no. 8 (2007): 231.